Separations of Biofuels and Bioproducts via Magnetic Mesoporous Carbons

by

Kyle Staggs

A Dissertation Presented in Partial Fulfillment
of the Requirements for the Degree
Doctor of Philosophy

Approved July 2017 by the
Graduate Supervisory Committee:

David Nielsen, Chair
Jerry Y.S. Lin
Cesar Torres
Mary Laura Lind
Xuan Wang

ARIZONA STATE UNIVERSITY

August 2017

ABSTRACT

The aims of this project are to demonstrate the design and implementation of separations modalities for 1) in situ product recovery and 2) upstream pretreatment of toxic feedstocks. Many value-added bioproducts such as alcohols (ethanol and butanol) developed for the transportation sector are known to be integral to a sustainable future. Likewise, bioproduced aromatic building blocks for sustainable manufacturing such as phenol will be equally important. The production of these compounds is often limited by product toxicity at 2- 20 g/L, whereas it may desirable to produce 20-200 g/L for economically feasible scale up. While low-cost feedstocks are desirable for economical production, they contain highly cytotoxic value-added byproducts such as furfural. It is therefore desirable to design facile detoxification methods for lignocellulose-derived feedstocks to isolate and recover furfural preceding ethanol fermentation by Escherichia coli. Correspondingly it is desirable to design efficient facile in situ recovery modalities for bioalcohols and phenolic bioproducts. Accordingly, in-situ removal modalities were designed for simultaneous acetone, butanol, and ethanol recovery. Additionally, a furfural removal modality from lignocellulosic hydrolysates was designed for upstream pretreatment. Solid-liquid adsorption was found to serve well each of the recovery modalities characterized here. More hydrophobic compounds such as butanol and furfural are readily recovered from aqueous solutions via adsorption. The primary operational drawback to adsorption is adsorbent recovery and subsequent desorption of the product. Novel magnetically separable mesoporous carbon powders (MMCPs) were characterized and found to be rapidly separable from solutions at 91% recovery by mass. Thermal desorption of value added products was found efficient for recovery of butanol and

furfural. Fufural was desorbed from the MMCPs up to 57% by mass with repeated adsorption/thermal desorption cycles. Butanol was recovered from MMCPs up to an average 93% by mass via thermal desorption. As another valuable renewable fermentation product, phenol was also collected via in-situ adsorption onto Dowex Optipore L-493 resin. Phenol recovery from the resins was efficiently accomplished with tert-butyl methyl ether up to 77% after 3 washes.

ACKNOWLEDGMENTS

This work has been made possible by the guidance and support of my advisor and committee members and collaborators. My advisor David Nielsen has been a significant help in focusing my work. His hard work and dedication on my behalf has made him an exemplary mentor. I would especially like to thank my loving and understanding wife Sherry for her steadfast dedication to my success. Without her support and encouragement, this work would not have reached completion. I would like to thank Dr. Lin, Dr. Torres, Dr. Lind and Dr. Wang for their input and assistance on this work. I would also like to thank Dr. Vogt and his postdoc Zhe Qiang for their work in developing and refining the magnetic mesoporous carbons which enabled rapid and selective sorption of bioproducts. I would be remiss if I did not mention the incredible support of my parents and all of my family who have been a much-needed encouragement throughout this project. Also, I would like to thank my lab mates for the witty banter and never to be underappreciated coffee runs which enabled me to refocus.

TABLE OF CONTENTS

Page

CHAPTER Page

CHAPTER Page

LIST OF TABLES

Table Page

LIST OF FIGURES

Figure Page

Figure Page

Figure Page

CHAPTER 1

1.0 IMPROVING N-BUTANOL PRODUCTION IN BATCH AND SEMI-CONTINUOUS PROCESSES THROUGH INTEGRATED PRODUCT RECOVERY

1.1.0 Preface

While the current global energy challenges have many proposed solutions, some of the most rapidly growing research generas are bioproducts and biofuels. The idea of a renewable bio-based alcohol energy economy is itself a recycled concept. Dating back to the 1820's inventors were creating internal combustion engines to run on ethanol and by the 1910's Henry Ford was producing tractors which ran on alcohol. (M. Guo, Song, & Buhain, 2015) With diminishing whale oil supplies, an energy crisis in the early1800's led to the use of ethanol as a fuel before the discovery of petroleum in 1859 by Edwin Drake. (Songstad et al., 2009) Alexander Graham Bell was quoted as saying, "Alcohol can be manufactured from corn stalks, and in fact from almost any vegetable matter capable of fermentation. Our growing crops and even weeds can be used. The waste products of our farms are available for this purpose and even the garbage of our cities. We need never fear the exhaustion of our present fuel supplies so long as we can produce an annual crop of alcohol to any extent desired." (Songstad et al., 2009) Alcohol taxes used to fund the Civil War helped make petroleum cheaper, leading to the development of a petroleum-based economy. (Songstad et al., 2009) Having never learned from the whale oil shortages, the global economy now seeks to replace the crude oil-derived economy of today. Surely then the renewable bioproduct research thrust is a new movement born from wisdom resulting from historical lessons. The Chemurgy movement, promoted by Henry Ford in the 1920s through the 1930s sought to promote

crop growth for bio-based materials such as ethanol-derived synthetic rubber. (Songstad et al., 2009)

A resurgence of research has been developing for many biomass-derived products and fuels. Bioproducts as a term has grown to include sustainable replacements for products derived from oil. This includes bioproduced commodity chemical building blocks such as phenol (Thompson, Machas, & Nielsen, 2016), styrene (McKenna & Nielsen, 2011), lactic acid (Kwan, Hu, & Lin, 2016), benzoate (Elshahed & McInerney, 2001), terpene alkaloids (Xu, Baunach, Ding, & Hertweck, 2012) and many other organic acids, aromatics and polycyclic hydrocarbons. (Keum, Seo, & Li, 2006) Likewise for alcohols, the developing research has included not only ethanol production from highly engineered strains of E. coli (L.P. Yomano, York, & Ingram, 1998), but also includes butanol (Berezina, Zakharova, Yarotsky, & Zverlov, 2012), isobutanol (X. Chen, Nielsen, Borodina, Kielland-Brandt, & Karhumaa, 2011), and aromatic alcohols such as cinnamyl alcohol. (W. Zhou et al., 2017) Other groups have focused on development of fatty acids from algae to develop biodiesel(Martarella, Rittmann, Lai, Chemical Engineering, & Barrett, 2015) and even gold particle synthesis. (Parial, Patra, Dasgupta, & Pal, 2012) With such a breadth of bioproducts under development, the future of the biomaterials and biofuels is decidedly more expansive than what was envisioned at the turn of the last century.

Bioproduction has limitations like any traditional process. As bioproduction relies on microorganisms to work as small chemical factories, the synthesis conditions are limited to the range of viable growth conditions for the microorganism. (C. Y. Chen et

al., 2013; Ikegami, Negishi, & Sakaki, 2011; Ikegami et al., 2007; Lau, Gunawan, Balan, & Dale, 2010; Patil, Veerapur, Patil, Madhusoodana, & Aminabhavi, 2007; Sasaki et al., 2013; Vane, 2008a; Vane & Alvarez, 2013; Vane, Alvarez, Rosenblum, & Govindaswamy, 2013) Additionally, bioproducts are often toxic to the microorganisms limiting the product accumulation. (C. Y. Chen et al., 2013; Vane, 2005, 2008a; Vane & Alvarez, 2013; Vane et al., 2013) As the bulk of the cost associated with bioproduction is the cost of the feedstock, much focus has been placed on bioproduction from waste biomass. In particular, lignocellulosic and hemicellulosic biomass have replaced glucose a broad range of products.(Bioenergy et al., 2005; Dalecka, Strods, & Mezule, 2015; Jonsson & Martin, 2016; Machado et al., 2016) These feedstocks have toxic compounds present which vary in concentration depending on the method of degradation from woody biomass to fermentable sugars. (Jonsson & Martin, 2016) Whether product or feedstock toxicity is the limiting factor for bioproduction, separations can alleviate the toxicity and improve product titers or cell growth. Many separations strategies have been applied, including: liquid-liquid extraction, pervaporation, vapor permeation, gas stripping, steam stripping, membrane assisted vapor stripping, hybrid distillation with molecular sieves, and others.(Cai et al., 2013; C. Y. Chen et al., 2013; Gudena, Rangaiah, & Lakshminarayanan, 2013; Paradis et al., 2013; Patil et al., 2007; Shi, Chen, Jean, & Chung, 2013; Vane, 2008a; Vane & Alvarez, 2013) Vapor phase separations such as pervaporation work well for products with high vapor pressure and low boiling points.(Cai et al., 2013; C. Y. Chen et al., 2013; Gaykawad et al., 2013; Kittur, Kariduraganavar, Kulkarni, & Aralaguppi, 2005; Vane, 2005) Solid phase separations such as molecular sieves (Aljundi, Belovich, & Talu, 2005; Xiao Lin, Kita, & Okamoto,

2001) and adsorbents (e.g. activated carbon, resins, etc.) often function best to separate hydrophobic products and those with high boiling points and low vapor pressure.(Niloofar Abdehagh, Gurnani, Tezel, & Thibault, 2015; Adnadevic, Mojovic, & Abu Rabi, 2008; Aljundi et al., 2005; Boyang et al., 2011; Hartmann, Vinu, & Chandrasekar, 2005; Jia et al., 2015; T. J. Levario, M. Z. Dai, W. Yuan, B. D. Vogt, & D. R. Nielsen, 2012; Maddox, 1982; Parajo, Dominguez, & Dominguez, 1996; Wiehn et al., 2013; Wiehn, Staggs, Wang, & Nielsen, 2014; Yapsaklı, Çeçen, Aktaş, & Can, 2009) Adsorbents are also particularly effective at recovery of analytes from low aqueous concentrations. (Fierro, Torné-Fernández, Montané, & Celzard, 2008; Hartmann et al., 2005; Jia et al., 2015; Nongonierma, Cayot, Le Quere, Springett, & Voilley, 2006) Liquid phase separations also work well for hydrophobic products though the selection of solvents is limited by biocompatibility of the solvent.(Cascon et al., 2011; Cheng & Wang, 2010; Groot et al., 1990; Heerema et al., 2011) The focus of this work will be to compare the known separations method for recovery of analytes from aqueous solutions to highlight the strengths and weaknesses of each method. Specifically, separations of bioalcohols and value-added coproducts are examined here.

Abstract

Although it represents a promising biofuel, n-butanol production by conventional batch fermentation is limited as a result of its cytotoxic effects. To address this limitation and facilitate semi-continuous fermentation, in situ n-butanol removal has proven to be an effective approach. Exploiting the phenomena of solvent extraction, adsorption, or vaporization, numerous integrated bioprocess configurations have been developed to facilitate selective n-butanol recovery. The objective of this review is to provide a broad overview of different technology options and process configurations to this end, highlighting notable achievements and recent developments. In each case, relevant design considerations critical for improving key production metrics will be discussed, with particular emphasis given to studies that, as a result of relieved product toxicity, have successfully demonstrated further enhanced n-butanol production through semi-continuous operation.

This work was published as:

Staggs, K. & Nielsen, D.R. Improving n-butanol production in batch and semi-continuous processes through integrated product recovery. *Process Biochem* **50(10)**, 1487-1498 (2015)

1.2.0 Background and Motivation

Produced by microbial biocatalysts from biomass-derived feedstocks, biofuels represent a promising solution to the growing global need for sustainable liquid transportation fuels (Connor & Liao, 2009; Keasling & Chou, 2008; Y. N. Zheng et al., 2009). In light of inherent shortcomings associated with ethanol, however, which include its high water solubility and low energy density (attributes that collectively diminish its compatibility with conventional engines and fuel distribution infrastructure) (Y. N. Zheng et al., 2009), interest continues to shift to the alternative fermentative production of higher (i.e., >2-carbon) alcohol biofuels (Connor & Liao, 2009; Keasling & Chou, 2008), including n-butanol (Dafoe & Daugulis, 2014; Garcia, Pakkila, Ojamo, Muurinen, & Keiski, 2011; Tashiro, Yoshida, Noguchi, & Sonomoto, 2013). With more similar physical and thermodynamic properties, n-butanol represents a potential 'drop in' compatible gasoline replacement (Berezina et al., 2012). Naturally synthesized by many *Clostridium* sp. (Jones & Woods, 1986a), n-butanol is produced as the major end-product along with acetone and ethanol as part of the so-called ABE fermentation. Efficient and commonly employed n-butanol production strains include, for example, the type strain *C. acetobutylicum* ATCC 824 and the hyper-producer *C. beijerinckii* (N. Qureshi & Blaschek, 2000). Notably, the novel and focal biosynthesis of n-butanol has also recently been engineered in a number of other heterologous microbes (Atsumi et al., 2008; Bond-Watts, Bellerose, & Chang, 2011; D. R. Nielsen et al., 2009).

Despite its promising attributes, however, several inherent limitations surround the n-butanol fermentation process, challenging its overall commercial prospects. Chief

among these is product toxicity, and the resultant feedback inhibition it causes against producing microbes at relative low aqueous n-butanol concentrations (Bowles & Ellefson, 1985; Ingram, 1990; Jones & Woods, 1986a). As with other alcohols and solvents, microbial activity is reduced as a result of n-butanol partitioning into the cytoplasmic membrane (Osborne, Leaver, Turner, & Dunnil, 1990; Vermue, Sikkema, Verheul, Bakker, & Tramper, 1993). As the membrane structure becomes disrupted (Bowles & Ellefson, 1985), increased membrane fluidity (Ingram, 1990; Ramos et al., 1997) and diminished function of several essential cellular functions results (Bowles & Ellefson, 1985). Consequently, maximal n-butanol titers of only 13 g/L are typical for wild-type *C. acetobutylicum* (Jones & Woods, 1986a), whereas strains engineered or selected for enhanced solvent tolerance fair only slightly better (e.g., maximal titers reaching no more than 20-24 g/L have been reported (Niloofar Abdehagh, Tezel, & Thibault, 2014; C. K. Chen & Blaschek, 1999; D. Liu et al., 2013; Chuang Xue et al., 2012)). At this output, large-scale bioreactors and high turnover rates are required to produce n-butanol in quantities sufficient for biofuel applications. Accordingly, there remains keen interest in the development of effective, process-level solutions for addressing n-butanol toxicity and promoting high rates of volumetric productivity.

As with many other toxic bioproducts, *in situ* product recovery has been demonstrated as an effective strategy for improving n-butanol production by circumventing its inhibitory effects (Schugerl, 2000; W. Van Hecke, Kaur, & De Wever, 2014; Chuang Xue et al., 2014; S. T. Yang & Lu, 2013). Utilizing an integrated bioprocess to synchronously incorporate fermentation and separation operations, n-butanol can be selectively removed from the fermentation medium as it is produced. With

typical yield coefficients of up to about 0.3 g-butanol/g-glucose (Barton & Daugulis, 1992; X. Chen et al., 2011; H.-W. Yen & Li, 2011; Y. Zhang, Ma, Yang, & Zhang, 2009), in traditional batch cultures the n-butanol toxicity threshold is readily reached when *Clostridium* sp. are provided with as little as 60 g/L glucose, with excess amounts typically going unused. Alternatively, by incorporating a second, product recovery phase to concentrate and sequester n-butanol away from susceptible cells, greater net substrate utilization is then possible as is n-butanol accumulation to above would be inhibitory levels. However, as high sugar concentrations can themselves be inhibitory (e.g., >100 g/L glucose (D. R. Nielsen & Prather, 2009), >250 g/L lactose (N. Qureshi & Maddox, 2005)), this is typically best accomplished through fed-batch operation. This semi-continuous approach to n-butanol production provides further practical benefits, including minimal wastewater generation, decreased frequency of culture turnover, and reduced between-run downtime for cleaning and sterilization. Time saved as a result of the latter features is often translated into rates of volumetric productivity, surpassing the 0.2-0.6 g/L-h typically achieved under conventional batch conditions (Jones & Woods, 1986a).

The selective separation of n-butanol from aqueous solutions can be achieved by exploiting of one of several unique physicochemical attributes.Effective strategies for *in situ* n-butanol recovery, however, must also satisfy several important prerequisites:

1. Cost: minimal energy and/or material costs to maintain favorable energetic and economic yields.

2. Biocompatibility: microbial activity and viability should not be adversely impacted by the conditions or materials required for the separation.
3. High affinity: effective n-butanol separation should be possible under dilute concentrations.
4. Regeneration: full regeneration possible with minimal energy input, enabling both facile release of recovered n-butanol and reuse of materials.
5. Robustness: separation materials and design should be resistant against non-ideal interactions with medium components and/or cells, as these can result in performance losses due to inhibition, (bio)fouling, concentration polarization, and degradation.
6. Modularity: important for improving implementation in retrofit applications and enabling different modes of operation.

Despite these stringent design considerations, numerous effective integrated bioprocesses have been developed to date and applied to enhance n-butanol production through its *in situ* recovery. The objective of this review is to provide a broad overview of different technologies, recent applications, and novel developments to this end (note: for earlier, complementary reviews see also the works of Schugerl *et al.* (Schugerl, 2000), Ramaswamy *et al.* (Ramaswamy, Huang, & Ramarao, 2013), and Ezeji *et al.* (Ezeji, Qureshi, & Blaschek, 2007)). In each case, as appropriate, specific emphasis is also given to relevant design considerations. Meanwhile, in light of known challenges related to the development of continuous n-butanol fermentations (Antoni, Zverlov, & Schwarz, 2007), of particular interest will be to highlight studies which, as a result of this approach, have led to the successful development of semi-continuous bioprocesses with further enhanced n-butanol production metrics (e.g., titer, yield, and/or rate of productivity). While it is of

course appreciated that n-butanol is synthesized alongside both acetone and ethanol (minor yet important co-products) to maintain tractability and focus, descriptions and discussions provided here will be confined to the production of n-butanol and, in some cases, total solvents. As perhaps the most promising strategies, specific focus will be given to processes employing solvent extraction, perstraction, adsorption, gas stripping, vacuum stripping and pervaporation. To facilitate the discussion, the structure of this review has been organized on the basis of the different separation media and equilibrium driving forces used to affect n-butanol separation in each case, namely solvent-based, adsorbent-based, and vapor-based processes. As a point of reference, the major advantages and disadvantages of the various technology options to be discussed are compared in Table 1.

Table 1.1.

Summarizing The Major Advantages and Disadvantages of The Different Separation Technologies Discussed in This Review.

Approach	Configuration	Advantages	Disadvantages
solvent-based	Direct addition	Easily implemented, maximal phase contact	High material costs, limited phase recovery, solvent toxicity, energy input required for phase dispersion
	External extractor	Improved control over separation conditions, increased modularity	Increased capital and energy costs, high material costs, limited phase recovery, solvent toxicity
	Perstraction	Reduced solvent toxicity, greater solvent options (cheaper and/or more effective), improved phase recovery	Solvent diffusion into media, mass transfer restriction (additional diffusion resistance, reduced surface area)
adsorbent-based	Direct addition	Easily implemented, maximal phase contact, high biocompatibility, low energy requirements	High material costs, high adsorbent load required, difficult phase recovery

	Packed bed	Modular design (amenable to retrofit applications), efficient separation conditions, high biocompatibility, low energy requirements	High operating pressure, pre-filtration required for cell removal
	Expanded bed	Modular design (amenable to retrofit applications), low operating pressure, no pre-filtration required, high biocompatibility, low energy requirements	Flow rate restrictions, larger column dimensions required
vapor-based	Gas stripping	Easily implemented amenable to retrofit applications), maximal biocompatibility, low capital and operating costs (no special equipment and few moving parts)	Significant co-removal of water, poor separation factor, must generate anaerobic carrier gas
	Vacuum stripping	Easily implemented amenable to retrofit applications), maximal biocompatibility	Significant co-removal of water, poor separation factor, increased capital and utility costs
	Pervaporation	Modular design (amenable to retrofit applications), increased separation factor, high biocompatibility, low energy requirements	Membrane fouling results in performance loss, higher capital cost

1.3.0 LLE Separation Technologies

Among the earliest integrated bioprocesses developed for *in situ* n-butanol recovery are those that exploit solubility differences to extract n-butanol from its aqueous environment and concentrate it within an immiscible solvent phase (Malinowski, 2001). Accordingly, such processes must be coupled with a second, downstream separation process (typically distillation) to ultimately recover and purify n-butanol, regenerating the solvent in the process (Kamiński, Górak, & Kubiczek, 2014). As a relatively mature technology, several useful algorithms have been developed to aid in designing LLE-based processes (Malinowski, 2001). A key design variable is the solvent partitioning coefficient (*K*), defined as:

$$K = \frac{C_S}{C_A} \tag{1.1}$$

Where C_S and C_A are the equilibrated n-butanol concentrations in the solvent and aqueous phases, respectively. In general, large *K*-values are desired to minimize material requirements, with several prior screening (Barton & Daugulis, 1992; Gonzalez-Penas, Lu-Chau, Moreira, & Lema, 2014) and modeling (Cheng & Wang, 2010; Kollerup & Daugulis, 1985; Y. P. Wang & Achenie, 2002) studies having identified effective solvent candidates for n-butanol extraction. For example, a classic screening study by Barton and Daugulis found that, among 63 screened solvents, 28 were found to be biocompatible, with 14 of those having $K > 2$ (Barton & Daugulis, 1992). Commonly employed solvents include oleyl alcohol (Bankar, Survase, Singhal, & Granström, 2012; Nasibuddin Qureshi & Maddox, 1995) and *1*-dodecanol (Tanaka et al., 2012), whose *K*-values have been reported as 3.56 and 5.14, respectively.

1.3.1 Direct Solvent Addition

In the simplest configuration, solvents are added directly to the bioreactor (Figure 1.1A). To provide sufficient capacity for n-butanol accumulation, solvent-aqueous phase ratios of around 0.4 and up to 2 (by vol.) have commonly been employed (Ishii, Taya, & Kobayashi, 1985; S. Roffler, Blanch, & Wilke, 1987b). In an early study by Roffler *et al*., for example, following an initial screening, oleyl alcohol was selected for n-butanol extraction from batch cultures, resulting in 25% greater glucose conversion and a 60% increase in volumetric n-butanol productivity (from 0.58 to 0.72 g/L-h) (S. Roffler, Blanch, & Wilke, 1987a). Ishizaki *et al.* later compared the utility of oleyl alcohol against that of methylated crude palm oil ($K = 0.9$) as solvents for n-butanol recovery from batch

cultures of *C. saccharoperbutylacetonicum* N1-4. Even despite its lower *K*-value, net n-butanol and total solvent production in cultures with methylated crude palm oil were found to be increased by 32% (15.9 to 20.9 g/L) and 41% (21.2 to 29.8 g/L), respectively (Ishizaki et al., 1999). A similar result was also obtained by Li *et al.*, who explored the potential of biodiesel (a mixture of oleic, palmitic, stearic, linoleic, linolenic, arachidic and myristic methyl esters) as the solvent phase (Q. Li et al., 2010).

Meanwhile, building upon the successful performance of oleyl alcohol in batch cultures, Roffler *et al.* later explored its effect on n-butanol production under fed-batch conditions. Further improvements in volumetric n-butanol productivity were demonstrated, in this case reaching up to 1.5 g/L-h (a 208% increase), due largely to the afforded ability to convert twice as much glucose substrate (S. Roffler et al., 1987b). Fed-batch operation was also explored by Baron and Daugulis, in this case, however, using poly(propylene glycol) 1200 as the solvent phase. Adding a concentrated glucose solution to the culture at an average frequency of every 13.5 h, it was demonstrated that the duration of solvent production phase could be increased from 70 to 202 h, during which time net glucose consumption and total solvent production both increased by ~360% (53.8 to 194.7 g/L and 15.9 to 58.6 g/L, respectively).

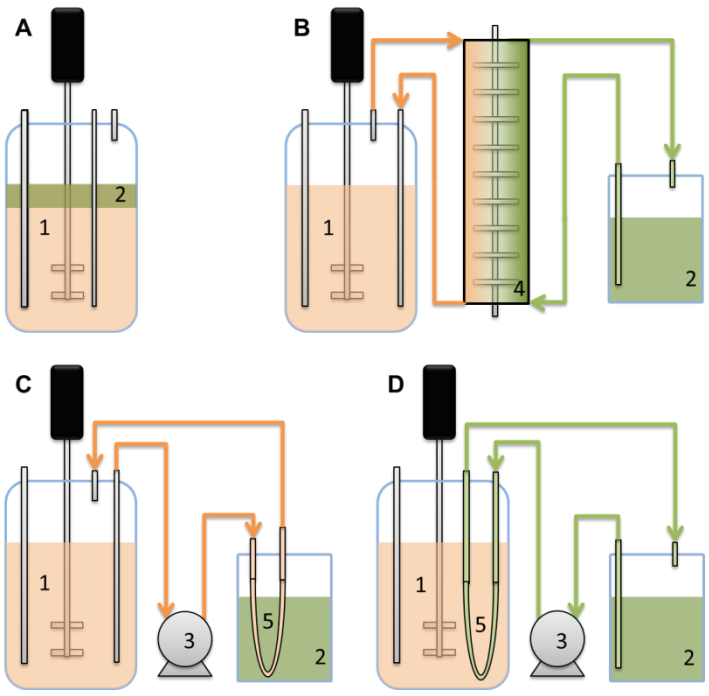

Figure 1.1. A Comparison of Different Solvent-Based Design Configurations Used For In Situ n-Butanol Recovery including: A) direct solvent addition, B) use of an external extraction unit, C) perstraction with culture circulation, and D) perstraction with solvent circulation. Legend: 1. bioreactor, 2. solvent, 3. pump, 4. extraction unit (reciprocating column shown), 5. tubular membrane.

1.3.2 Re-circulation Through an External Solvent Extractor

Despite its straightforward implementation (i.e., requiring no additional equipment), direct solv5ent addition presents several practical challenges, particularly with respect to process scale-up. Achieving rapid mass transfer, for instance, requires large interfacial areas and thus high energy inputs for agitating the biphasic mixture (S. R. Roffler, Blanch, & Wilke, 1988). Alternatively, improved separation conditions, as well as enhanced n-butanol production, have been realized with designs that integrate an external solvent extractor. In this case, the cell containing media is continuously re-circulated between the bioreactor and external extractor. Roffler *et al.*, for example, also

developed a looping process for n-butanol recovery in an external solvent extractor by employing a Karr reciprocating plate extraction column (Figure 1.1B) containing oleyl alcohol (S. R. Roffler et al., 1988). Although the per pass extraction efficiency of n-butanol in the column was low (only 15-40%), continuous re-circulation of the culture through the column maintained aqueous n-butanol concentrations below 8 g/L throughout 55 h of fed-batch fermentation. In that time, a total of 214 g/L glucose was consumed with 40 g/L n-butanol produced (67 g/L total solvents) at an overall productivity of 1.0 g/L-h – a 70% increase over traditional batch cultures.

1.3.3 Membrane-Assisted Extractive Fermentation (Perstraction)

In addition to the risk of productivity losses due to solvent-induced toxicity (Cascon et al., 2011), solvent entrainment due to mutual solubility and stable emulsion formation commonly leads to costly material losses (Cascon et al., 2011; Vane, 2008b). These shortcomings have been addressed through the development of membrane perstraction, wherein an n-butanol-permeable membrane barrier is additionally incorporated to provide physical separation between the culture and solvent phases (Groot et al., 1990; Y. J. Jeon & Lee, 1987; Vane, 2008b). Moreover, by shielding cells from the solvent, better performing and/or cheaper solvents can be employed, independent of their potential biocompatibility. In contrast to direct addition, this approach further promotes facile solvent recovery and replacement with minimal disruption of the culture. However, as the membrane introduces an additional mass transfer resistance, potentially slowing rates of n-butanol uptake, the selection of effective membrane materials and dimensions (e.g., thickness, area) are important design considerations. In most case, membranes composed of polydimethylsiloxane (PDMS; i.e.,

silicone) have performed well in perstraction designs due to their high n-butanol diffusivity. Tanaka *et al.*, meanwhile, also demonstrated enhanced n-butanol production metrics in a perstraction design using a polytetrafluoroethylene (PTFE) membrane (Tanaka et al., 2012).

In general, membrane perstraction can be performed according to one of two prototypical configurations, differing with respect to the circulated phase: culture vs. solvent (Figures 1.1C and 1.1D, respectively). An early study by Groot *et al.* provided a comparison of both designs, using ethylene glycol or isopropyl myristate as solvents in an external reservoir (Groot et al., 1990). In the case of solvent circulation (Figure 1.1D), however, it was found that the high solvent permeability through the silicone tubing membrane lead to its significant accumulation in the fermentation broth. Reaching levels of up to 80 g/L in the case of ethylene glycol, this represents not only a significant material loss, but also a point of concern should more toxic solvents instead be employed. In this case, this limitation was addressed by modifying the process to instead circulate the culture through the external solvent reservoir (Figure 1.1C). As a result, n-butanol accumulation in the isopropyl myristate phase was found to top 20 g/L after 160 h of operation, with a total of 100 g/L glucose consumed in the process.

Incorporating the lessons learned from Groot *et al.*, subsequent studies have predominantly been directed towards the development of perstraction processes employing culture circulation. Also using silicone tubing as a membrane and oleyl alcohol as solvent, a perstraction process was developed by Qureshi *et al.* wherein the entire contents of the bioreactor were circulated through the extractor an average of every

~3.3 min (N. Qureshi & Maddox, 2005). Meanwhile, to maintain a high extraction driving force, solvent removal and replacement (i.e., with fresh solvent) was performed whenever the extracted n-butanol concentration exceeded 6.65 g/L. By producing and removing n-butanol from the bioreactor in this semi-continuous manner, the n-butanol content in the bioreactor was maintained below 3 g/L for the duration of the 391 h fermentation, during which time total solvent production reached 136.58 g, including 66.4 g n-butanol. Jeon *et al.* demonstrated similarly impressive results under fed-batch conditions using oleyl alcohol and a membrane composed of silicone tubing (Y. J. Jeon & Lee, 1987). In this case, a total of 147.7 g/L n-butanol was produced from 601 g/L glucose over course of 209 h of continuous operation (Y. J. Jeon & Lee, 1987).

1.4.0 SLE Separation Technologies

As an alternative to the use of solvents, increasing focus continues to be directed towards the development of novel process configurations and materials for *in situ* n-butanol recovery via adsorption (Ezeji, Qureshi, & Blaschek, 2004b; Garcia et al., 2011; M. Kumar & Gayen, 2011; Oudshoorn, van der Wielen, & Straathof, 2009b). Adsorbents are generally more biocompatible than solvents (promoting maximal biocatalyst activity), as well as fully immiscible and unsusceptible to emulsification – features that facilitate their separation from cultures and improve prospects for repeated regeneration and reuse (Rehmann, Sun, & Daugulis, 2007). As with solvents, additional downstream processing is required to ultimately recover the adsorbed n-butanol product, as has been achieved by thermal treatment (Eom et al., 2013), steam stripping (N. Qureshi, Hughes, Maddox, & Cotta, 2005a), gas stripping (Nongonierma et al., 2006), vacuum application (Wiehn et

al., 2014), or solvent elution (Eom et al., 2013). Combined thermal treatment (heating to 100^{o}C) and vacuum application, for example, proved an effective strategy for recovering up to 85% of adsorbed n-butanol from Dowex® Optipore L-493, a polymer resin adsorbent, as a condensable vapor (D. R. Nielsen & Prather, 2009). Through the same process, the adsorbent was also thereby regenerated for reuse without loss of separation performance. Several prior studies have demonstrated that successive reapplication of regenerated adsorbents is possible with little to no loss in separation performance (Groot & Luyben, 1986a; L. Nielsen, Larsson, Holst, & Mattiasson, 1988). Adsorption-based processes have been suggested to be among the most energy efficient for n-butanol recovery, with estimates of at least a 10% decrease in required energy relative to other approaches (specifically, conventional distillation, extraction/perstraction, gas stripping, pervaporation) (Oudshoorn et al., 2009b; N. Qureshi, Hughes, et al., 2005a).

Typically selected via *ad hoc* materials screening, numerous classes and types of adsorbents have been characterized and employed for n-butanol separations (Vane, 2008b), in forms ranging from powders to pellets (N. Abdehagh, Tezel, & Thibault, 2013). Particularly promising n-butanol adsorbents include silicalite and other inorganic zeolites (Adnadevic et al., 2008; Hashi, Tezel, & Thibault, 2010; Maddox, 1982; Milestone & Bibby, 1981; Oudshoorn, van der Wielen, & Straathof, 2009a; Saravanan, Waijers, Ziari, & Noordermeer, 2010), activated (Groot & Luyben, 1986a; Hashi et al., 2010; Silvestre-Albero, Silvestre-Albero, Sepulveda-Escribano, & Rodriguez-Reinoso, 2009) and mesoporous (T. J. Levario et al., 2012) carbons, as well as polymer resins (Groot & Luyben, 1986a; D. R. Nielsen & Prather, 2009; D. R. Nielsen, Prather, & Amarasiriwardena, 2010; L. Nielsen et al., 1988). Key attributes of an effective adsorbent

include a high capacity and affinity for n-butanol, along with biocompatibility, as well as chemical, thermal and mechanical robustness. Adsorption capacity and affinity are determined via the equilibrium isotherm, typically represented by either the Langmuir or Freundlich isotherm models (given by Equations 1.2 and 1.3, respectively).

$$q = \frac{q_{max} k_l C_A}{1 + k_l C_A} \tag{1.2}$$

$$q = k_f {C_A}^{1/n} \tag{1.3}$$

Where q is equilibrium capacity, q_{max} is maximum equilibrium capacity, k_l and k_f are Langmuir and Freundlich constants, respectively, n is the Freundlich exponent, and C_A is defined as above. In most cases, adsorbent behavior has been characterized using model solutions (e.g., n-butanol in water). It should be noted, however, that adsorption capacity is often decreased in fermentation broths as a result of competitive inhibition by other adsorbed species (e.g.,, broth components or co-products), with n-butanol capacity reductions of up to 29% having been reported (N. Abdehagh et al., 2013). Meanwhile, whereas whole cell biofouling of the adsorbent surface is a common concern in such applications, several recent studies have found such occurrences to be minimal with little to no impact on either separation performance or n-butanol production (Groot & Luyben, 1986a; Wiehn et al., 2014).

The separation performance of several previously investigated n-butanol adsorbents is compared in Figure 1.2. As a result of van der Waals interactions (Carey & Sundberg, 2000; N. Qureshi, Hughes, et al., 2005a; Regdon, Dekany, & Lagaly, 1998), adsorbents with hydrophobic surface chemistries display some of the highest capacities

and affinities (Hashi et al., 2010; D. R. Nielsen & Prather, 2009; D. R. Nielsen et al., 2010; Oudshoorn et al., 2009a; Saravanan et al., 2010). Effective polymer adsorbents are those that include more hydrophobic monomer substituents (e.g., long n-alkyl acrylates and aromatic groups (M. H. Zhou & Cho, 2003)), whereas zeolite hydrophobicity has been improved by increasing the Si/Al ratio (N. Abdehagh et al., 2013; Saravanan et al., 2010). Separation performance is also strongly influenced by adsorbent structure; high specific surface areas offer more adsorption sites and thus high adsorption capacity (Hartmann et al., 2005; D. R. Nielsen & Prather, 2009; D. R. Nielsen et al., 2010; Nunes, Pires, Carvalho, Calhorda, & Ferreira, 2008; Oudshoorn et al., 2009a) while regular and interconnected pores facilitate intraparticle transport to promote enhanced uptake rates (T. J. Levario et al., 2012; Xiaoqing Lin et al., 2012).

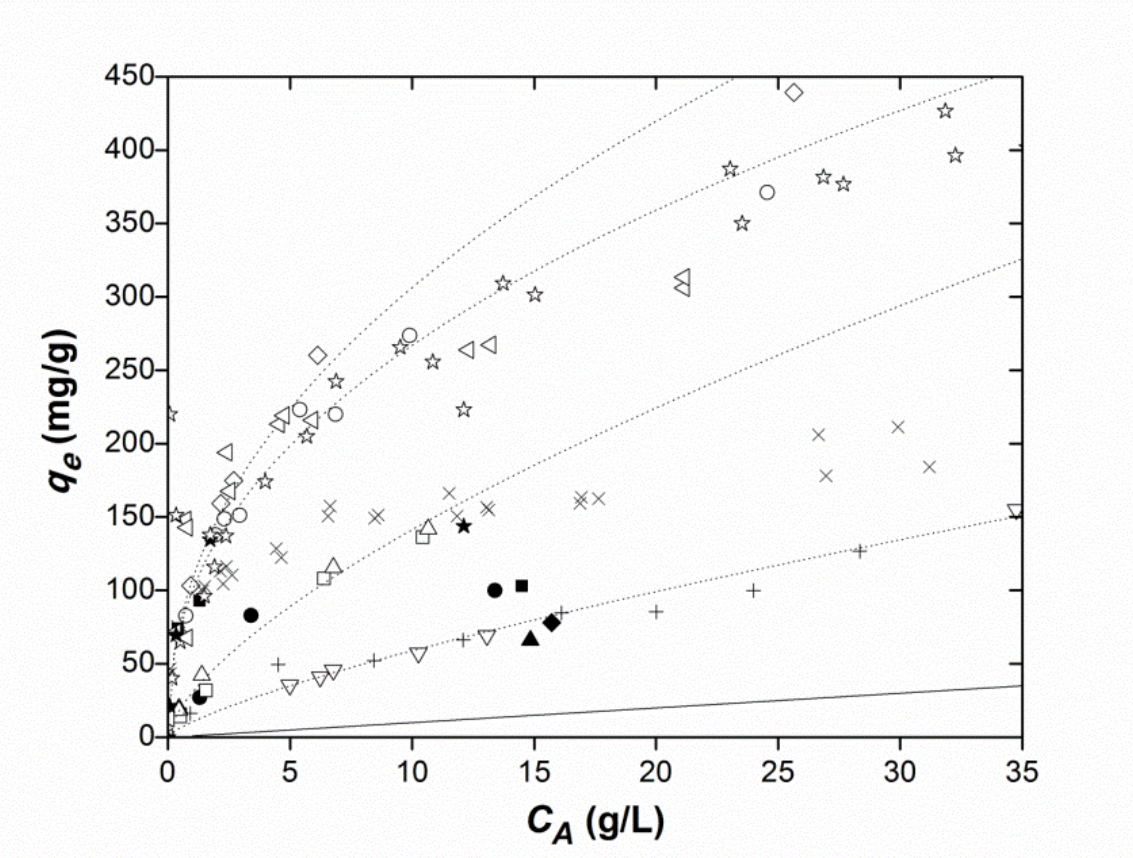

Figure 1.2. Comparing Equilibrium Isotherms For Various n-Butanol Adsorbents. Polymer resins: Dowex® Optipore L-493 (open diamonds), Dowex® Optipore SD-2 (open circles), Diaion HP-20 (open upright triangles), poly(4-ethylstyrene-*co*-divinylbenzene) (open squares), Dowex® M43 (open inverted triangles), all Nielsen and Prather (2009); Amberlite XAD-4 (solid circles), (Groot & Luyben, 1986a; L. Nielsen et al., 1988); Amberlite XAD-16 (solid squares), Ennis et al. (1987); Amberlite XAD-8 (solid upright triangles), (Groot & Luyben, 1986a); Amberlite XAD-2 (solid diamonds), (Groot & Luyben, 1986a); Silica aerogels: TLD302-330 ('+'), Wiehn *et al.* (2013); Zeolites: silicalite-1 (solid squares), Milestone and Bibby (1981); Activated carbon: AC F-400 (open left triangles), AC F-600 (solid stars), both Abdehagh *et al.* (2013). Mesoporous carbon: FDU-16-800 ('X'), CS-81-800 (open stars), both Levario *et al.* (2012). Trend lines, shown for reference and indicated by dotted lines, represent the best fit Freundlich isotherm models for each of (in decreasing order): Dowex® Optipore L-493, Dowex® Optipore SD-2, Diaion HP-20, Dowex® M43, and Amberlite IRA-900. Solid line indicates y = x.

1.4.1 Direct Adsorbent Addition

As with solvents, the simplest adsorbent-based designs also involve their direct addition to cultures (Figure 1.3A). An early study by Yang *et al.* explored the use of a poly(vinyl pyridine) ion exchange resin (Reillex 425) to adsorb n-butanol in batch cultures, demonstrating a 56% increase in glucose consumption and 54% increase in total solvent production (reaching up to 29.8 g/L). Volumetric productivity was also improved to 0.92 g/L-h, a 130% increase over conventional batch culture. However, the low specific surface area of the selected adsorbent (only ~90 m^2/g) resulted in only a modest n-butanol loading capacity (~52 mg/g), thus necessitating the use of a high adsorbent phase ratio (300 g-adsorbent/L-culture) to achieve the requisite total level of product removal. While adsorbent phase ratios of 50 to 400 g/L are common in such designs (L. Nielsen et al., 1988; N. Qureshi, Hughes, et al., 2005a), this design parameter should be minimized to reduce material costs. Moreover, owing to their low specificity (which can deplete the media of essential nutrients), excessive adsorbent addition has in some cases also led to reduced growth and productivity (D. R. Nielsen & Prather, 2009; L. Nielsen et al., 1988). A lower adsorbent phase ratios is possible when using a higher capacity adsorbent. As seen in Figure 1.2, among the top performing adsorbents identified to date are those notably capable of adsorbing n-butanol at up to ~300 mg/g (i.e., ~30% of their dry weight) by the time the aqueous toxicity threshold is reached (i.e., 13 g/L). This includes, for example, both Dowex® Optipore L-493 and SD-2 (macroporous, poly(styrene-*co*-DVB)-derived resins with specific surface areas of 1100 and 800 m^2/g, respectively) (D. R. Nielsen & Prather, 2009). Based on their high adsorption affinities and capacities, said resins were identified as the most promising n-butanol adsorbents amongst a pool of 17 candidates with different polymer chemistries and functionalities.

Ultimately, the in a batch culture containing just 50 g/L Dowex® Optipore SD-2, net n-butanol production reached 22.2 g/L, nearly doubling the titers achieved in conventional batch culture (D. R. Nielsen & Prather, 2009).

1.4.2 Fixed Bed Adsorption

In contrast to their direct addition, adsorbents may also be housed in external adsorption beds through which the culture broth is the re-circulated (continuously or intermittently; Figure 1.3B). With increased accessibility external to the fermenter, adsorbent removal and replacement is facilitated with reduced risk for compromising the integrity of the culture. Early adoptions of this approach focused on the application of adsorbents in fixed beds (i.e., packed columns); an approach that affords efficient n-butanol recovery. Abdehagh *et al.*, for example, showed that packed column containing activated carbon F-400 could be used to recover up to 80% of n-butanol from a model ABE mixture (Niloofar Abdehagh et al., 2015). The approach has also been integrated with cultures. For example, using a poly(vinyl pyridine) resin (Reillex 425) as the adsorbent, Yang and Tsao developed a fixed bed process to enhance n-butanol production by *C. acetobutylicum* (X. Yang & Tsao, 1995). The contents of the 0.7 L bioreactor were continuously circulated through a 0.3 L cylindrical column packed with 423 g resin. However, due to the presence of the cells (which can become entrained in and block flow through the bed), the process further incorporated microfiltration to remove and recycle cells prior to entering the adsorbent bed (Pierce et al., 1999). Operating in a fed-batch manner for ~240 h, n-butanol and total solvent production reached 38.7 and 47.2 g/L, with total solvent productivity reaching 1.69 g/L-h. Increased modularity also enables facile integration of adsorbent beds with different bioreactor configurations, including

those poorly compatible with direct adsorbent addition (e.g., non-planktonic cultures). For example, Liu *et al.* recently coupled a fixed bed adsorption column containing macroporous KA-I resin with a *C. acetobutylicum* biofilm reactor (D. Liu et al., 2014). With the culture immobilized, upstream microfiltration was no longer required. Through repeated batch culture, n-butanol production ultimately reached 92.6 g/L at a productivity of 1.51 g/L-h, representing 4- and 3-fold improvements over traditional batch fermentation using planktonic culture, respectively.

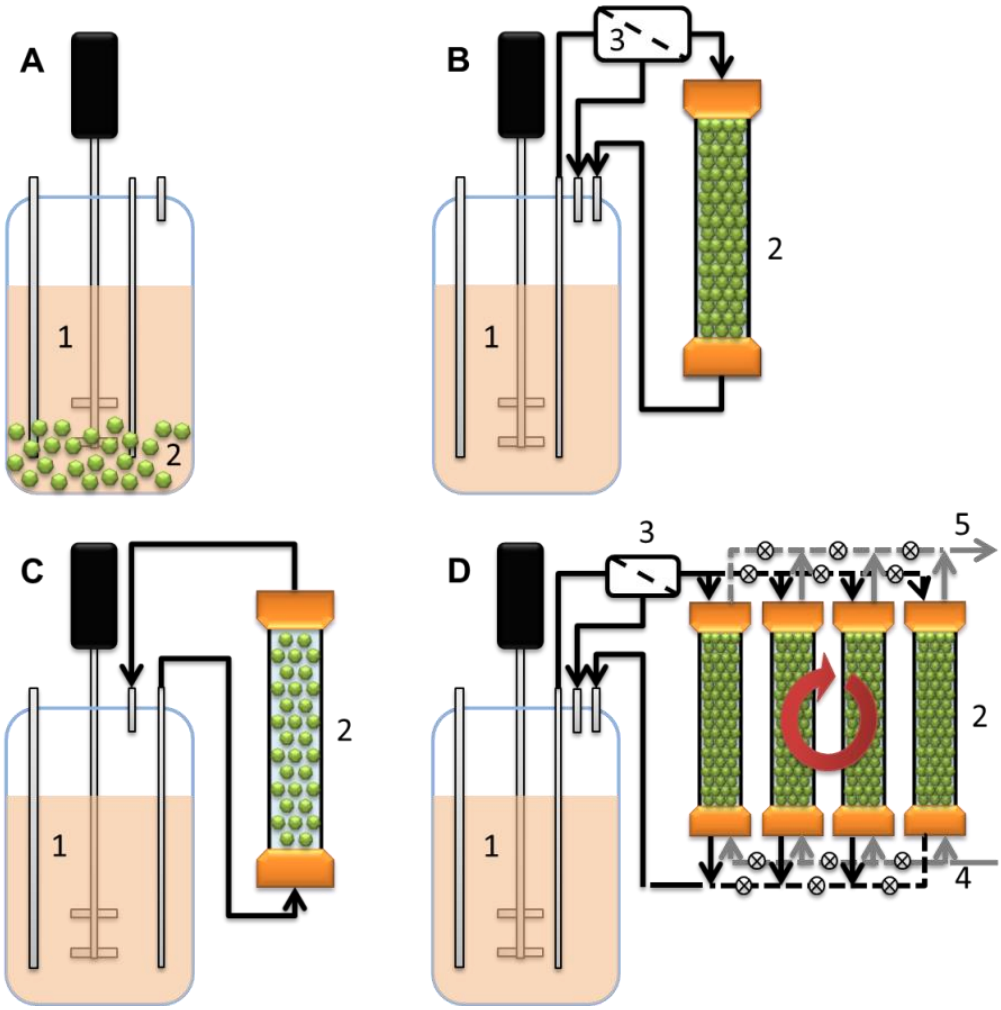

Figure 1.3. A Comparison of Different Adsorbent-Based Design Configurations Used For In Situ n-Butanol Recovery, including: A) Direct adsorbent addition, B) packed bed adsorption,

C) expanded bed adsorption, and D) simulated moving bed operation. Legend: 1. bioreactor, 2. adsorbent, 3. microfiltration unit, 4. regeneration media, 5. n-butanol-rich recovery stream.

1.4.3 Expanded Bed Adsorption

In contrast to fixed bed operation, alternative operation of the adsorption column in an expanded bed mode provides sufficient void space between adsorbent particles to accommodate direct cell passage (Figure 1.3C). Fluidization is achieved in this case by circulating the culture through the bed in an up-flow manner; however, it should be noted that maintaining a stable bed and avoiding inversion imposes restrictions on the circulation rate of the media through the adsorption column. While this approach eliminates the requirement for upstream microfiltration, reduced separation efficiency is experienced relative to packed bed operation (Menkhaus & Glatz, 2005). Initially developed and applied to improve the fermentative production of both succinic (J. Li et al., 2011) and propionic acid (P. Wang, Wang, Liu, Shi, & Su, 2012) (using ion exchange resins as adsorbents in both cases), the authors recently applied expanded bed adsorption to improve n-butanol production by *C. acetobutylicum* ATCC 824 (Wiehn et al., 2014). In this case, the expanded bed consisted of 0.17 L glass column containing 75 g of Dowex® Optipore L-493 (thereby leaving ~55% of the column volume unoccupied to accommodate for bed expansion). The contents of the 1 L culture were continuously re-circulated between the bioreactor and adsorption bed at a rate of about 100 mL/min, expanding the bed height by ~50%. Fed-batch operation with this design ultimately enabled volumetric n-butanol and total solvents production to be increased to 27.1 and 40.7 g/L, respectively, each ~2.2-fold improvements over batch culture (Wiehn et al., 2014). The modular nature of the adsorbent bed design was further exploited in said

study during the regeneration cycle, wherein direct vacuum application to the liquid-drained column (i.e., without adsorbent transfer) was used to recover 81% of the produced n-butanol (Wiehn et al., 2014). By facilitating the cycle of adsorbent recovery, regeneration, and reuse, such increasingly modular designs will remain crucial to the continued optimization of semi-continuous n-butanol production. Meanwhile, through further process evolution, continuous n-butanol production will also likely be realized through the future incorporation of simulated moving bed (SMB) operation (Figure 1.3D) (Imamoglu, 2002). A staple of the modern biopharmaceutical industry, to facilitate the continuous production and recovery of proteins, SMB is an unexplored yet particularly promising technology for enhancing n-butanol production.

1.5.0 VLE Separation Technologies

Solvent- and adsorbent-based processes expose cultures to foreign chemicals/materials, a practice that, in spite of careful material selection, presents increased risk of phase induced toxicity while also introducing opportunities for biofouling. Vapor-based processes circumvent these challenges by exploiting relative volatility for *in situ* n-butanol removal by vaporization, with condensation subsequently used to trap the evolved vapors. Operating under dilute conditions, Henry's Law describes n-butanol's vapor-liquid equilibrium behavior (Equation 1.4), with differences from this equilibrium condition providing the driving force for separation.

$$p = HC_A \tag{1.4}$$

Where p is the partial pressure of n-butanol in the vapor phase, H is the Henry's Law coefficient, and C_A is defined as above. In general, however, vapor-based processes for n-butanol recovery are commonly challenged by its relatively low vapor pressure relative to that of water (e.g., 0.0109 vs. 0.0312 atm at 25^{o}C). In vapor-based processes, the ability of n-butanol to be selectively removed over water is determined by the separation factor:

$$\alpha_{12} = \frac{C_1^v / C_2^v}{C_1^l / C_2^l} \tag{1.5}$$

Where C_1 and C_2 are concentrations of vaporized species (i.e., n-butanol and water, respectively) and superscripts v and l indicate the vapor and liquid phases, respectively.

1.5.1 Gas Stripping

Requiring only a carrier gas to be sparged through the fermentation media (Figure 1.4A); gas stripping is an easily implemented and effective *in situ* recovery technique for n-butanol (Niloofar Abdehagh et al., 2014; Y. Chen et al., 2014; N. Qureshi, Hughes, et al., 2005a). For example, with stripping rates on the order of 4-4.5 g/L-h having been reported (Y. Chen et al., 2014; Chuang Xue et al., 2012) – nearly an order of magnitude greater than typical production rates – aqueous accumulation of n-butanol to inhibitory levels is readily precluded. To maintain anaerobic conditions, however, an inert carrier gas (typically a mixture of H_2 and CO_2) must be utilized (Ezeji, Qureshi, & Blaschek, 2004a, 2013), the generation of which increases capital and operating costs. Pre-humidification of the carrier gas, meanwhile, is also typically performed to reduce culture volume losses (Ezeji et al., 2013).

Using an engineered strain of *C. acetobutylicum* (developed to produce isopropanol in lieu of acetone), Lee *et al.* recently demonstrated the utility of gas stripping for promoting solvent production under fed-batch conditions (J. Lee et al., 2012). With 132.9 g/L glucose consumed in 45 h, 35.6 g/L total solvents were produced, a ~75% increase relative to batch mode operation (J. Lee et al., 2012). In earlier works, Ezeji *et al.* likewise employed continuous gas stripping under fed-batch conditions, in this case to improve the ABE fermentation (Ezeji et al., 2004a). Although productivity was continuously maintained for an initial period of over 201 h, accumulating 152 g/L n-butanol and 233 g/L total solvent from 500 g/L glucose, production was ultimately and unduly halted as a result of gradually declining culture conditions. Though uncharacterized, it was postulated that said limitation perhaps resulted from either the depletion of an essential micronutrient or the accumulation of non-viable cells, acids, and/or other byproducts in the aqueous phase.

As most separation strategies are selective towards only the target product, such productivity-limiting factors are a common challenge faced by *in situ* product recovery designs, particularly in long-term applications (e.g., fed-batch). In many cases, however, this problem has been effectively addressed by performing periodic exchanges of the culture medium, thereby replenishing nutrients while diluting byproducts. In a follow-up study, for example, Ezeji *et al.* successfully demonstrated that by adopting a medium exchange protocol, their semi-continuous gas stripping process could be operated under fed-batch conditions for an uninterrupted period of up to 504 h (Ezeji et al., 2013). Specifically, at an average dilution rate of 0.03 h-1, a portion of the bioreactor contents were continuously exchanged for a glucose-rich feed solution (containing 250-500 g/L

glucose). By this approach, 461 g/L total solvents were produced from 1125 g/L of glucose, representing a 3-fold further improvement relative to their initial gas stripping/fed-batch design and a 25-fold increase over traditional batch culture (Ezeji et al., 2013).

The ease of implementation of gas stripping makes it an amenable approach for integration with a variety of bioreactor configurations. In a recent study by Chen *et al.*, for example, its utility was explored in fed-batch cultures of immobilized *C. acetobutylicum* (Y. Chen et al., 2014). Following 175 h of continuous operation, 290 g/L glucose was consumed resulting in the production of 66 g/L n-butanol and 106 g/L total solvents. The approach is equally effective for use with cultures grown on complex, biomass-derived substrates. Lu *et al.*, for example, demonstrated a 56% improvements in n-butanol production from wood pulping hydrolysate as a result of integrated gas stripping (Congcong Lu, Dong, & Yang, 2013). Xue *et al.*, also studied the use of gas stripping in fed-batch cultures of immobilized *C. acetobutylicum* (Chuang Xue et al., 2012). In this case, however, gas stripping was applied intermittently, and only when aqueous n-butanol concentrations exceeded >8 g/L. This approach not only maximized achievable separation factors, but also reduced energy input and operating costs. Ultimately, 113 g/L n-butanol (nearly a 6-fold increase) along with 172 g/L total solvents were produced from 475 g/L glucose over the course of 326 h of continuous operation. To further enhance their design by reducing energy requirements associated with n-butanol purification, Xue *et al.* later investigated two-stage gas stripping protocol (Chuang Xue et al., 2014; Chuang Xue et al., 2013). While the first stage served to remove n-butanol from the fibrous bed bioreactor, the second served to then recover n-

butanol at further increased purity from the initial condensate. In the final design, n-butanol selectivity of up to 33.2 was achieved, rendering a recovered product phases containing 515.3 g/L n-butanol and 671.1 g/L total solvents (Chuang Xue et al., 2014).

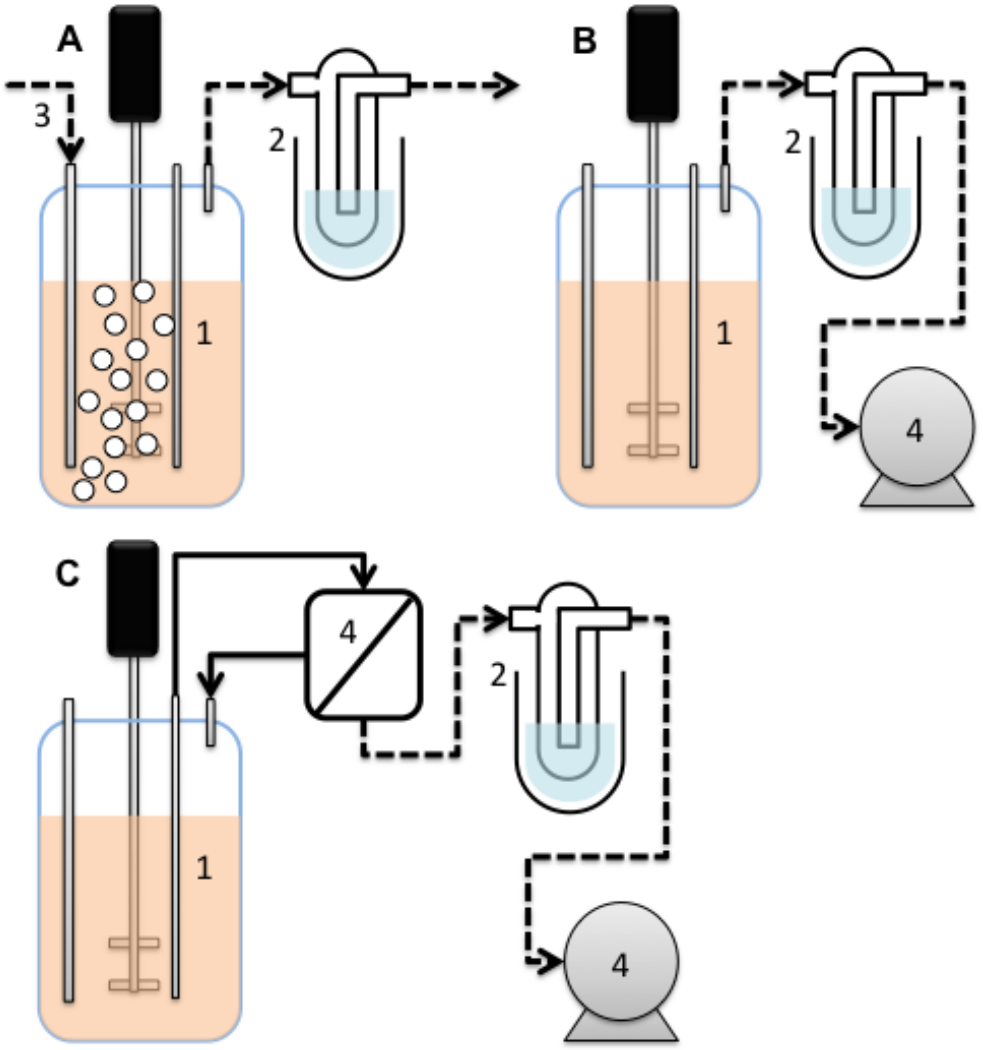

Figure 1.4. A Comparison of Different Vapor-Based Design Configurations Used For In Situ n-Butanol Recovery, including: A) gas stripping, B) vacuum stripping, and C) pervaporation. Legend: 1. bioreactor, 2. vapor condensation trap, 3. sparged carrier gas, 4. vacuum pump.

1.5.2 Vacuum Stripping

In contrast to evolving n-butanol vapors from the culture via its displacement into a sparged gas, vacuum stripping renders a similar outcome by reducing pressure above the bioreactor headspace (Figure 1.4B). As it is not limited by poor gas solubility at physiological temperatures (Y. Chen et al., 2014), vacuum stripping has been reported to support n-butanol removal rates as much as 10-fold faster than by gas stripping (Mariano, Qureshi, Maciel Filho, & Ezeji, 2012). However, whereas a study by Mariano *et al.* showed that vacuum stripping can be used to increase n-butanol and total solvent production by as much as ~31% under batch conditions, to date, vacuum stripping has seen limited application with respect to semi-continuous operation (Mariano et al., 2012).

1.5.3 Pervaporation

Despite their proven ability to enable enhanced n-butanol production, the fundamental weakness of both of gas and vacuum stripping ultimately lies in their lack of selectivity. In vapor-based processes, low separation factors are undesirable as significant co-removal of water vapor results in a hydrous solvent product in need of additional downstream purification (Chuang Xue et al., 2012). In practice, separation factors for n-butanol are inversely proportional to its concentration in the media (Ezeji et al., 2013), with typical values for gas stripping having been reported to range between 4 to 12 (Ezeji et al., 2013) and up to 20 for vacuum stripping (Mariano et al., 2012). One effective approach for improving the separation factor in vapor-based process involves the use of a membrane barrier to reject evolved water vapor. In pervaporation, for example, an n-butanol permselective membrane is contacted directly with the fermentation broth while a sweep gas or vacuum conditions (more common due to improved mass transfer rates (Nasib Qureshi & Blaschek, 1999)) are applied on the permeate side to provide the

separation driving force. Following permeation into the membrane, n-butanol diffuses through it, becoming vaporized as it reaches the permeate side (Figure 1.4C) (Nasib Qureshi & Blaschek, 1999). The overall process requires minimal energy input, prompting the U.S. Department of Energy to label pervaporation is among the most efficient methods recovering bio-alcohols (D.O.E., 1990).

Separation factor and flux are important measures of membrane performance and as such serve as key design parameters for the overall process (Vane, 2008b). Whereas separation factor remains as defined in Equation 1.5, flux, is determined as:

$$J = \frac{m_p}{A_m \Delta t} \tag{1.6}$$

Where m_p is mass of the permeate, A_m is membrane area, and t is time. Higher fluxes support efficient pervaporation designs by minimizing the total membrane surface area necessary to achieve rapid n-butanol recovery. It should be appreciated, however, that, as with most membrane separations, an inverse relationship exists between pervaporation flux and separation factor (N. Qureshi, M. M. Meagher, H. J. Huang, & R. W. Hutkins, 2001a).

Hydrophobic, non-porous polymer membranes have been the most intently studied for n-butanol pervaporation, the most common being those composed of PDMS (Menchavez & Ha, 2013). Although high fluxes have been reported using PDMS membranes (ranging between 10-400 g/m^2-h (Wouter Van Hecke et al., 2012)), achievable separation factors typically remain <20 (Wouter Van Hecke et al., 2012). Both using PDMS disk membranes, for example, Groot *et al.* reported an n-butanol separation

factor of ~11 and an average flux of 10.4 g/m^2-h using a PDMS disk membrane (Groot & Luyben, 1987), while Van Hecke *et al.* reported values of ~14.7 and ~367 g/m^2-h, respectively (Wouter Van Hecke et al., 2012). It has been suggested, however, that to offset the increased capital and operating cost requirements associated with pervaporation and achieve economically viable n-butanol recovery, a minimum separation factor of at least 30 should be achieved (Vane, 2008b). Thus, although it remains a commonly employed material in research studies, commercial prospects of PDMS membranes remain limited (Vane, 2008b). Accordingly, there remains keen interest in the development of novel pervaporation membranes with improved separation performance, including those composed of poly(tetrafluoroethylene) (PTFE), poly(ether-block-amide) (PEBA) (H.-W. Yen, Lin, & Yang, 2012), and other related tuned block copolymers (Niloofar Abdehagh et al., 2014; Ikegami, Negishi, Nakayama, Kobayashi, & Sakaki, 2014; H.-W. Yen, Chen, & Yang, 2012; H.-W. Yen, Lin, et al., 2012). Meanwhile, more recent studies have also explored the potential of various nanoporous inorganic (e.g., zeolites (Wee, Tye, & Bhatia, 2008)) and 'composite' membranes (e.g., PDMS coated silicalite (Ikegami et al., 2014) and PEBA mixed with carbon nanotubes (H.-W. Yen, Chen, et al., 2012)), materials with improved prospects for enhanced and tunable separation performance (J. Li et al., 2014; N. Qureshi et al., 2001a; Wu et al., 2012). Key performance metrics of select polymer, inorganic, and composite membranes are compared in Table 1.2. It should be noted, however, that in addition to differences in polymer chemistry (N. Qureshi et al., 2001a), performance also varies due to membrane thickness (H.-W. Yen, Lin, et al., 2012), feed temperature (H.-W. Yen, Lin, et al., 2012),

level of vacuum (or sweep gas flow rate) (Nasib Qureshi & Blaschek, 1999), and other process/environmental conditions.

A recent study by Yen *et al.* provided a direct comparison of the relative performance of two different polymer membranes, namely PDMS and PEBA, and their resultant impact on n-butanol separation and production (H.-W. Yen, Lin, et al., 2012). PEBA membranes ultimately supported the greatest separation factor and flux in model solutions (17.4 and 9.98 g/m^2-h vs. 14 and 3.91 g/m^2-h, respectively) and, when applied to fed-batch fermentation, enabled n-butanol and total solvent production at up to 16.6 and 27.3 g/L, respectively (from a total of 130 g/L glucose) (H.-W. Yen, Lin, et al., 2012). Further improvements to PEBA membrane performance were made by the same authors in a subsequent study, notably through the incorporation of 5%wt. multi-walled carbon nanotubes (CNT) (H.-W. Yen, Chen, et al., 2012). Using this composite membrane, flux was improved to 16.1 g/m^2-h and the separation factor to 19.4, along with a 20% further increase in volumetric productivity. The efficacy of composite membranes for n-butanol pervaporation was similarly explored by Li *et al.*, in this case using silicalite-1 filled PDMS on a poly(acrylonitrile) support (J. Li et al., 2014). Using model solutions, separation factors of 30-33 were demonstrated, along with fluxes ranging from 40 to 173 g/m^2-h. When applied to fed-batch fermentation, after 288 h of continuous operation a biphasic solution was ultimately recovered in the condensed permeate. Owing to the high separation factor (>30), the n-butanol content in the condensate exceeded its solubility in water, leading an organic-rich phase with 446 g/L n-butanol along with an aqueous phase containing 89.6 g/L n-butanol (J. Li et al., 2014).

Spontaneous phase separation by the condensate is advantageous as it reduces energy requirements associated with further downstream purification.

One challenge commonly faced in pervaporation designs is diminished separation performance due to membrane fouling. Surface fouling can occur in the presence of other medium components, biomolecules, and/or whole cells. For example, using a tubular silicalite-1 membrane coated with silicone rubber, Ikegami *et al.* compared relative n-butanol separation performance between both binary solutions and cell-free fermentation broths (Ikegami et al., 2014). Separation factor averaged 294 and 413 between model solutions and broths, whereas average flux was maintained at 35 and 22.3 g/m^2-h, respectively (Ikegami et al., 2014). Though detrimental to performance, fouling effects can be addressed through additional process improvements. For example, Qureshi *et al.* used ultrafiltration to eliminate potential foulants from the fermentation broth prior to contacting it with a silicalite-PDMS composite membrane (N. Qureshi et al., 2001a). As a result, separation performance was sustained throughout the course of a 36 day fed-batch fermentation, enabling n-butanol separation factor and flux to be maintained at average values of 203 and 89 g/m^2-h, respectively. By this approach, a total of 445 g/L glucose was consumed to yield 105 g/L n-butanol and 155 g/L total solvents (N. Qureshi et al., 2001a).

Table 1.2.

Comparing The n-Butanol Separation Performance of Different Pervaporation Membranes and Under Different Test Conditions. 'Binary' refers to a binary mixture of n-butanol in water; 'ABE' refers to a model solution of acetone, n-butanol, and ethanol in water; 'Broth' refers to a Clostridium sp. fermentation broth, typically cell-free and applied as a downstream separation.

Membrane	Separation factor	Flux (g/m^2-h)	Feed type	Reference
Polymer Membranes				
PDMS tubing	45-64	6.2-14.5	Binary	(Larrayoz & Puigjaner, 1987)
PDMS	15-37	70-1000	Binary	(Nasib Qureshi & Blaschek, 1999)
PTFE	2.7-4.8	35-2100	Binary	(Nasib Qureshi & Blaschek, 1999)
PDMS	14	3.91	Binary	(H.-W. Yen, Lin, et al., 2012)
PEBA	17.4	9.98	Binary	(H.-W. Yen, Lin, et al., 2012)
Polypropylene	6.3	1400-1600	Fermentation broth	(Nasib Qureshi & Blaschek, 1999)
Composite Membranes				
CNT filled PEBA	19.4	16.1	Binary	(H.-W. Yen, Chen, et al., 2012)
CNT filled PDMS	32.9	244.3	Binary	(C. Xue, G. Q. Du, L. J. Chen, J. G. Ren, J. X. Sun, et al., 2014)
5% ZSM-5-PEBA	~21.8-33.3	190-719.3	Binary	(Tan, Wu, & Li, 2013)
Silicalite filled PDMS	30-33	40-173	Binary	(J. Li et al., 2014)
Silicalite filled PDMS	10-180	12.5-240	ABE	(N. Qureshi et al., 2001a)
PDMS-PVDF composite	35.2	769.6	ABE	(C. Xue, Du, Chen, Ren, & Bai, 2014)
PDMS-PVDF composite	14.4–21.2	93.3–108.8	Fermentation broth	(C. Xue, G. Q. Du, L. J. Chen, J. G. Ren, & F. W. Bai, 2014)
Liquid Membranes				
Polymer supported ionic liquid	11	560	Binary	(Heitmann et al., 2012)
Inorganic				

Membranes				
Phenyltrimethyls iloxane (PhTMS)/PDMS Coated Alumina	~10-30	200-900	Binary	(E. J. Jeon, Kim, & Lee, 2012)
Methylated Silica	~0.0001	~10-200	Binary	(Campaniello, Engelen, Haije, Pex, & Vente, 2004)

1.6.0 Conclusion and Biofuels Outlook

By circumventing the toxic effects associated with the in culture accumulation of n-butanol, *in situ* product recovery has emerged as an effective strategy for enhancing its key production metrics. Whereas multiple effective process strategies have been developed for this purpose, it should be appreciated that each approach carries its own unique pros and cons. Future advancements in terms of both materials and process development will ultimately enable *in situ* product recovery to evolve from its current laboratory bound incarnations into a viable strategy for enhancing commercial-scale n-butanol production.

Although *in situ* n-butanol removal has proven to be an effective approach for circumventing toxicity and facilitating semi-continuous fermentation, the field remains ripe for further innovation. Future advancements in the field will be facilitated by the development of novel materials and/or process configurations, the likes of which will continue to address some of the key inherent shortcomings identified here within. With respect to novel separation materials, the objective will be to develop and/or identify those with enhanced separation performance, including in terms selectivity, recovery rate, fouling resistance, and robustness, while also simultaneously reducing material costs and

energy requirements. Such efforts are already underway, and leading to promising new candidates. For example, as a departure from the traditional focus on organic solvents in solvent-based designs, non-ionic and liquid polymer surfactants have recently emerged as effective alternatives (Dhamole, Wang, Liu, Wang, & Feng, 2012). Ionic liquids, meanwhile, offer a wide range of physical and separation properties along with an unprecedented degree of tunability (Cascon et al., 2011; Fadeev & Meagher, 2001). Furthermore, with nearly negligible vapor pressure, volatile losses of these solvents during fermentation are virtually eliminated while also streamlining downstream processing (Kamiński et al., 2014). Tunability is a similarly attractive feature with respect to hybrid or composite membrane materials. Combining the processability of polymer membranes with the selectivity of inorganic membranes, such materials are expected to draw increasing interest for n-butanol pervaporation. Increased development and application of engineered adsorbent materials is likewise expected, in particular with respect to the development of increasingly hydrophobic materials with defined pore structures (e.g., mesoporous carbons).

Meanwhile, the development of increasingly modular process will continue to provide several important benefits, including: *i)* improved control over the separation conditions (maximizing the return on material costs), *ii)* protection of the cells from the separation media (and vice versa), *iii)* ease of semi-continuous operation with minimal process disruption for phase separation/regeneration, and *iv)* improved prospects for process integration, especially in retrofit applications. (e.g., packed or expanded bed adsorption vs. direct addition). This trend can already be seen in the each of solvent-, adsorbent-, and vapor-based processes, and is likewise expected to extend into the future.

1.7.0 Acknowledgments

This work was supported by the National Science Foundation (Award Nos. CBET-1067684 and CBET-1159200). The authors declare no conflicts of interest.

1.8.0 Dissertation Organization

This proposal is organized into four chapters. Chapter 1 details a brief history of the separation of biofuels, namely butanol with its coproducts ethanol and acetone. It is composed of 3 separations categories, namely liquid-liquid, solid-liquid and vapor-liquid equilibrium. In chapter 2, the focus is *in situ* separation of butanol with engineered magnetically responsive mesoporous carbon powders (MMCPs). Butanol causes product toxicity to the producing organisms, necessitating separation. These MMCPS, developed by collaborators at the University of Ackron, were found to perform comparably to commercially used activated carbons while boasting 89% by mass recoverability from aqueous solution via magnetic retrieval. Furthermore, up to 93% by mass of adsorbed butanol was recovered, which is the highest recovery percentage for butanol the authors are aware of. This was also the first such demonstration of a magnetically separable carbon employed for *in situ* capture of butanol and its co-products, as far as the authors are aware. Chapter 3 employs the same MMCPs to recover furfural from simulated lignocellulosic hydrolysates. Furfural causes growth toxicity, preventing bacterial growth, necessitating furfural removal prior to fermentation. Because furfural is a value-added byproduct, its adsorption and desorption characteristics were evaluated with MMCPs. Chapter 3 also describes the development of a magnetic MMCP recovery column which captured up to 91% MMCP mass. An efficient thermal regeneration

protocol was developed for furfural as it was for butanol, recovering up to 57% furfural by mass. The simulated hydrolysate was successfully pretreated by MMCPs and fermented to ethanol by *E. coli* LY180 up to 62.8 g/L after pretreatment. Control fermentation reached titers as high as 64.2 g/L ethanol, which may be the highest ethanol titer achieved by *E. coli*. Chapter 4 applies the adsorption process design principles from the other chapters for phenol recovery. Phenol is another important renewably producible bioproduct which has not been produced at more than ~33% of the toxicity limit by engineered strains. It was speculated that phenol caused feedback inhibition, limiting its production. To investigate this, adsorbents were applied as an intracellular diagnostic tool by reducing the aqueous concentration of phenol and thereby reduce feedback inhibition. The adsorption of phenol onto Dowex Optipore L-493 was found to be more efficient for phenol adsorption than MMCPs. The adsorption and desorption were characterized for phenol as for butanol and furfural. Phenol desorption by solvent recovery was found more efficient than thermal regeneration. This method confirmed feedback inhibition was not the cause of limited phenol titer. The 5^{th} chapter summarizes the findings of the 4 preceding chapters and details the experimental plans for continuance of the work presented here. Specifically, this chapter details the importance of the findings of this work with regards to adsorption performance, especially for desorption. It also includes the recommendations for improving the MMCP design for improved functionality.

CHAPTER 2

2.0 HIGH EFFICIENCY AND FACILE BUTANOL RECOVERY WITH MAGNETICALLY RESPONSIVE MESOPOROUS CARBON ADSORBENTS

Abstract

The in-situ recovery of n-butanol from conventional batch fermentation is an effective strategy to overcome cytotoxic titer limitations. Here, we demonstrate efficient butanol recovery using magnetically responsive micro/mesoporous carbon adsorbents. While large surface areas (>1400 m2/g) promote adsorption, inclusion of magnetic Ni nanoparticles enables direct and facile magnetic retrieval of spent adsorbents, bypassing the need for column configurations (e.g., packed or expanded bed). Butanol loading capacities of a family of mesoporous powders (4-10 wt% Ni content) are not significantly impacted by Ni content, performing comparably to commercial resins and activated carbons (e.g., up to 0.26 g/g at 12.5 g/L equilibrated butanol). Magnetic recovery of the mesoporous powder is dependent on the Ni content, with up to 89 wt% recovery achieved in 6 min with 10 wt% Ni. Desorption studies using retrieved adsorbents demonstrated an average of 93% recovery of the total adsorbed butanol. Biocompatibility studies using an Escherichia coli model showed no discernable toxicity, even at high Ni content and levels of adsorbent addition. Kinetic studies indicate that neither the effective adsorption or desorption rates should constitute a bottleneck with respect to the future development of a semi-continuous butanol fermentation process using these novel, magnetically responsive adsorbents.

This work was published as:

Staggs, K., Qiang, Z., Madathil, K., Gregson,C., Xia, Y., Vogt, B., & Nielsen, D.R. High Efficiency and Facile Butanol Recovery with Magnetically Responsive Micro/Mesoporous Carbon Adsorbents. ACS Sustainable Chem. Eng., 5(1), 885–894, (2017)

2.1.0 Background and Motivation

Biofuels produced via the microbial conversion of biomass feedstocks represent a promising, sustainable solution for the escalating global demand for liquid transportation fuels.(Connor & Liao, 2009; Keasling & Chou, 2008; Y. N. Zheng et al., 2009) As a potential drop-in replacement for conventional gasoline, n-butanol (butanol) is one of the most promising second-generation biofuel candidates.(Berezina et al., 2012; Dafoe & Daugulis, 2014; Garcia et al., 2011; Tashiro et al., 2013) However, butanol toxicity, remains an inherent challenge that limits its microbial production at economically viable rates.(Bowles & Ellefson, 1985; Ingram, 1990; Jones & Woods, 1986a) Moreover, due to its low toxicity threshold (typically just 12-13 g/L), downstream recovery of butanol from dilute fermentation broths (as conventionally accomplished via two-stage distillation(Luyben, 2008)) is low-efficiency and energy-intensive.(Pfromm, Amanor-Boadu, Nelson, Vadlani, & Madl, 2010) In order to address these challenges, integrated bioprocesses employing *in situ* butanol recovery have emerged as a promising alternative for enhancing volumetric productivity while also facilitating economical downstream product recovery.(Schugerl, 2000; W. Van Hecke et al., 2014; Chuang Xue et al., 2014; S. T. Yang & Lu, 2013) Numerous different separation media and process configurations have been demonstrated for *in situ* butanol recovery to date, including liquid-liquid extraction (*via* direct solvent addition(Ishizaki et al., 1999; Q. Li et al., 2010; S. Roffler et al., 1987a) and perstraction(Groot et al., 1990; Y. J. Jeon & Lee, 1987; Oudshoorn et al., 2009a, 2009b; Vane, 2008b)), vapor-liquid extraction (*via* gas stripping (Y. Chen et al., 2014; Ezeji et al., 2004a; N. Qureshi & Blaschek, 2001; Chuang Xue et al., 2012) and pervaporation(Ezeji et al., 2013; Groot & Luyben, 1987; S. Y. Li, Srivastava, & Parnas,

2011; Mariano et al., 2012; N. Qureshi, M. M. Meagher, J. Huang, & R. W. Hutkins, 2001b)), and solid-liquid extraction or adsorption.(Niloofar Abdehagh et al., 2015; N. Abdehagh et al., 2013; Faisal, Zhou, Hedlund, & Grahn, 2016; Groot & Luyben, 1986a; T. J. Levario, M. Dai, W. Yuan, B. D. Vogt, & D. R. Nielsen, 2012a; Xiaoqing Lin et al., 2013; Xiaoqing Lin et al., 2015; D. Liu et al., 2014; Maddox, 1982; D. R. Nielsen & Prather, 2009; Oudshoorn et al., 2009a; N. Qureshi, Hughes, et al., 2005a; Wiehn et al., 2014; X. Yang & Tsao, 1995) Among these, adsorption is often considered among the lowest cost and least energy intensive method for *in situ* butanol recovery.(Faisal et al., 2016; Oudshoorn et al., 2009b; N. Qureshi, Hughes, et al., 2005a)

A wide range of adsorbent materials have been investigated for *in situ* butanol recovery, including silicalites (Milestone & Bibby, 1981; N. Qureshi, Hughes, et al., 2005a), zeolites (Oudshoorn et al., 2009b; Oudshoorn, van der Wielen, & Straathof, 2012), aerogels (Wiehn et al., 2013), activated carbons (Eom et al., 2015; Groot & Luyben, 1986b), mesoporous carbons (Thomas J. Levario et al., 2012a) and various polymer resins.(X. Lin et al., 2012; L. Nielsen et al., 1988; X. P. Yang, Tsai, & Tsao, 1994) Typically, adsorptive butanol recovery uses either *a)* circulation of the fermentation broth through an external column containing the adsorbent and operated in either packed or expanded bed mode (N. Abdehagh et al., 2013; Eom et al., 2015; Wiehn et al., 2014), or *b)* direct addition of the adsorbent to the fermentation broth within the bioreactor.(Groot & Luyben, 1986b; D. R. Nielsen & Prather, 2009; L. Nielsen et al., 1988) Packed bed adsorption is appealing because it typically offers higher separation efficiency (Menkhaus & Glatz, 2005), however, said approach requires that an additional upstream filtration step be performed to remove cells in order to avoid column plugging.

Expanded bed adsorption does not require such pre-filtration (due to increased bed void volumes) but suffers from slightly reduced separation efficiency compared to packed bed configurations.(Menkhaus & Glatz, 2005) In both cases, meanwhile, rates of culture broth circulation through the column are typically responsible for controlling the overall butanol recovery rate.(Wiehn et al., 2013) Both designs, however, suffer from challenges associated with continuous pumping requirements. More specially, in addition to increased utility costs, mechanical pumping can impose sheer stress towards sensitive microorganisms (Groot, van der Lans, & Luyben, 1992; Saravanan et al., 2010), reducing cell fitness and productivity.

Conversely, direct adsorbent addition provides significant and continuous solid-liquid contact to enable near equilibrium adsorption thereby maximizing the degree of separation on a mass basis of the adsorbent. Additionally, the separation can be achieved without introducing additional capital costs associated with the adsorption column and pump, utility costs associated with pumping, and productivity limitations incurred due to damaging sheer stresses imposed upon the microorganisms. However, the challenge associated with the direct adsorbent addition approach is how to efficiently retrieve the adsorbent without disrupting the fermentation. Presently, filtration is most commonly employed to end (Boyang et al., 2011; Faisal et al., 2016; Saravanan et al., 2010; Wiehn et al., 2014), however, doing so likewise requires pumping of the culture broth and, as such, can again impose significant stress upon the microorganism.

To begin to address these shortcomings, here we examine the development and application of magnetically-responsive adsorbents that can be both directly added to and then easily retrieved from fermentation broths. Mesoporous carbon powders have been

demonstrated to be effective adsorbents for butanol (Thomas J. Levario et al., 2012a) and can be readily produced in bulk quantities from relatively low cost commodity precursors of phenolic resin and Pluronic® surfactants.(Z. Qiang et al., 2015) Here, a series of novel magnetically responsive microporous/mesoporous carbon powders (MMCPs) containing embedded Ni nanoparticles (formed *in situ* from nickel nitrate during carbonization) in the carbon framework were fabricated. With these MMCPs we systematically developed a model semi-continuous process for acetone, butanol, ethanol (ABE) production through its simulated *in situ* recovery (Figure 2.1). In the process, we demonstrate that *i)* the Ni nanoparticles do not adversely impact the adsorption capacity or kinetics, *ii)* MMCPs are efficiently removed from the solution by magnet, *iii)* adsorbed butanol can be efficiently recovered by thermal treatment, and *iv)* re-generated MMCPs can be readily re-used without significant decrease in adsorption or magnetic separation performance. Furthermore, preliminary experiments indicate that, despite the incorporation of Ni nanoparticles, MMCPs maintain high biocompatibility. Overall, the proposed approach represents a versatile and new strategy for *in situ* product recovery with the potential to improve the production of a range of other inhibitory biofuels and biochemicals.

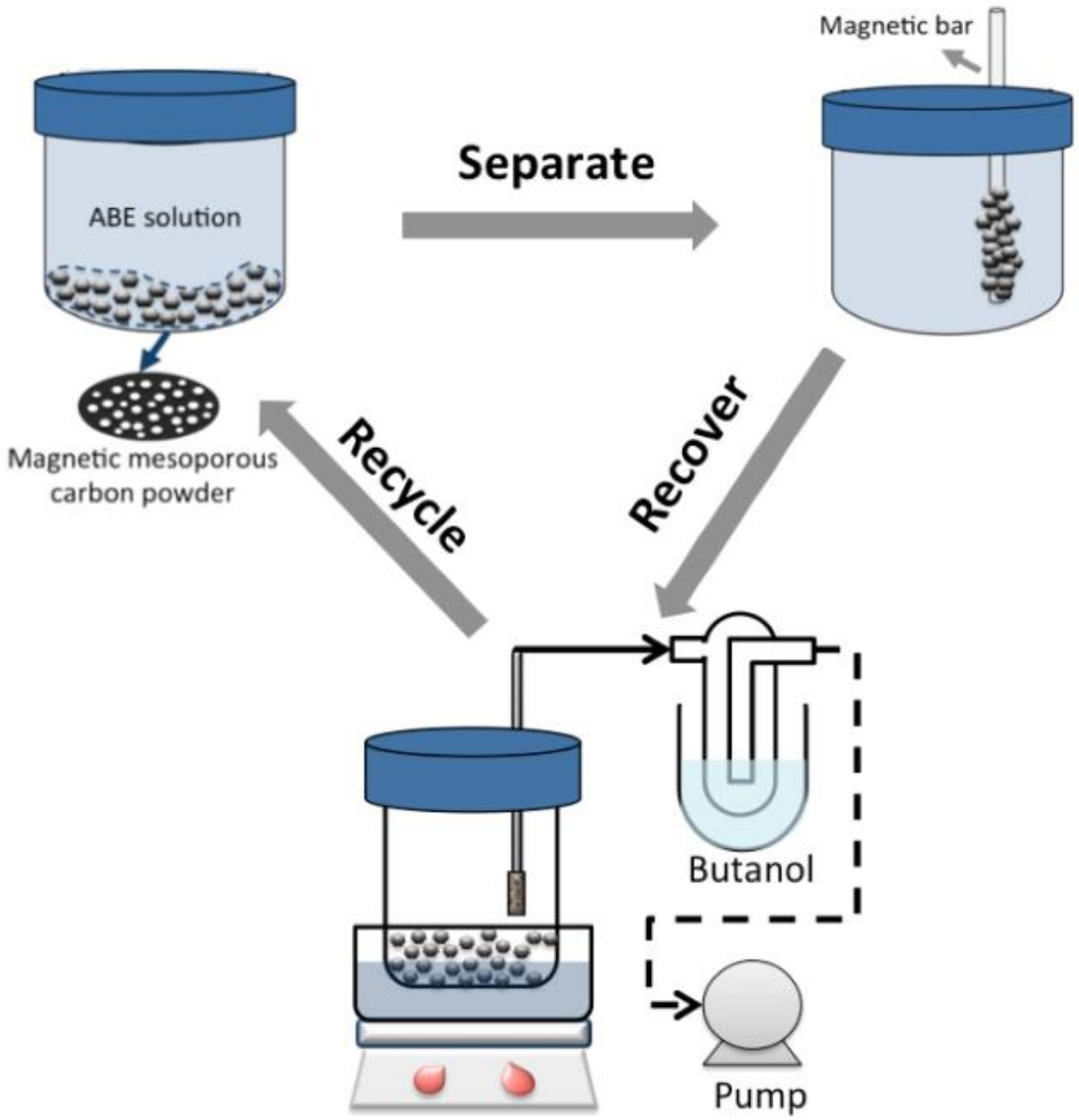

Figure 2.1. Schematic of Semi-Continuous Adsorption and Recovery. Schematic illustration of the model, semi-continuous process evaluated as part of this study which involved assessing the absorption, magnetic retrieval, and desorption capabilities of novel MMCPs as adsorbents for next generation biofuels.

2.2.0 Materials and Methods

2.2.1 MMCP Synthesis and Characterization

Phenol (>99%), formaldehyde (ACS reagent, 37% in H_2O, containing 10-15% ethanol as stabilizer), tetraethyl orthosilicate (TEOS) (>98%), Pluronic F127, nickel nitrate hexahydrate (>99.999%, trace metal basis), ethanol (>99%), potassium hydroxide (KOH, >85%) and sodium hydroxide (NaOH, >97%), and hydrochloric acid (37 %) were purchased from Sigma-Aldrich (St. Louis, MO) and used as received. Thermally-stabilized polyethylene terephthalate (PET) (125 μm thick) was purchased from Terphane Inc. (Bloomfield, NY) and used as the support substrate. A low-molecular weight phenolic resin was synthesized according to previous reports.(Yan Meng et al., 2006; Y. Meng et al., 2005) The synthesis of the MMCPs follows a modified procedure for the synthesis of mesoporous materials using a roll-to-roll process.(Zhe Qiang et al., 2016) Briefly, 96 g Pluronic F127 was dissolved in 80 g of H_2O and 240 g of ethanol at 40°C under magnetic stirring. Next, 120 g of resol solution (50 wt% in ethanol), 150 g of TEOS, and 10-18 g of nickel nitrate hexahydrate were added to the Pluronic solution. After stirring for 2 h at 40°C, the solution was cast onto the PET substrate *via* doctor blade at 50 cm/min with a wet film thickness of approximately 400 μm. The film was first heated at 50°C for 3 h to evaporate the solvent, followed by heating at 100°C for 3 h to crosslink the resol.(Yuanzhong Zhang, 2014) The crosslinked film was carefully peeled from the PET substrate and ground into a powder. The powder was carbonized in a tube furnace (SentroTech Inc., Strongsville, OH) under a N_2 atmosphere. The furnace was first heated to 600 °C at 1 °C/min, followed by heating at 5 °C/min to 800 °C, and held at 800 °C for 3 h. The sample was cooled to ambient temperature in N_2 atmosphere. Silica was removed by etching using daily-refreshed 3M KOH in ethanol/deionized water (1:1 v/v) over 4 days. The MMCPs were then rinsed with deionized water 10 times and

dried under vacuum at 80 °C for 24 h. For activation, a mixture of 30 g of MMCP and 60 g of KOH was heated at 5 °C/min to 600 °C and held for 30 min. Resultant powders were neutralized by dilute HCl solution (0.02M) and rinsed with deionized water 30 times. Powders were finally dried under vacuum at 80 °C overnight. The nickel content of three resulting MMCP samples was approximately 4.4%, 6.3% and 10.1% as determined by the thermogravimetric analysis based on 10 g, 14 g, and 18 g of nickel nitrate hexahydrate in the synthesis, respectively, which are accordingly named as MMCP-4, MMCP-6, and MMCP-10.

To investigate pore architecture, N_2 adsorption and desorption isotherms were obtained using a Micromeritics Tristar (Norcross, GA). The Barrett-Joyner-Halenda (BJH) model was used to determine the mesopore size distributions were calculated from the adsorption isotherm using the Barrett-Joyner-Halenda (BJH) model.(Storck, Bretinger, & Maier, 1998) Surface areas were determined by the Brunauner-Emmett-Teller (BET) methodology. The nanostructure of the MMCPs was elucidated using transmission small-angle X-ray scattering (SAXS; Rigaku MicroMax 002+ instrument, The Woodlands, TX) with a 2D multiwire area detector and a sealed copper tube operating at 45 kV to produce 0.154 nm X-rays. The scattering vector (q) was calibrated using the primary reflection peak of silver behenate at q = 1.076 nm^{-1}. The two-dimensional X-ray patterns were obtained from $0.12 < q < 2$ nm^{-1} and the domain spacing, d, of the MMCP was determined as:

$$d = 2\pi/Q^* \tag{2.1}$$

where Q^* is the primary peak position. Transmission electron microscopy (TEM) was

performed on the film using JEOL-1230 microscope operating with an accelerating voltage of 120 KV and bright field images were recorded by a digital CCD camera.

2.2.2 Adsorption Isotherm Studies using Aqueous Binary and ABE Model Solutions

Adsorption experiments were performed using 22 mL glass scintillation vials containing approximately 100 mg MMCP and 2 mL aqueous solution. Preliminary studies focused on the use of binary solutions (i.e., acetone, butanol, or ethanol in water) at initial concentrations ranging from 0.1-34 g/L. For model ABE solutions, samples were prepared at the 3:6:1 mass ratio of acetone, butanol and ethanol associated their native co-production by *Clostridium acetobutylicum*.(Jones & Woods, 1986b) Once mixed, samples were equilibrated at 37 °C overnight while mixing on an orbital shaker. This time is confirmed to be sufficient for the adsorbents to reach equilibrium. The supernatant (1 mL) was then removed for analysis by high-performance liquid chromatography (HPLC; Agilent 1100 series; Santa Clara, CA) equipped with a refractive index detector. Binary solutions were separated on a Hypersil GOLD aQ Polar C-18 column (Thermo Scientific; Grand Island, NY) using 5 mM H_2SO_4 as the mobile phase at 0.8 mL/min. ABE solutions were separated using an Aminex HPX-87H anion exchange column (Bio-Rad Laboratories; Hercules, CA) with 5mM H_2SO_4 as the mobile phase. A variable flow rate rising from 0.55-0.7 mL/min at 18 min with a 22 min final hold was used to reduce the elution time for butanol. External standards of known concentrations of butanol, acetone, and ethanol in water were used for calibration. The equilibrium adsorption capacity (Q_i) of each solute *i* was calculated using a mass balance:

$$Q_i = \frac{(C_{i,0} - C_i)V}{m} \tag{2.2}$$

where $C_{i,0}$ and C_i (g/L) are initial and equilibrium aqueous concentrations of species *i*, *V* (L) is aqueous volume, and *m* (g) is mass of MMCP. Equilibrium adsorption data were fit to the Freundlich isotherm models as shown in equation 3.

$$Q_i = k_{f,i} C_i^{1/n_i} \quad (2.3)$$

where Q_i (g/g adsorbent) are equilibrium adsorption capacity for the adsorbed species *i*, $k_{f,i}$ (g/g) and n_i (dimensionless) are the Freundlich constant and exponent, respectively. Freundlich exponent, the approximate Gibbs energy of adsorption was estimated from the following relation. (D. R. Nielsen et al., 2010)

$$\Delta G_i = -R * T * n_i \quad (2.4)$$

Where ΔG_i (kJ/mol) is the approximate energy of adsorption of component I, R (kJ/(mol·K)) is the universal gas constant, T (K) is temperature, and n_i is as defined above.

2.2.3 Characterizing the Kinetics of Butanol Adsorption from Aqueous Butanol Solutions

Butanol adsorption kinetic experiments were performed using media bottles containing approximately 2.6 g MMCP and 52 mL of a 10 g/L butanol solution, sealed with a butyl rubber septa. After mixing at 37°C on an orbital shaker for various time (0.5, 2, 5, 8, 10, 15, 30, 60, 120, 180, 240 min), 1 mL aqueous samples were drawn for HPLC analysis and characterized as described previously. The time dependent adsorption capacity was calculated using equation 2. The temporal dependence of the adsorption was

fit to both pseudo-first and pseudo-second order kinetic models(Ho & McKay, 1999), given by equations 2.4 and 2.5, respectively:

$$\frac{dQ_t}{dt} = k_1(Q_e - Q_t) \quad (2.4)$$

$$\frac{dQ_t}{dt} = k_2(Q_e - Q_t)^2 \quad (2.5)$$

where Q_t (g/g adsorbent) is the adsorption capacity at time t (min), Q_e (g/g adsorbent) is the equilibrium adsorption capacity, and k_1 (1/min) and k_2 (g/g min) are the first and second order rate constants, respectively.

2.2.4 Magnetic Recovery of MMCPs from Aqueous Slurries

The MMCPs were removed from aqueous slurries using a magnetic rod (Figure 2.12) to assess the efficacy of the Ni nanoparticle inclusions for magnetic recovery and provide a preliminary proof of concept. The magnets used to construct the rod were N32 neodymium ring magnets (0.75”/0.375” outer/inner diameter). Approximately 1.6 g of MMCPs were dispersed in 300 mL deionized water and continuously stirred at 200 rpm. The efficacy of MMCP retrieval was assessed by immersion of the magnetic rod in the slurry for a period of 2 min. In this case, the recovered MMCPs were then released from the rod by gently rinsing with water. The MMCPs were dried at 25°C in an updraft drying chamber for a minimum of 24 h until no further mass loss was detected. To assess the limitation for the magnetic recovery, this immersion process was repeated 3 times, giving a total of 6 min of immersion of the magnetic rod for each slurry.

2.2.5 Desorption of Adsorbed Butanol from MMCPs

MMCP samples (4.1 g) were equilibrated with 200 mL of a 16.2 g/L butanol solution in a sealed media bottle at 37°C. The supernatant was removed through a

stainless steel solvent bottle filter with application of vacuum (Figure 2.13). The crudely dried MMCP in the media bottle was then immersed in a water bath at 95°C with an applied house vacuum (77 kPa below ambient) to evolve and remove butanol vapors that were subsequently collected in a cold trap submerged in an acetone/dry ice mixture. Vacuum application was performed in discrete intervals until the crystalized condensate coated the entire condenser surface area (between 30 to 60 min). The condensate was diluted with 10 mL of distilled water. The solution was analyzed by HPLC using methods described above. The vacuum recovery of the adsorbate from the MMCPs continued in this manner until no further condensate was observed. This butanol adsorption-recovery process (equilibration, supernatant removal, heat and vacuum application, vapor collection, and condensate analysis) was repeated for a total of 5 consecutive 'cycles', in each case using a 16.2 g/L butanol solution and the same regenerated MMCP sample

2.2.6 Assessing MMCP Biocompatibility

A seed culture of *Escherichia coli* BW25113 was prepared by inoculating a 5 mL Luri-Bertani broth (LB; Thermo Fisher Scientific, Waltham, MA), incubated overnight in a shaking incubator at 32°C. Seed cultures were used to inoculate 50 mL LB broth in a 250 mL shake flask also containing either 0 (control) or 1.0 g of MMCP-10. A third flask that included 1.0 g of Dowex Optipore L-493 resin (hereafter referred to as L-493) was also prepared as an additional control, as this poly(styrene-divinylbenzene) resin is known to be both an effective butanol adsorbent as well as biocompatible with *E. coli*.(D. R. Nielsen & Prather, 2009) All cultures were incubated at 32°C while shaking for a total of 48 h, at which point the entire aqueous slurry was transferred to a 50 mL Falcon tube and centrifuged at 3000 rpm for 5 min using an Allegra X-22R centrifuge (Beckman

Coulter, Indianapolis, IN). The supernatant was decanted and the solid pellet (containing both cells and the MMCP-10 or L-493 sample) was washed 4 times with deionized (DI) water before then being resuspended in a minimum volume of DI water. The resuspended sample was then transferred to a weigh boat and dried in an oven at 37^{o}C until no further mass loss was detected (~48 h). Final dry cell mass was determined by subtracting the initial mass of MMCP-10 from the resultant total dry mass of the combined sample.

2.3.0 Results

2.3.1 MMCP Characterization

Figure 2.2 demonstrates the ordered mesoporous structure of the MMCPs. From TEM, the degree of ordering decreases and cylindrical nanostructures are ordered only locally with short-range correlations with increasing Ni content, which is consistent with previous reports.(Zhai et al., 2011) Moreover, the Ni-containing nanoparticle size increases approximately from 11 nm to 16 nm to 19 nm for MMCP-4 (Figure 2.2A), MMCP-6 (Figure 2.2B), and MMCP-10 (Figure 2.2C), respectively. The nature of the nanoparticles is confirmed with X-ray diffraction (XRD), as illustrated in Figure 2.14. The three well-resolved diffraction peaks in the XRD profile are assigned to the (111) and, (200) reflections of FCC metallic Ni. To better investigate the nanostructure ordering, small angle X-ray scattering (SAXS) was used to complement the TEM imaging. The primary ordering peak from SAXS in Figure 2D becomes broader with increasing amount of incorporated Ni nanoparticles. This change in the shape of the peak is suggestive of a gradual degradation of regularity in the mesostructures and agrees well with the observations from TEM micrographs in Figure 2.2A-C. The domain spacing of

MMCP-4 (4.4% Ni) is approximately 11.2 nm and the domain spacing is increased to 12.3 nm for MMCP-6 (6.3% Ni) due to the enhanced rigidity of the framework from the embedded Ni nanoparticles, which reduces contraction from stress developed during the carbonization step. The domain spacing of MMCP-10 (10.1% Ni) is reduced to 10.1 nm, which may be associated with decreased thickness of the walls due to migration of Ni to grow nanoparticles during carbonization. No higher-order peaks are observed in the SAXS profiles for all three MMCPs. This behavior is consistent with prior reports for the loading of high Z metal nanoparticles in ordered mesoporous carbons(Dai & Vogt, 2012; Hao et al., 2013; Y. Meng et al., 2005; X. Wang & Dai, 2009) and is attributed to the heterogeneous distribution of Ni nanoparticles in the carbon walls, which leads to additional correlation length scales beyond the pore-pore spacing.

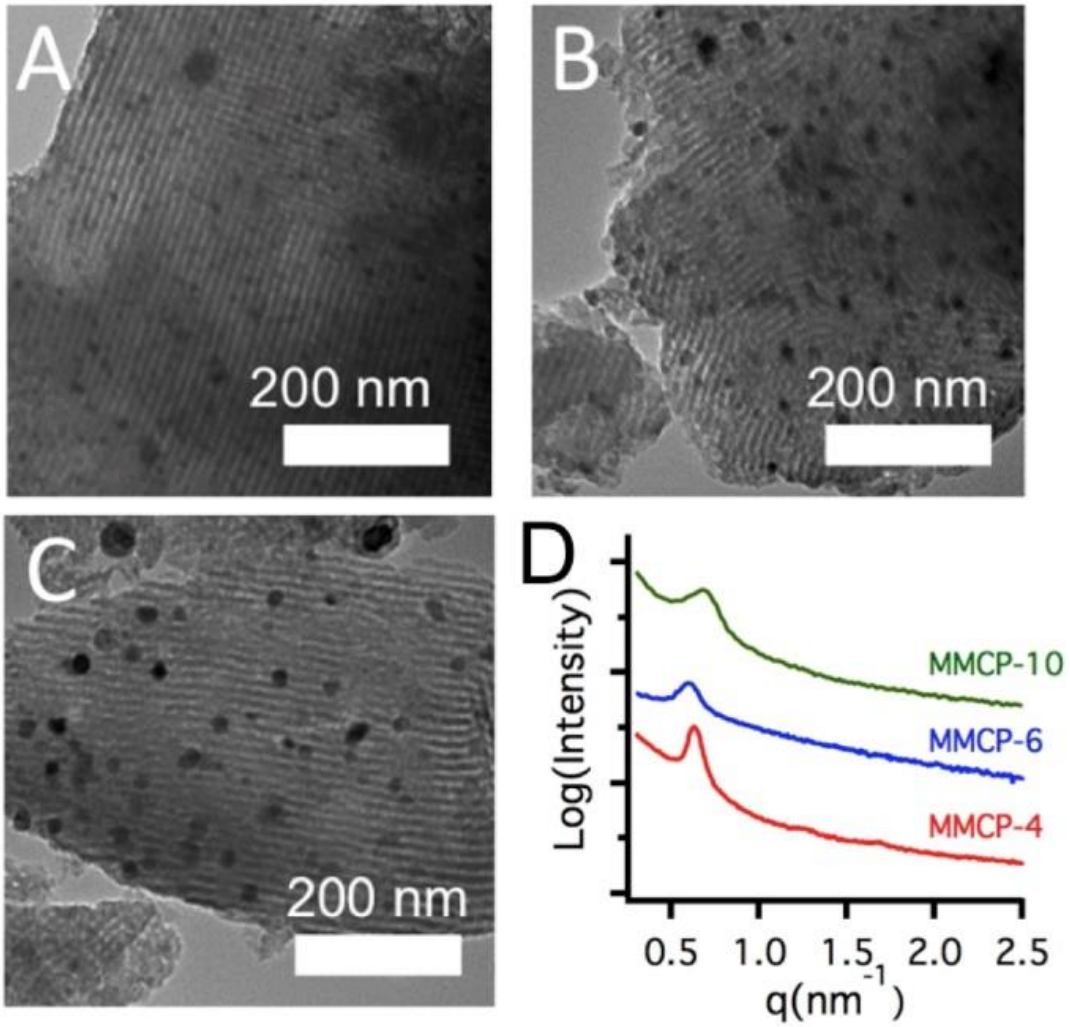

Figure 2.2. TEM Micrographs. TEM micrographs of (A) MMCP-4; (B) MMCP-6 and (C) MMCP-10, and (D) SAXS profiles for all three samples.

The N_2 adsorption-desorption isotherms (Figure 2.3A) for all three MMCP samples show typical type-IV behavior with an H_1 hysteresis loop. A well-defined step in the isotherms occurred at approximately p/p_0=0.5-0.7 due to the capillary condensation of nitrogen in the mesopores. Pore size distributions (Figure 2.3B) determined from the N_2 adsorption isotherms confirm the presence of both micropores (from activation and removal of silica) and mesopores (from the Pluronic F127 template). The average

mesopore size for MMCP-4, -6, and -10 is approximately 6.6, 7.2, and 5.6 nm, respectively. The shift in average pore size agrees well with the change in domain-spacing determined from SAXS. The associated specific surface areas are approximately 2200, 1400, and 1800 m^2/g for MMCP-4, -6, and -10, respectively. These surface areas are significantly higher than other magnetic porous carbon composites for biofuel absorbents (<1000 m^2/g) previously reported.(Boyang et al., 2011; X. Liu, Wang, Wu, & Wang, 2015; Oliveira et al., 2002)

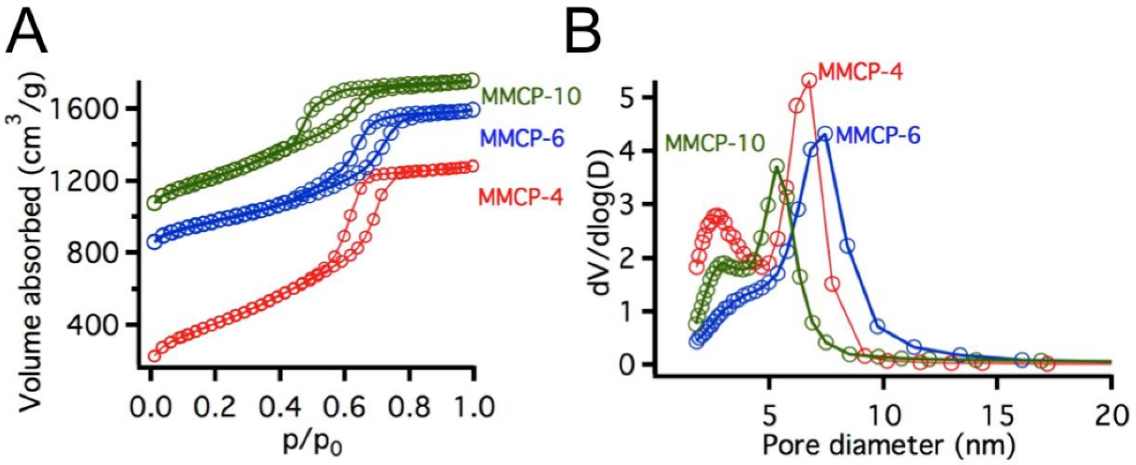

Figure 2.3. MMCP Characterization (A) N_2 adsorption-desorption isotherms of MMCP-4, MMCP-6 and MMCP-10; The isotherms of MMCP-6 and MMCP-10 are vertically offset by 500 and 750 m^2/g to improve comparison. (B) Pore size distributions derived from adsorption isotherms.

2.3.2 Aqueous Butanol Adsorption

The adsorption behavior of MMCPs for *in situ* butanol recovery was assessed using model solutions and cell-free conditions to reduce complexity and focus on separation performance. Figure 2.4 illustrates the equilibrium isotherms obtained using the MMCPs with binary aqueous solutions. As shown in Figure 2.4A, the Ni content in

the MMCP does not significantly impact the adsorption behavior of butanol from water. Surprisingly, higher Ni content in the MMCP tends to lead to a slight increase in the gravimetric adsorption capacity despite the lower surface area of MMCP-10 (~1800 m^2/g) than MMCP-4 (~2200 m^2/g). For all three MMCPs the adsorption capacity reaches >0.3 g/g MMCP near butanol's approximate inhibitory threshold (12.5 g/L). These isotherms are well described by the Freundlich model ($R^2 > 0.961$), which is consistent with prior reports for butanol adsorption by other hydrophobic materials.(Thomas J. Levario et al., 2012a; D. R. Nielsen & Prather, 2009; Rudling, 1988) Other isotherm models were applied and it was found that the Dual Site Langmuir model(Nguyen & Do, 2000) describes the data with similar residuals to Freundlich isotherms as shown in Figure 2.16. Table 2.1 shows the resultant best-fit Freundlich parameters, as compared with similar mesoporous carbons without Ni nanoparticles and chemical activation. In general, the Freundlich constant is increased for the MMCPs examined here in comparison to FDU-15 and its analogs previously reported for the separation of butanol.(Thomas J. Levario et al., 2012a) Freundlich exponents, the Gibb's energy of adsorption was approximated using equation 2.4. Gibb's energy of adsorption values determined for MMCP-4, 6 and 10 were -4.7±0.4, -3.5±0.3 and -5.4±0.4 kJ/mol, respectively. These negative values suggest the adsorption process is spontaneous which is consistent with physisorption rather than chemisorption where energy input is required. Figure 2.4B shows that the equilibrium uptake for ethanol by the MMCPs is again nearly invariant of Ni content and the isotherms can be fit by the Freundlich model. However, the capacity for ethanol is significantly reduced (by nearly a factor of 3) in comparison to butanol, although the Freundlich constants for the MMCPs are still generally larger than

for previously reported mesoporous carbons.(Thomas J. Levario et al., 2012a) Figure 2.4C shows that the equilibrium uptake for acetone. Unlike ethanol and butanol, the adsorption is dependent on the Ni content in the MMCP with the adsorption on MMCP-4 significantly greater than the other two MMCPs examined. Overall, the observation that adsorption of acetone and ethanol on MMCPs was less than that of butanol is consistent with other ABE adsorbents, including zeolites(Faisal et al., 2016; Saravanan et al., 2010) and polymer resins.(Niloofar Abdehagh et al., 2015; D. R. Nielsen & Prather, 2009; Wiehn et al., 2014) These adsorption isotherms obtained for the binary solutions associated with the individual ABE components derived via most *Clostridium* sp. fermentations suggest that the MMCPs exhibit sufficient capacity for use with *in situ* recovery applications.

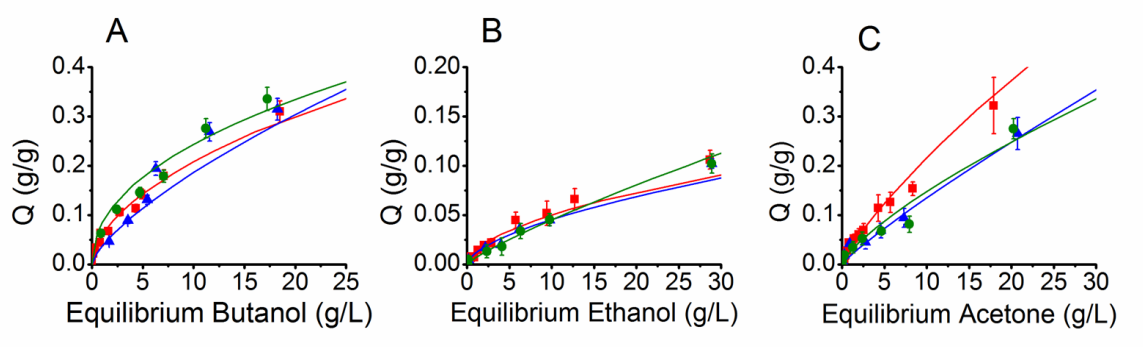

Figure 2.4. Adsorption Isotherms and Corresponding Freundlich Isotherm Model Fits for binary (i.e., in water) solutions of (A) butanol, (B) ethanol, and (C) acetone for each of MMCP-4 (squares), MMCP-6 (triangles), and MMCP-10 (circles).

Table 2.1

Freundlich Isotherm Model Fit Parameters Obtained For Previously Investigated Mesoporous Carbons and The MMCPs Developed in This Study.

	Acetone		Butanol		Ethanol		
Adsorbent	k_f (g/g)	n	k_f (g/g)	n	k_f (g/g)	n	Reference
FDU-15-	-	-	0.027±0.006	3.7±0.5	0.005±0.001	2.4±0.2	36

800							
FDU-16-800	-	-	0.052±0.005	4.6±0.3	0.007±0.001	2.5±0.2	36
CS-68-800	-	-	0.018±0.004	1.9±0.1	0.003±0.001	1.8±0.1	36
CS-81-800	-	-	0.033±0.007	2.4±0.2	0.003±0.001	1.9±0.1	36
MMCP-4	0.034±0.005	1.2±0.1	0.060±0.004	1.9±0.2	0.014±0.001	1.8±0.1	This study
MMCP-6	0.018±0.004	1.1±0.1	0.037±0.005	1.4±0.1	0.009±0.001	1.4±0.1	This study
MMCP-10	0.027±0.005	1.3±0.1	0.085±0.003	2.2±0.2	0.006±0.001	1.2±0.1	This study

As the primary liquid biofuel of interest, butanol adsorption performance is of particular importance in this work. Figure 2.4 provides a comparison of the isotherm for MMCP-10 (highest Ni content, so most likely to be magnetically separable) with several previously investigated butanol adsorbents, each selected to represent among the best performance for their respective material classes. MMCP-10 behaves and performs in a comparable manner, despite its unique, magnetically-responsive attributes. At 12.5 g/L (selected to represent the approximate inhibitory threshold of *C. acetobutylicum*), for example, the performance of MMCP-10 (0.26 g/g) equals that of the best commercial activated carbons (i.e., AC F-400), while surpassing most other carbon materials investigated to date, as shown in Table 2.3.

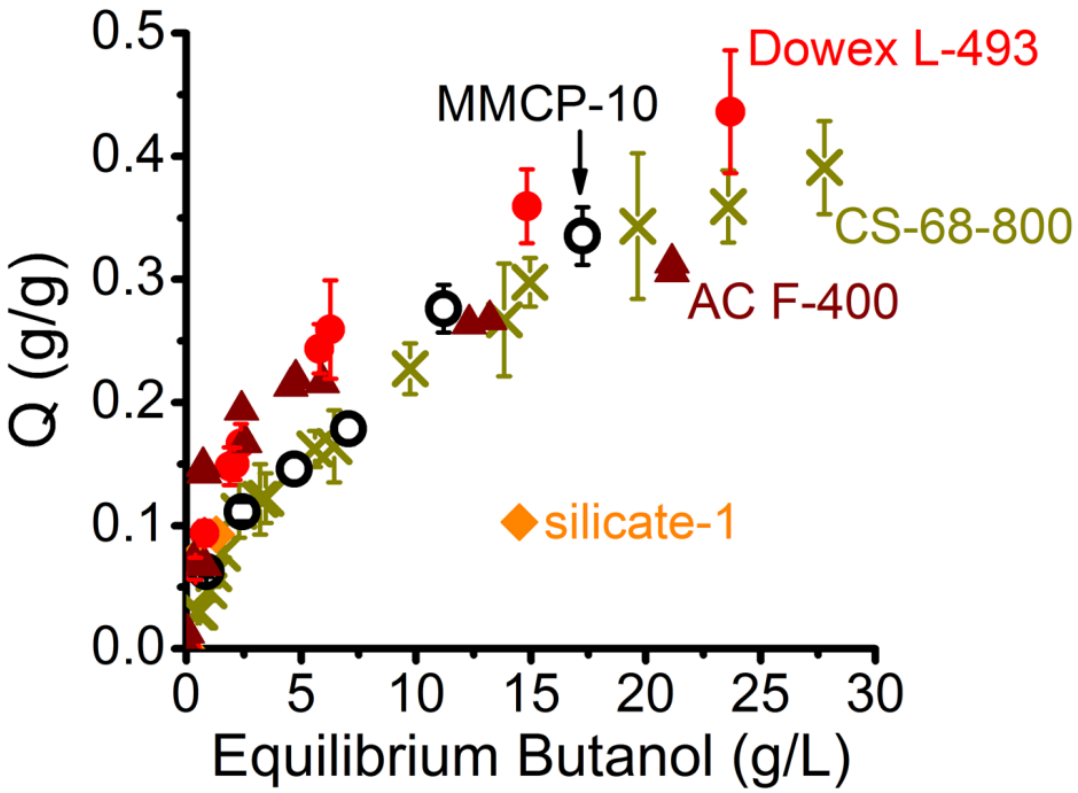

Figure 2.5. Comparing Butanol Adsorption Isotherms between MMCP-10 (open circles) and other, previously investigated butanol adsorbents, including: activated carbon (AC) F-400 (solid triangles), the mesoporous carbon CS-68-800 (Crosses) (T. J. Levario et al., 2012), silicalite-1 (solid diamonds) (Milestone & Bibby, 1981), and the macroporous poly(styrene-co-divinylbenzene) resin Dowex Optipore L-493 (solid circles) (T. J. Levario et al., 2012).

2.3.3 Adsorption Behavior of ABE Solutions

Most *Clostridium* sp. fermentations yield a mixture of products that includes acetone, butanol, and ethanol (i.e., the so-called ABE fermentation), synthesized at a typical mass ratio of 3:6:1 (acetone:butanol:ethanol). Accordingly, adsorption behavior was next investigated using a series of aqueous ABE mixtures, each initially prepared to represent said ratio. Figure 2.6 shows the adsorption isotherms obtained for these

mixtures on MMCP-10. For all species, adsorption from the ABE mixture is decreased relative to binary mixtures (note: lines in Figure 2.6 represent Freundlich isotherm model fits obtained using the data in Figure 2.4). Competition for the same adsorption sites reduces the overall adsorption of each species relative to the binary case. As adsorption of all three components is driven by both van der Waals (Carey & Sundberg, 2000; N. Qureshi, Hughes, et al., 2005a; Regdon et al., 1998) and hydrophobic interactions,(Hashi et al., 2010; D. R. Nielsen et al., 2010; Oudshoorn et al., 2009a; Saravanan et al., 2010) butanol adsorption is impacted less than that of less hydrophobic acetone.(Sangster, 1989) Adsorption of ethanol, meanwhile, is limited due to its lower concentration in the ABE solution as well as the lower intrinsic equilibrium capacity of the MMCPs (Figure 2.4). These behaviors are consistent with prior studies of other ABE adsorbents. (Niloofar Abdehagh et al., 2015; D. R. Nielsen & Prather, 2009; Wiehn et al., 2014)

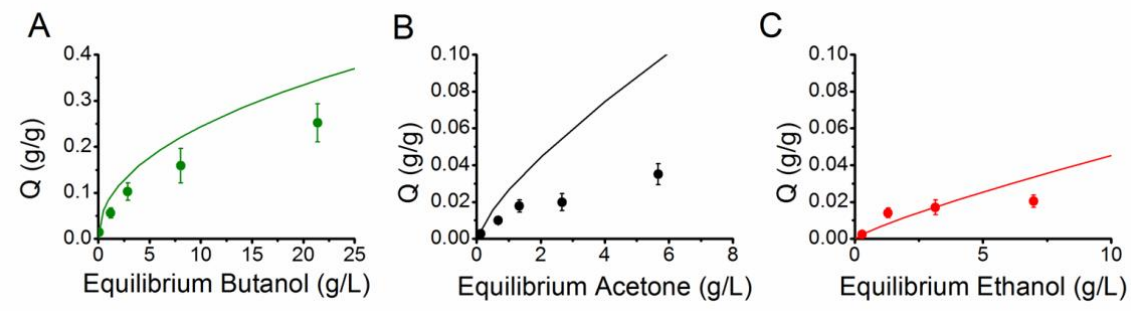

Figure 2.6. Equilibrium Adsorption of Model ABE Solutions using MMCP-10 with respect to (A) butanol, (B) acetone, and (C) ethanol (solid circles). Freundlich isotherm model fits obtained for binary solutions are shown for comparison in each case (solid lines).

2.3.4 Characterizing Butanol Adsorption Kinetics from Binary Solutions

In addition to total adsorption capacity, the rate of butanol uptake is furthermore critical for the efficacy of MMCPs as adsorbents for *in situ* product recovery. Figure 2.7 illustrates the rates of butanol uptake from model binary solutions for MMCP-4, -6, and -10. The initial butanol uptake was rapid in each case, reaching 80-90% of the equilibrium capacity within the first 15-30 min, with equilibrium attained in less than 1 h. Although faster adsorption rates have been reported for other butanol adsorbents, this performance is acceptable for *in situ* product recovery.(Thomas J. Levario et al., 2012a; Xiaoqing Lin et al., 2012; D. Liu et al., 2014; N. Qureshi, Hughes, Maddox, & Cotta, 2005b) For instance, as typical butanol production rates by *Clostridium* sp. have been reported as 0.32-0.48 g/(L·h),(C. Lu, Zhao, Yang, & Wei, 2012; H. W. Yen, Li, & Ma, 2011) the maximum (i.e., initial) rate of butanol uptake by MMCP-10 was nearly 123 g/(L·h). The adsorption kinetics of all MMCPs are similar and can be well represented by a pseudo-second order kinetic model (R^2 > 0.994 in all cases). The pseudo-second order rate constants (Table 2.2) indicate that MMCPs enable almost an order of magnitude increase (9.3 fold) in the butanol uptake rate in comparison to commercial activated carbons, AC F-400 and AC F-600.(N. Abdehagh et al., 2013) Accordingly, adsorption kinetics are not expected to arise as a bottleneck for *in situ* butanol recovery applications using MMCPs.

Table 2.2

Kinetic Parameters Determined for Pseudo-Second Order Model.

Adsorbent	k_2 (g/g min)	Reference
AC F-400	0.8	38
AC F-600	1.1	38
MMCP-4	6.5	This study
MMCP-6	3.6	This study

MMCP-10	7.4	This study

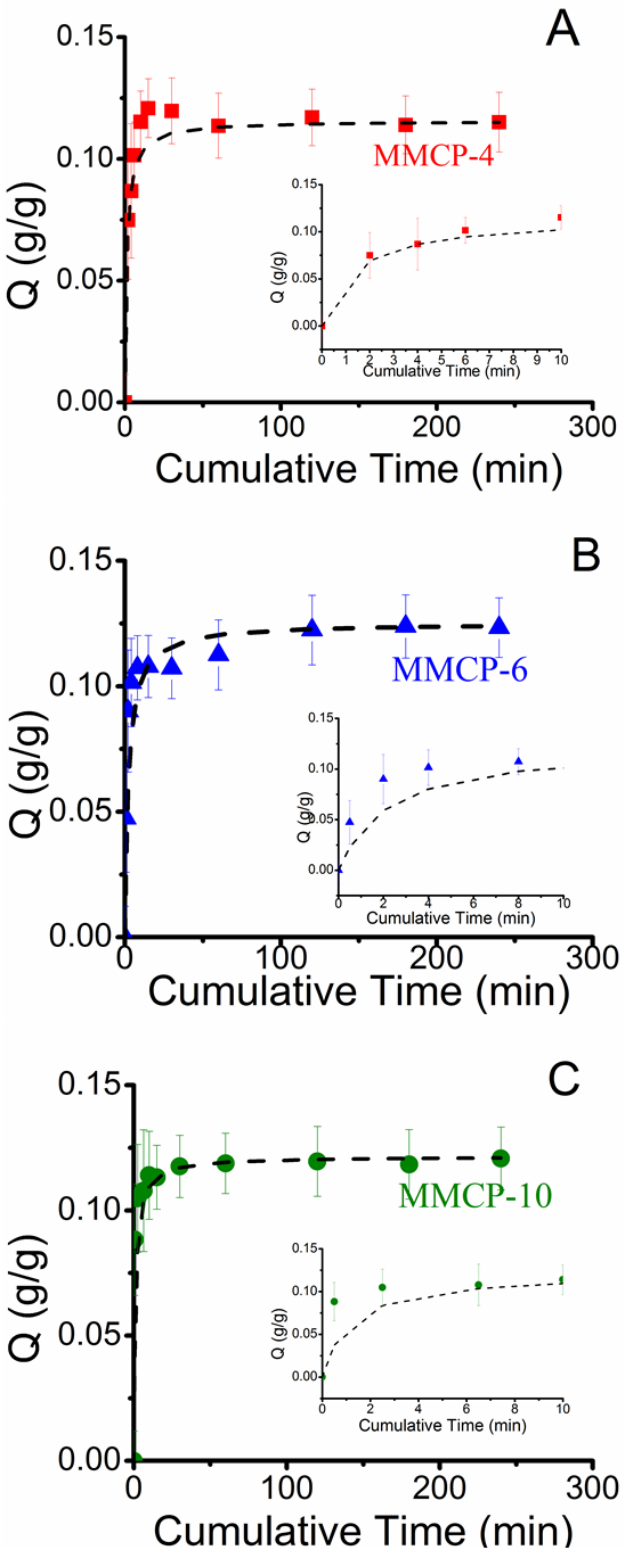

Figure 2.7. Kinetics of Butanol Adsorption by MMCP-4 (A), MMCP-6 (B), and MMCP-10 (C), along with the corresponding best-fit predictions obtained using a pseudo-second order kinetic model. Inset figures show the first 10 min of each respective dataset.

2.3.5 Magnetic MMCP Retrieval

The rationale for inclusion of Ni nanoparticles in the MMCPs is to enable their facile removal from the fermentation broth following adsorption. Model experiments were conducted by simply immersing a magnetic rod (Figure 2.12, Supplementary Information) into an aqueous suspension of MMCPs for a period of 2 min, after which the rod together with adhered MMCP, was then removed. Figure 2.8 illustrates the efficacy of this simple design and approach for MMCP removal. Here, 'Retrieval Number' refers to the number of serial attempts performed (each 2 min in duration) to retrieve MMCP samples from the same initial solution. The initial retrieval (Retrieval Number 1) always led to the highest fractional recovery of the MMCPs for a given Ni content in the MMCPs. As expected, increasing the Ni content results in greater initial MMCP recovery during the 1st retrieval. This recovery was reproducible with the fraction of MMCP-4, MMCP-6, and MMCP-10 recovered in the initial retrieval being 0.22 ± 0.06, 0.36 ± 0.09, and 0.77 ± 0.03, respectively. These results demonstrate that the ability of MMCPs to adhere to the magnetic rod is proportional to the Ni content, although there a significant, non-linear uptick is observed in the fraction recovered at the highest Ni content examined (MMCP-10). For the subsequent retrieval cycles, the amount of MMCP collected is a function of both the Ni content and remaining MMCP content. As the majority of the MMCP-10 was removed during the first cycle, the fraction (based on the initial concentration) removed during the 2nd retrieval is only 0.1 ± 0.03, or nearly

50% of the remaining particles in the suspension (see Figure 2.15). For MMCP-4, the fraction (based on the initial concentration) removed during the 2nd retrieval is 0.17 ± 0.04, nearly the same fractional recovery (based on the remaining particles) as for 1st retrieval. This result confirms that the initial removal of MMCPs is limited by the Ni content and decreases with MMCP content. This decrease is also observed when re-using magnetically separated MMCPs, so the lack of recovery is not due to non-magnetically active materials from the synthesis. For the 6 min of total retrieval time examined here (3 x 2 min cycles), half of the MMCP-4 was recovered from the suspension, while the fraction of MMCP-10 retrieved was 0.89 ± 0.03 overall. When applied in a semi-continuous process, however, unrecovered MMCPs can be recovered in a subsequent retrieval cycle and so are not irreversibly lost.

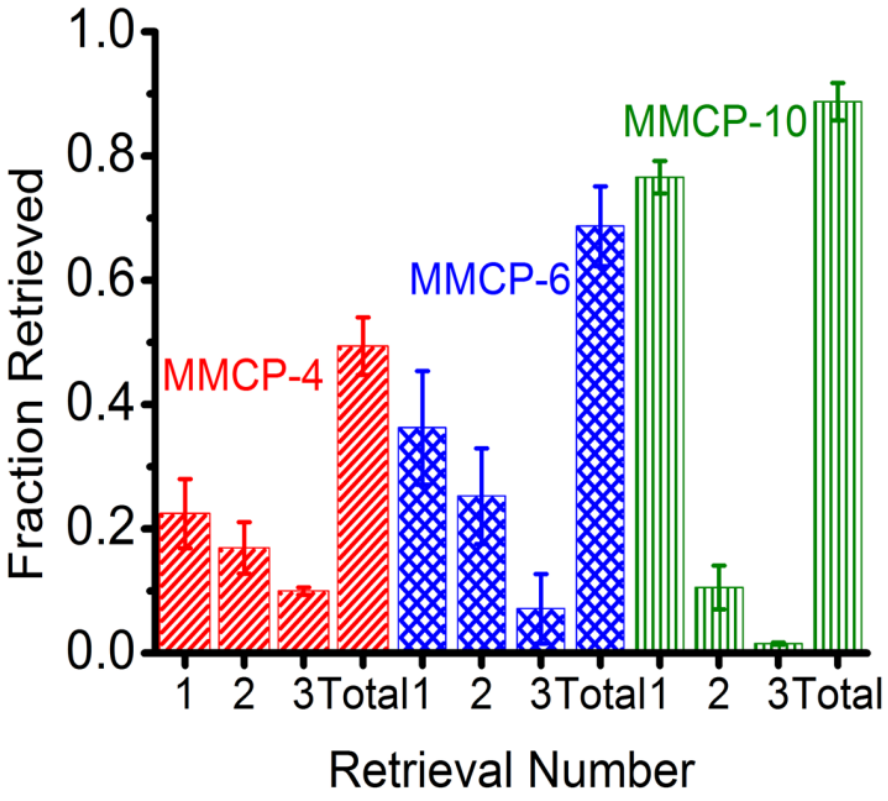

Figure 2.8. Fractional Retrieval of MMCPs. Fraction of MMCP-4 (diagonal stripes), MMCP-6 (crosshatch) and MMCP-10 (vertical stripes) retrieved per application of the magnetic retrieval tool, as well as total retrieved (sum total of 3 sequential applications).

2.3.6 Desorption and Recovery of Butanol from MMCPs and Recycling of MMCPs

With the demonstration of efficient adsorption and magnetic retrieval, the final key requirements for the potential use of MMCPs are the desorption/recovery of butanol and regeneration of the MMCPs for subsequent reuse. For butanol recovery from adsorbents, thermal treatment(Sutikno & Himmelstein, 1983; Wei et al., 2014) is generally the most efficient method.(Wiehn et al., 2014) MMCPs were equilibrated with an aqueous solution initially containing 16.2 g/L butanol before then being recovered. Adsorbed butanol was removed from the recovered MMCP by heating (95 $^{\circ}$C) under vacuum. The evolved vapors were collected in an integrated cold trap (Figure 2.13). Figure 2.9A demonstrates that a majority of the adsorbed liquid within the MMCPs (~85-90%) was recovered within the first 90 min. Initially, the rate of butanol desorption reached as high as ~3.5 g/L-h which, much like rates of adsorption, also greatly exceeds typical rates of butanol production. Unlike for initial adsorption, however, there is a clear difference in the butanol recovery for the different MMCPs. In total, 92.9%, 86.4%, and 99.7% of initially adsorbed butanol sample was recovered from MMCP-4, -6, and -10, respectively, by this approach. While the most butanol was evolved from the MMCP-4 and least from MMCP-10, a significant amount of butanol can still be recovered from all of the MMCPs examined. For comparison, we have previously demonstrated that 83% of adsorbed butanol was recoverable from L-493 resin adsorbent via an analogous thermal processing approach.(D. R. Nielsen & Prather, 2009; Wiehn et al., 2014)

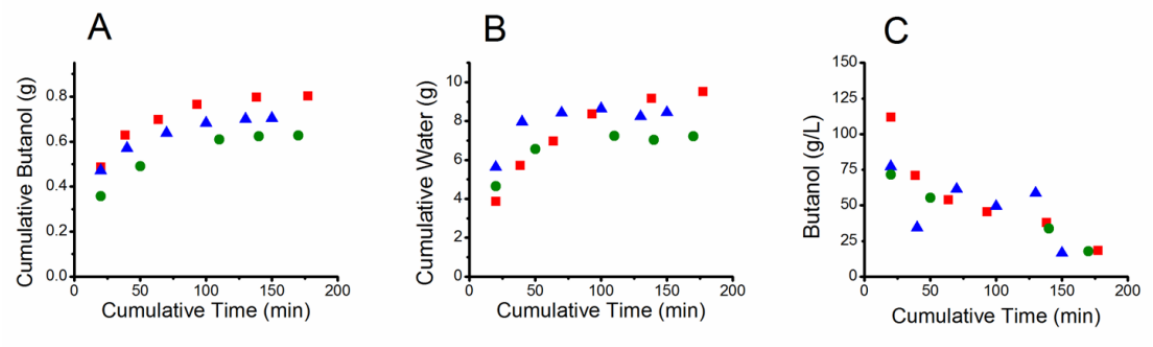

Figure 2.9 Desorption of Butanol from MMCPs. Recovery of vapors desorbed from MMCP-4 (squares), MMCP-6 (triangles), and MMCP-10 (circles) for (A) butanol and (B) water (note: cumulative time refers to the total duration for which vapor collection occurred). (C) Concentration of butanol in the collected condensate at each time point.

The adsorbed fluid contains water in addition to butanol. Figure 2.9B illustrates the amount of water co-evolved from the MMCP samples. While the mass of water collected is an order of magnitude greater than that for butanol, an overall significant increase in the concentration of butanol compared to the initial solution (16.2 g/L) is still realized. More specifically, the total recovered products have butanol concentrations of 76.9 g/L, 77.8 g/L and 80.8 g/L for MMCP-4, MMCP-6 and MMCP-10, respectively, corresponding to effective separation factors of 4.7, 4.8 and 5.0. The purity of the butanol collected is time dependent with higher butanol concentrations recovered initially. The butanol concentration of the collected product during each desorption interval (each lasting 30-60 min) is shown in Figure 2.9C. The maximum butanol concentration in the product (obtained in the first 30 min of desorption) was approximately 112 g/L for MMCP-4. This represents a 6.9-fold enrichment over the initial aqueous concentration (16.2 g/L). For the other two MMCPs, the maximum concentration of butanol in the product was approximately 75 g/L, still nearly a 5-fold enhancement.

MMCPs must also be re-usable to constitute a cost effective separation process. Figure 2.10 illustrates that separation performance is not degraded during subsequent cycles of reuse for regenerated samples of MMCP-4. As can be seen, relative changes with respect to the efficiency of butanol recovery and its collected purity during a total of five repeated adsorption-desorption cycles were minimal. The reused MMCP-4 displays comparable performance to that of the fresh material (Figure 2.9A). This is consistent with prior reports for recycled L-493 resin(D. R. Nielsen & Prather, 2009) and zeolite(Oudshoorn et al., 2012) adsorbents, which similarly been reported to retain consistent adsorption behavior when regenerated under similar process conditions.

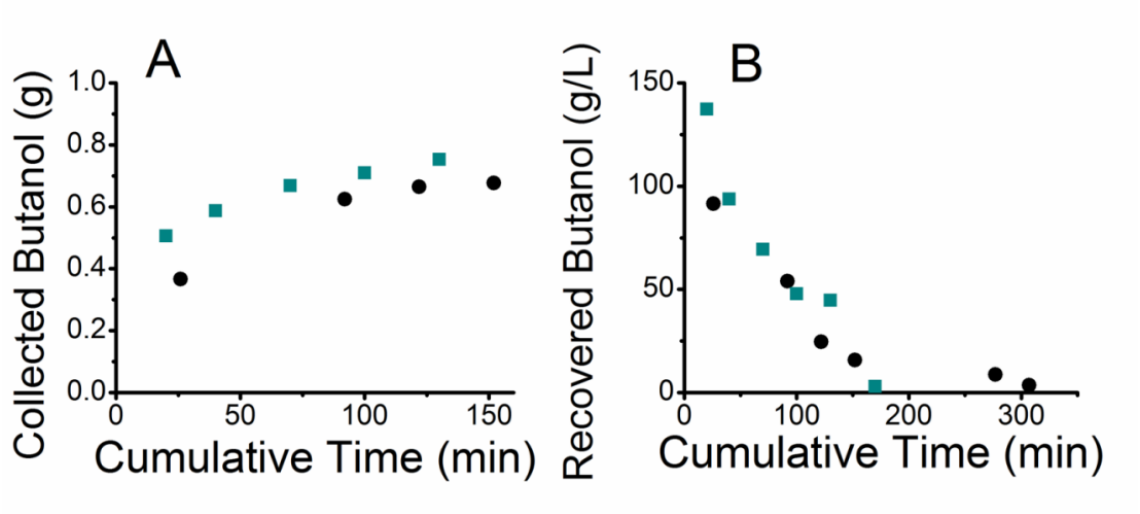

Figure 2.10. Reusability of MMCPs After Multiple Cycles. Characterizing the repeated reuse and performance of regenerated MMCP-4 over the course of 5 consecutive adsorption-desorption cycles. For clarity, only the 1st (solid circles) and 5th cycle (solid squares) are shown. Compared are A) the cumulative evolution and collection of butanol and B) the instantaneous concentration of butanol in the collected condensate (i.e., per each 30-60 min treatment duration).

2.3.7 Magnetic Retrieval Field Modeling

To better understand the magnetic field parameters involved in the retrieval process, modeling was performed to approximately map magnetic flux densities used in this study. Understanding the magnetic flux density is prerequisite to optimization of the magnetic recovery strategy. Magnets were simulated as N32 neodymium with 0.5" inner diameter and 0.75" outer diameter on both steel and aluminum cores. The actual magnets used in the development of the retrieval tool were rated for a 5 lb lifting strength. The simulated lifting strength was approximately 4.8 lbs at the same distance, validating the material and magnet geometry used in the simulation. Figure 2.8 charts the field lines and magnetic flux density regions in Tesla which are equivalent to 10,000 Gauss. Visually the collected MMCPs were conformal to the shape of the yellow region of magnetic flux density seen in Figure 2.8A as would be expected. As can be seen in Figure 2.8B, a steel core would concentrate the magnetic flux density at the end of the tool, whereas an aluminum core provides regions of high magnetic flux density which extend more than 5 mm from the surface of the recovery tool. Also represented in Figure 2.8C-F are the magnetic flux densities of 1-4 magnet recovery tool configurations. The modeling results here showed that the main difference in the number of magnets is the increased surface area with high magnetic flux density. Additionally the models indicate that the magnetic flux density immediately adjacent to the recovery tool increases from approximately 0.3 to 0.4 T from 1 to 4 magnet configurations. The insignificant influence of the magnetic field compared to Ni composition simplifies the required design parameters for scalable MMCP recovery.

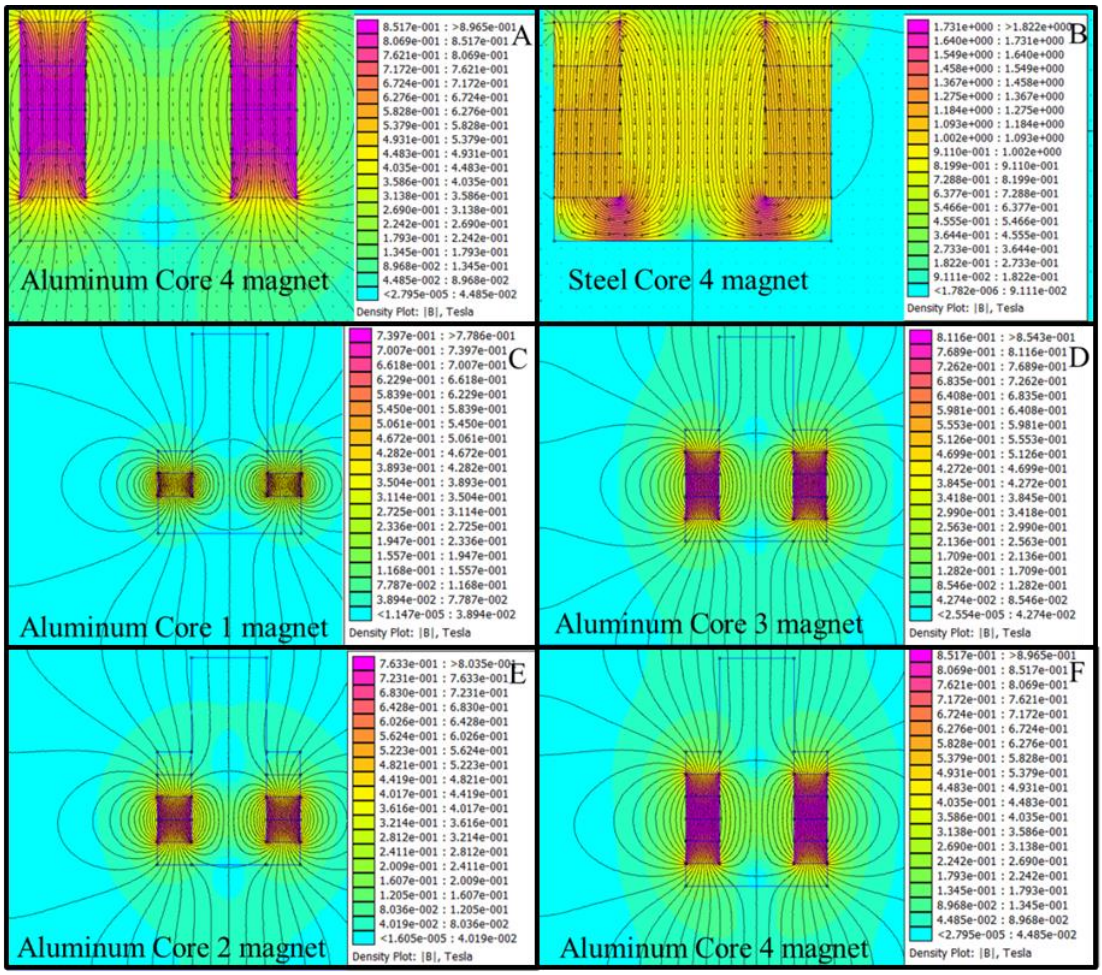

Figure 2.11. Magnetic Flux Density Distributions For Magnetic Recovery Tools. A) T6 aluminum core with 4 magnets demonstrating the magnetic flux density extending into the solution around the magnetic tool. B) 1018 steel core with 4 magnets where the magnetic flux density is concentrated at the base of the magnetic tool. C) Single magnet, D) 2 magnets, E) 3 magnets and F) 4 magnets on a T6 aluminum recovery tool.

2.3.8 Examining MMCP Biocompatibility

A preliminary assessment of MMCP biocompatibility was performed using *E. coli* as a model microbe and MMCP-10 (selected because it contained the highest Ni content and thus posed the greatest potential risk of inhibition). Dowex Optipore L-493, a resin adsorbent previously reported as biocompatible with *E. coli*, (D. R. Nielsen &

Prather, 2009) was also included as an additional control. While in absence of either adsorbent a final cell density of 53 g/L was reached, a similar final density (52 g/L) was also achieved in the presence of 1 g of MMCP-10. This mark was comparable to yet slightly better than with L-493 (50 g/L). From this cursory demonstration of biocompatibility it is expected that MMCPs will furthermore perform as effective adsorbents for *in situ* butanol recovery, as part of future investigations by our group.

2.4.0 Conclusion

In this work, we demonstrated the efficacy of a series of novel MMCPs as magnetically retrievable adsorbents for butanol recovery. The adsorption capacity and kinetics of the MMCPs are competitive with conventional butanol adsorbents studied to date, but the embedded Ni nanoparticles in the adsorbents enable facile separation from aqueous slurries via magnetic field application. Using an *E. coli* model, initial studies suggest that MMCPs further demonstrate high inherent biocompatible. By enabling key limitations associated with current adsorption-based designs to be effectively circumvented, MMCPs are promising candidate adsorbents for *in situ* butanol recovery and the development of semi-continuous butanol fermentation processes.

2.5.0 Acknowledgments

This work was supported by the National Science Foundation (Award Nos. CBET-1067684 and CBET-1159200). The authors declare no conflicts of interest.

2.6.0 Supporting Information

Supporting information describes the magnetic retrieval device, physical properties of the MMCPs relative to other adsorbents, the desorption apparatus, XRD profile, fractional recovery of MMCP versus remaining concentration, and the desorption

profile for all performed cycles. Figure 2.12 reveals the construction of the magnetic retrieval tool used to recover the MMCPs. Aluminum was chosen for its low remanence, meaning that the aluminum does not become magnetized like steel does, as explained in section 2.3.7.

Figure 2.12. Magnetic Retrieval Tool. The magnetic retrieval tool used in this study was fabricated using aluminum hardware and most notably included a stack of 4 neodymium ring magnets (0.75”/0.375” outer/inner diameter) covered by aluminum tape.

It is important to have certain physical parameters characterized by which to compare adsorbents. Adsorption is very highly dependent on surface area, but the other factors such as the mean pore diameter can impact kinetics. For a more complete comparison, Table 2.3 presents additional physical properties of MMCPs from earlier generations to the present generation of varied Ni composition and compares them to commercial carbon.

Table 2.3

Physical Properties of Previously Investigated Carbon Adsorbents and MMCP Adsorbents Examined in This Study.

Adsorbent	Surface Area (m^2/g)	Mean Pore Diameter (nm)	Butanol Adsorption Capacity (g/g) at 12.5 g/L	Reference
AC F-400	1,090	-	0.26	[38]
AC F-600	710	-	0.15	[38]
FDU-15-800	538	5	0.12	[36]
FDU-16-800	671	5.8	0.15	[36]
CS-68-800	1287	8.2	0.25	[36]
CS-81-800	1307	7.2	0.28	[36]
MMCP-4	2205 ± 93	6.6	0.23 ± 0.02	This study
MMCP-6	1405 ± 73	7.2	0.22 ± 0.02	This study
MMCP-10	1805 ± 98	5.6	0.26 ± 0.01	This study

Adsorption is a key performance metric for adsorption, but equally important for value-added products is desorption. This has been accomplished for ABE component recovery by thermal methods. The custom apparatus designed to facilitate thermal desorption is detailed in Figure 2.13. By heating the MMCPs under vacuum, the solvents are volatilized by order of boiling point following bulk phase water removal. The ABE components are then captured in the cold trap at higher concentrations.

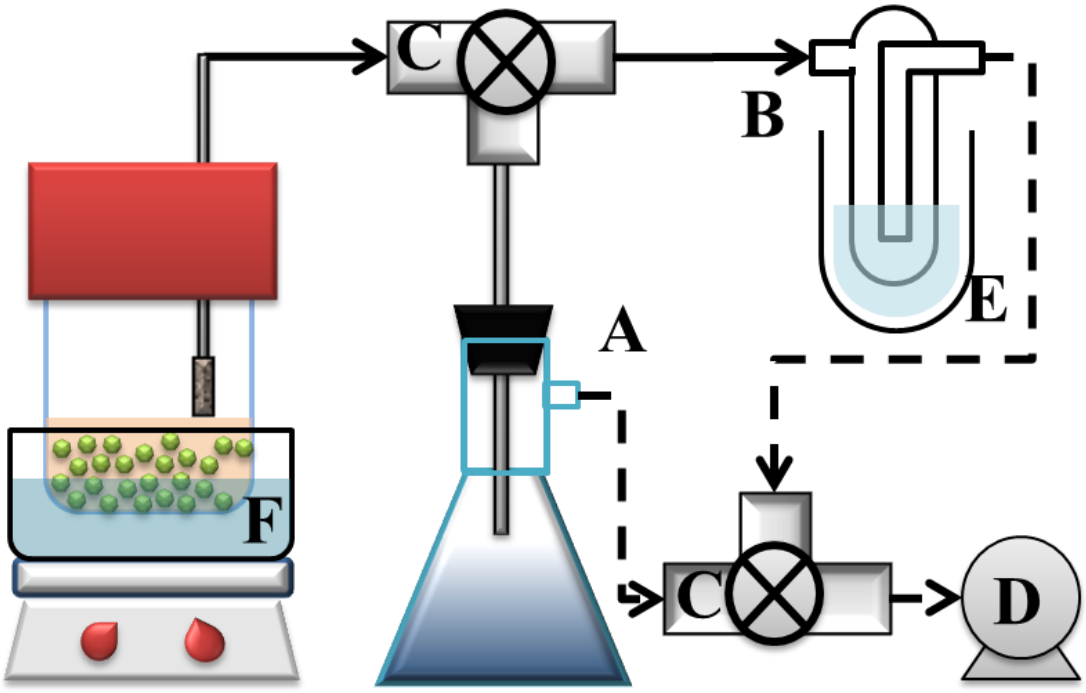

Figure 2.13. Apparatus Used for Butanol Desorption and MMCP Regeneration. Following adsorption equilibration, the bottle containing the crudely dried MMCP sample was fitted with a chromatography cap through which nylon tubing was passed. Said tubing was connected to a solvent bottle filter which was then submerged into the aqueous slurry. A series of 3-way valves (C) were used to direct flow either through (A) a vacuum flask (for bulk aqueous retrieval), or (B) a glass cold trap (E) submerged in an acetone/dry ice mixture (for vapor condensation), both of which were connected to vacuum pump (D). Following removal of the bulk aqueous solution, crudely dried MMCP samples were heated in a water bath (F).

Another means of physical characterization is X-ray Diffraction (XRD), which provides information about crystallinity. Figure 2.14 reveals 2 peaks for crystallinity, which accounts for the mostly uniform carbon matrix and the disrupted carbon matrix loaded with Ni nanoclusters. Because the two carbon structures are distinct, there are only two corresponding structural peaks for the carbon.

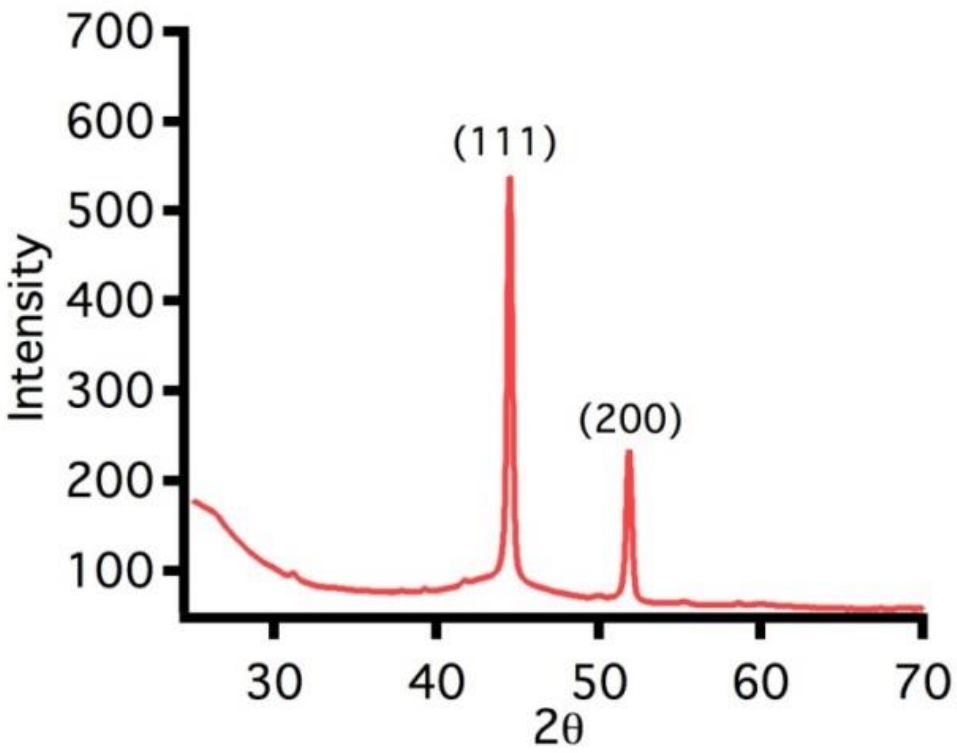

Figure 2.14. XRD Profile of MMCP-10.

Structural details of adsorbents partially determine the recovery performance, however the adsorption data will conform to different equilibrium models depending on the most reasonable mechanism. This system conforms to physisorption (reversible surface attachment) rather than chemisorption (surface reaction). To verify this, additional equilibrium isotherm models were applied including dual site Langmuir. Figure 2.15 compares the dual-site Langmuir and Freundlich isotherms. While the red lines are seemingly a good fit, the dual-site Langmuir presumes surface features for the adsorbent which are not consistent with the measured adsorption performance. The dual-site model assumes that the adsorbent has distinct surface sites with notably different adsorption energies and therefore loading capacities.

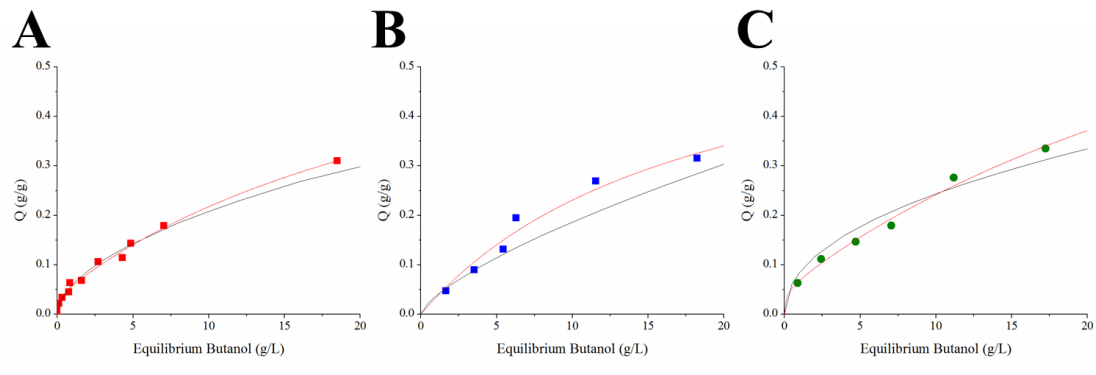

Figure 2.15. Additional Adsorption Model Fits. Comparing the Dual Site Langmuir (red line) and Freundlich (black line) fit for butanol adsorption onto A) MMCP-4, B) MMCP-6 and C) MMCP-10.

Other environmental impacts on adsorption performance are important to consider in a well-rounded study. For this study, the effects of pH and temperature were examined and the results are represented in Figure 2.16. For the biologically relevant pH range of 4-10, there is little effect on adsorption performance. Likewise in the narrow biologically relevant temperature range, there is no discernible effect on adsorption performance. Likely if the pH and temperature range were shifted farther outside the biologically relevant ranges there would be more prominent effects.

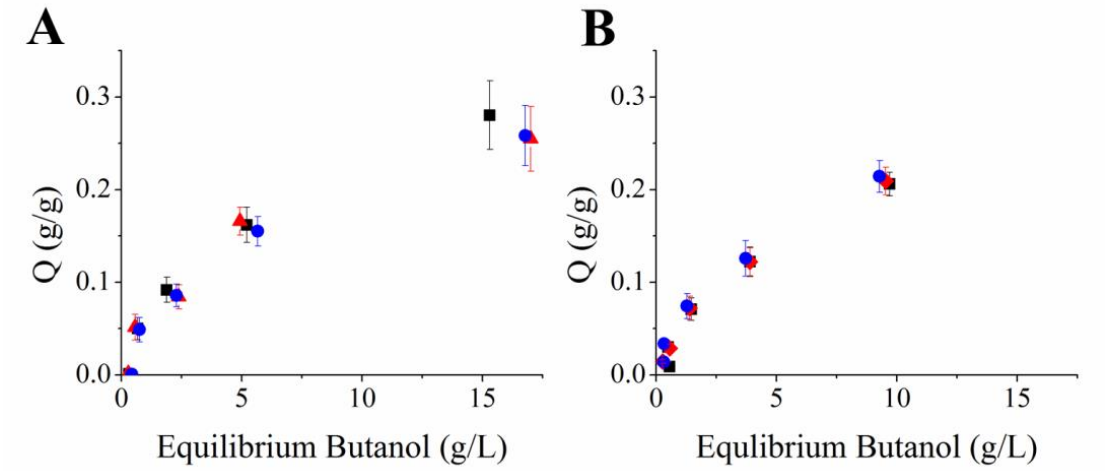

Figure 2.16. Other Isotherm Factors. Butanol adsorption by MMCP-10 as a function of A) pH: 4 (squares), 7 (triangles) and 10 (circles), and B) temperature: 25^{o}C (squares), 32^{o}C (diamonds) and 37^{o}C (circles).

Like desorption, an adsorbent's separability from culture is an important design consideration when recovering a value-added product. Figure 2.17 compares the magnetic response of varied Ni composition within the MMCPs. The important to note that the total retrieved fraction for each composition is proportional to the Ni content. Each retrieval gathers more MMCP mass with a diminishing return such that the 5th retrieval is essentially complete recovery.

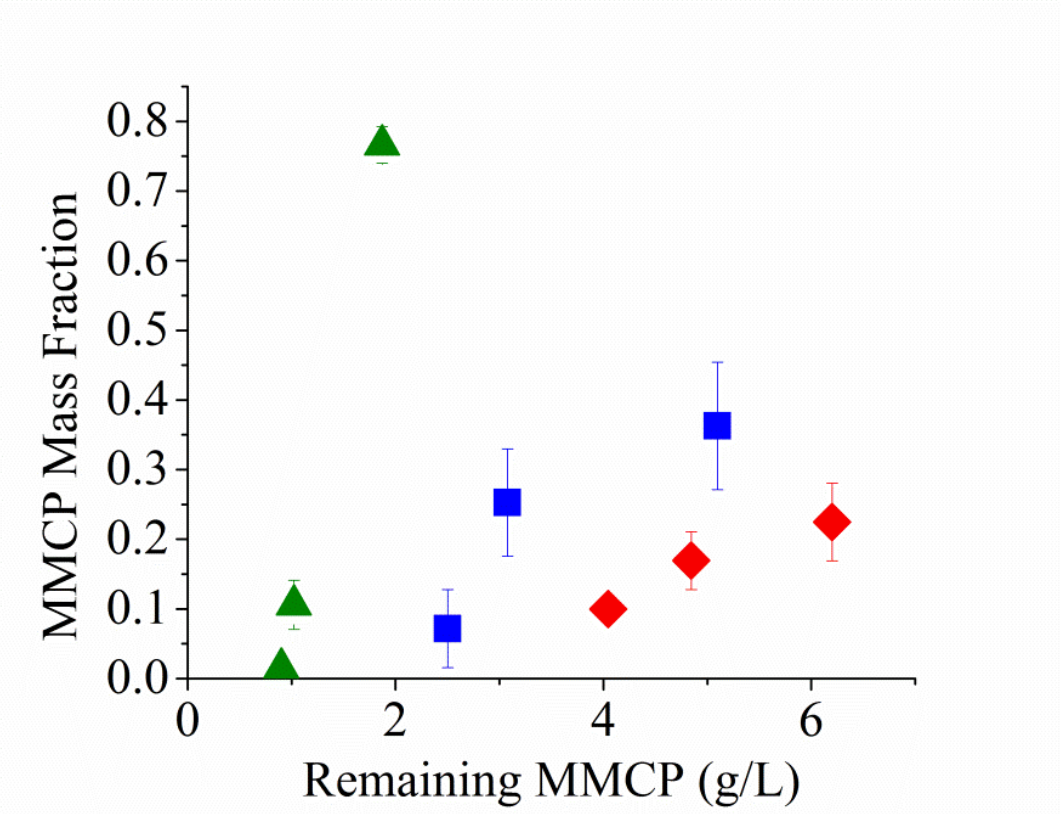

Figure 2.17. Fractional Recovery of MMCP. Fraction of MMCPs retrieved versus the concentration remaining in suspension as determined for MMCP-4 (diamond), MMCP-6 (square) and MMCP-10 (triangle) as obtained for a series of three sequential retrievals.

The final, though important aspect of adsorbent performance is presented in Figure 2.18. When designing a recovery system based on adsorbents for value-added products, there will be a final stage where products are recovered and adsorbents are regenerated. Accordingly, it is important to measure the repeatability of use for the adsorbent. The MMCPs performed consistently for 5 regeneration/reuse cycles.

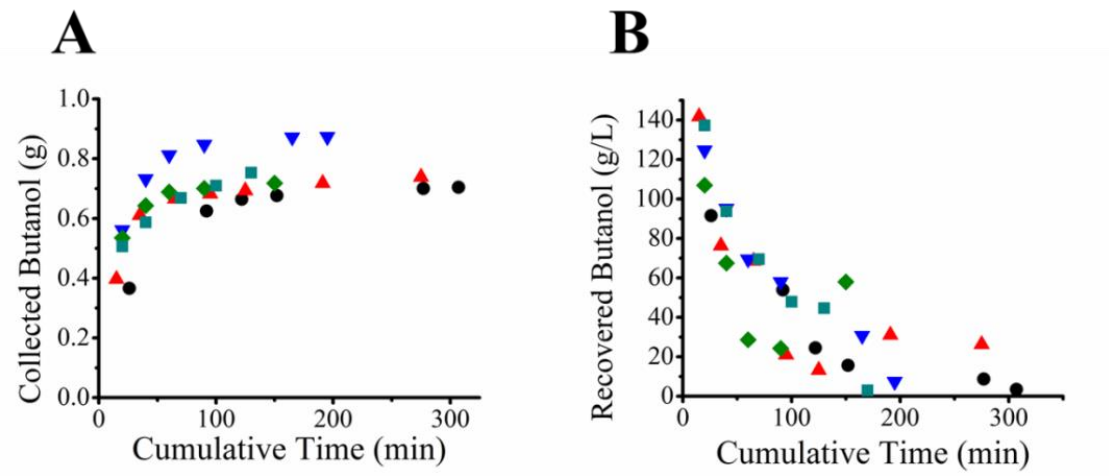

Figure 2.18. Multiple Adsorption/Desorption Cycles. Characterizing the repeated reuse and performance of regenerated MMCP-4 over the course of 5 consecutive adsorption-desorption cycles. Compared are A) the cumulative evolution and collection of butanol and B) the instantaneous concentration of butanol in the collected condensate (i.e., per each 30-60 min treatment duration) obtained throughout a series of 5 sequential adsorption-desorption cycles. The legend is as follows: cycle 1 (circles), cycle 2 (triangle), cycle 3 (inverted triangle), cycle 4 (diamonds) and cycle 5 (squares).

CHAPTER 3

3.0 LIGNOCELLULOSIC BIOMASS DERIVED ETHANOL PRODUCTION FROM PRETREATMENT BY MAGNETICALLY RESPONSIVE MESOPOROUS CARBON ADSORBENTS

Abstract

The selective capture and recovery of furfural from model biomass hydrolysate mixtures was investigated using magnetic mesoporous/microporous carbon powders (MMPCs), with the objective of detoxifying the feedstock and facilitating ethanol fermentation by *Escherichia coli*. The mesoporous structure and high surface area of these carbons promotes rapid loading of furfural (~5.1g/L-min) resulting in high selectivity, while magnetic functionalization of carbon adsorbents promotes their facile separation from media during pretreatment up to 91% within 15 minutes. *E. coli* ethanol production compared well between furfural-free (up to 64.2 g/L) and pretreated model hydrolysates (up to 62.8 g/L). MMCPs are retrievable by magnetic column up to 91% by mass. Desorption of furfural from magnetic mesoporous carbons reached ~57% by thermal means, facilitating their re-use. Moreover, this recovery of furfural converts an otherwise waste stream toxin to a valuable byproduct to the fermentation of ethanol from lignocellulose-derived feedstock. This approach with novel magnetic mesoporous carbons shows great promise in efficient treatment of real hydrolysates without stripping the high value fermentable sugars.

Keywords: furfural; *in-situ* recovery; mesoporous carbon; magnetic; bioproduct

This work is being prepared as a manuscript for submission to Green Chemistry with the following authorship: Staggs, K., Flores, A., Qiang, Z., Xia, Y., Wang, X., Vogt, B., and Nielsen, D. R.

3.1 Introduction

Renewable bioproducts such as ethanol can be produced from numerous biomass feedstocks (Gaykawad et al., 2013; Pfromm et al., 2010), which also determines the bulk of the production cost. (Pfromm et al., 2010) Corn-derived feedstock is composed of starches readily hydrolyzed to glucose with no toxic byproducts compared to lignocellulose-derived biomass but is more expensive. (Pfromm et al., 2010) Lignocelluolsic biomass has been well evaluated as the most cost effective bioproduct feedstock. (Garcia et al., 2011; Gaykawad et al., 2013; J. Li et al., 2011; Congcong Lu et al., 2013; Machado et al., 2016) Hydrolysis of lignocellulosic biomass forms cytotoxic feedstocks requiring extensive pretreatment before fermentation to valuable bioproducts, further adding to process costs and limiting the economic feasibility of biofuels.(Balan, 2014; Dalecka et al., 2015; P. Kumar, Barrett, Delwiche, & Stroeve, 2009; J. Li et al., 2011) Among the most cytotoxic constituents of lignocellusolic hydrolysate, furfural content varies widely depending on the hydrolytic protocol used (Jonsson & Martin, 2016), e.g.: 0.5g/L (Parajo et al., 1996), 1.75 g/L (Y. Zhang et al., 2015), 0.22 g/L (Jonsson & Martin, 2016), and 3.8 g/L (Larsson et al., 1999). Furfural is toxic at or below 2 g/L to *E. coli*. Other inhibitors are also formed from hydrolysis such as acetic acid, phenolics and other furans.(K. Zhang, Agrawal, Harper, Chen, & Koros, 2011) The focus of this work however is the capture and recovery of furfural from the model hydrolysates as it is often the most highly concentrated cytotoxin.

It is known that separation of low concentration compounds relative to commercial production (e.g. bioalcohol at more than 100g/L) is more energy intensive and costly. (N. Qureshi, Hughes, et al., 2005a) Furfural at no more than 4 g/L is

considered a low concentration separation. Furfural has been removed from model and real hydrolysates by adsorption onto activated carbon (S. C. Lee & Park, 2016; Sulaymon & Ahmed, 2008; K. Zhang et al., 2011), charcoal (Parajo et al., 1996), XAD-4 resins (Weil et al., 2002), and D141 resins (Jia et al., 2015). Other furfural separation techniques such as distillation are not suitable due to furfural's high boiling point. (Brownlee & Miner, 1948) Pervaporation of furfural by polydimethyl siloxane (Hu et al., 2015) and polyurethaneurea (Ghosh, Pradhan, & Adhikari, 2007, 2010) has also been evaluated. With furfural flux up to 3.9 g/m^2-h pervaporation can separate 10g/L feed, concentrating furfural up to ~54 wt%.(Ghosh et al., 2007) While greater flux and selectivity are possible by pervaporation, furfural caused membrane swelling and decreased separation factor. As furfural is not the only phenolic compound present in a real hydrolysate, it is likely the separation factor would be greatly reduced compared to furfural/water feed from industrial waste streams. By contrast, typical adsorbents such as activated carbon and polymeric resins have a lesser effective separation factor (up to 0.5 g/g at 50C by XAD-7 resins (Weil et al., 2002), ~0.37 g/g for activated carbon (Sulaymon & Ahmed, 2008)) and are not readily separable from aqueous slurries without the use of gravity settlement, filtration, or isolation in a packed column.(Sulaymon & Ahmed, 2008; K. Zhang et al., 2011) This is particularly challenging for bacterial cultures because of the toxicity of activated carbons, specifically that of carbon nanoparticles.(Karnib, Holail, Olama, Kabbani, & Hines, 2013)

To address these limitations, magnetically-responsive mesoporous carbons have been previously fabricated and evaluated for butanol recovery (a similarly oleophilic compound) in Chapter 2. The promising butanol recovery performance suggests furfural

loading should be similarly efficient with rapid kinetics. Importantly, furfural selectivity is desired for pretreatment such that the core saccharides are not stripped, decreasing the economic value of the feedstock. Meanwhile, although not typically removed from the adsorbent following its separation, if it could be efficiently recovered, furfural could itself serve as a value-added biochemical co-product, with uses as a precursor to resins, adhesives, solvents and flavoring agents (note: there is presently no known synthetic route for furfural production and it is exclusively produced from natural pentoses such as xylose).(Machado et al., 2016) It is therefore desirable to not only separate furfural during pretreatment, but to isolate it in higher concentration as a secondary product.. Accordingly, this work seeks to evaluate: A) the sorption performance of furfural, B) furfural pretreatment viability from model hydrolysates, C) ethanol production from pretreated vs untreated model hydrolysates, D) furfural recovery potential by thermal desorption.

3.2 Materials and Methods

3.2.1 MMCP Characterization

Detailed characterization of the MMCPs has been previously reported in Chapter 2. Virgin MMCP were mounted on carbon tape adhered to pin stubs and either gold or carbon sputter coated using a Technics Hummer V sputter coater (Anatech, Union City, CA). The sputter coating chamber was evacuated by vacuum and filled with argon gas with the flow rate maintained such that the chamber pressure was maintained at 100-125 mTorr. Substrates were sputter coated for 5 minutes maintaining approximately a 7-10

microamp current. Imaging was performed on a JEOL JSM6300 Scanning Electron Microscope (Peabody, MA) at 15 kV.

3.2.2 Adsorption Isotherm Studies of Furfural

Adsorption performance was determined using 22 mL glass scintillation vials loaded with 100 mg MMCP suspended in 2 mL aqueous solution. Whereas preliminary isotherms were constructed for binary solutions (i.e. furfural/water) coadsorption isotherms with furfural and simple sugars were also constructed. Initial furfural concentrations ranged from 0.1-10 g/L. The exact concentration of furfural in a lignocellulosic hydrolysate is both batch and process condition dependent.(Machado et al., 2016) Model hydrolysate was composed of glucose and xylose in 50/50 ratio ranging from 2-50 g/L with furfural concentrations ranging from 0.4-10 g/L.

Following overnight equilibration at 37 °C overnight while mixing on an orbital shaker, 1 mL aliquots were drawn for analysis by high-pressure liquid chromatography (HPLC; Agilent 1100 series; Santa Clara, CA) equipped with both diode array and refractive index detectors. Separation of binary solutions were separated on an Aminex HPX-87H anion exchange column External standards were developed for furfural, glucose, xylose as calibrations. Equilibrium adsorption capacity (Q_i) of each analyte *i* was calculated from the following mass balance:

$$Q_i = \frac{(C_{i,0} - C_i)V}{m} \tag{3.1}$$

where $C_{i,0}$ and C_i are the initial and equilibrium aqueous concentrations of analyte i, V is volume, and m is mass of MMCP. Adsorption data were fit by the Freundlich model as follows:

$$Q_i = k_{f,i} C_i^{1/n_i} \quad (3.2)$$

where Q_i is the equilibrium adsorption capacity of species i, $k_{f,i}$ and n_i are the Freundlich constant and exponent, respectively.

3.2.3 Closed Loop Magnetic Retrieval of MMCPs

Retrieval of MMCPs was accomplished by column retrieval (Figure 3.1). Two identical columns were prepared. A peristaltic pump was used to circulate the aqueous solutions through the magnetic column. Solutions were drained and the magnetic core was removed from the inner tube. MMCPs were rinsed off the inner tube with deionized water for subsequent regeneration. For 300 mL of aqueous volume, approximately 9 g of MMCP was suspended and magnetically stirred in a 500 mL vessel. When pretreating model hydrolysates, the MMCPs were added to the media from an autoclaved slurry and stirred to equilibration for 15 minutes. The slurry was then pumped through silicone tubing and a retrieval column both sterilized by autoclave. Media was drained into the reactor vessel and the column was recovered as described above.

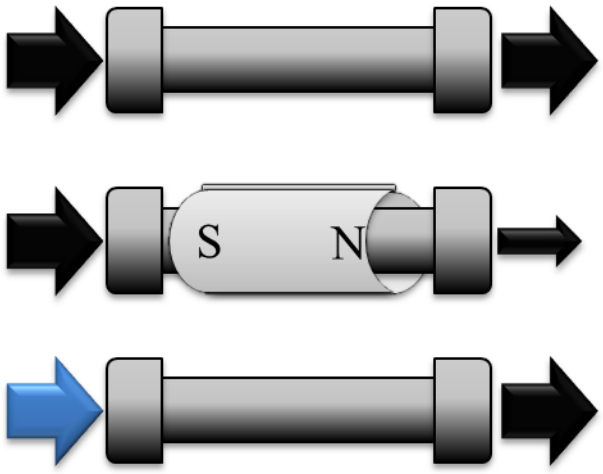

Figure 3.1 Closed Loop Magnetic Retrieval. Column with carbon slurry (top), magnetic capture (middle), carbon flush with DI water (bottom).

3.2.4 Desorption of Adsorbed Furfural from MMCPs

Recovery of adsorbed furfural was accomplished by comparing two recovery modes. For each study, approximately 4 g of MMCPs were suspended in approximately 200 mL of 10 g/L furfural and equilibrated for 3 hours at 37°C. The first recovery mode was solvent washes with DMSO, chosen for the high solubility of furfural compared to other solvents.(K. Zhang et al., 2011) Each DMSO wash was diluted by a factor of 10 before 1 mL aliquot was drawn for analysis by HPLC as described above. For the second mode, thermal desorption of furfural was investigated. Supernatant was extracted by a stainless solvent bottle filter and the partially dried MMCPs were heated to 95°C in a water bath under vacuum (77 kPa below ambient). A cold trap with an acetone/dry ice mixture collected the evolved enriched furfural/water mixture. Within 30-60 minute intervals, the cold trap was occluded with solidified product, and the cold trap was

thawed. 1 mL aliquots were analyzed by HPLC using methods described above. For both modes of recovery, a total of 5 ‘cycles’ were repeated.

3.2.5 Assessing MMCP Biocompatibility

Seed cultures of *E. coli* LY180 (L.P. Yomano et al., 1998; H. Zheng, Wang, Yomano, Shanmugam, & Ingram, 2012) were prepared by inoculation in 5 mL of Luri-Bertani broth (LB; Thermo Fisher Scientific, Waltham, MA), incubated overnight in a shaking incubator at 32°C. MMCPs were added to the culture tubes at the following concentrations: 0, 4, 8, 20, 40, 80, 120, and 160 g/L. From these culture tubes, 100 µL aliquots were added to 900 µL DI water and cell density was determined by optical density (OD600) at 600 nm using a DU800 spectrophotometer (Beckman Coulter, Brea, CA). Biocompatibility was further studied by growing LY180 with 30 g/L MMCPs in culture tubes. MMCPs were drawn up by pipette and deposited on carbon tape mounted to pin stubs for SEM imaging. After air drying, the SEM preparation was followed as described above. Sputter coated samples were also imaged at 15 kV.

3.2.6 Fermentation of Pretreated Model Hydrolysates

Seed cultures of *E. coli* LY180 were grown in culture tubes as described above. Seeds were added to a 250 mL media bottle with a 50 mL working volume at 2% inoculum by volume with the following media composition: ammonium phosphate (dibasic 26.3 g/L, monobasic 8.7 g/L) 5mL, 500 g/L Xylose 12 mL, 200 g/L Glucose 7 mL, 1M MOPS 5 mL, trace metals 0.075 mL, 1M Mg 0.075 mL, 1M KCl 0.05 mL, Betaine 0.05 mL and the balance sterile DI water. Media components were filter sterilized rather than autoclaved. This high total sugar content was consistent with that of

other studies with LY strains of ~140 g/L.(L.P. Yomano et al., 1998) For cultures with MMCP pretreatment, furfural was added to the media to raise the aqueous concentration to 3g/L, above the toxicity threshold for *E. coli*. MMCPs were added to the media at ~50 g/L and equilibrated for 1 hour before being passed through the magnetic retrieval column. With the majority of the MMCPs captured magnetically, the finer MMCPs were separated by sterile vacuum filtration. This served to 1) sterilize the pretreated media, 2) enable comparison of growth by OD600 without optical interference from the MMCPs. Media bottles were topped with septa caps and custom ¼" thick butyl rubber discs to allow syringe sampling and maintain anaerobic conditions. Cultures were grown at 37°C in a shaking incubator at 160 rpm with samples taken every 24 hours up to 72 hours. Samples were centrifuged before analysis of the 1 mL aliquots by HPLC as described above.

3.3.0 Results and Discussion

3.3.1 Aqueous Furfural Adsorption from Model Solutions

It well known that 'oily' or 'greasy' contaminants are the most difficult to isolate from water (S. Kang & Choi, 2005; Pintor, Vilar, Botelho, & Boaventura, 2016) and furfural is an oleophilic substance with low water solubility. Adsorption behavior for furfural pretreatment was assessed first by adding MMCPs to cell-free, binary furfural/water mixtures. As seen in Figure 3.3, the specific loading of furfural on MMCP exceeded 0.42 g/g when equilibrated with a solution containing 2.8 g/L residual furfural. Below the 1 g/L where increasingly robust cell growth occurs, loading exceeds 0.18 g/g at 0.84 g/L residual furfural. This adsorption performance compares well to commercial granular activated carbon Norit-1240, whose maximal adsorption capacity was reported

to reach as high as 0.28 g/g at ~4g/L residual furfural.(K. Zhang et al., 2011) XAD-4 resins have reported adsorption as high as 0.09 g/g at ~2.1 g/L residual furfural.(Weil et al., 2002) As a more complete comparison, Figure 3.2 further compares adsorption isotherms of MMCP with that of Norit-1240, as reported by Zhang *et al*.(K. Zhang et al., 2011) As can be seen in Figure 3.2, at concentration below 1 g/L the adsorption performance of MMCPs is directly comparable to that of Norit 1240. Some of the difference may be due to MMCPs surface area of ~1800 m^2/g approximately 1.5-fold that of Norit-1240 (reported as 1175 m2/g).(Yapsaklı et al., 2009)

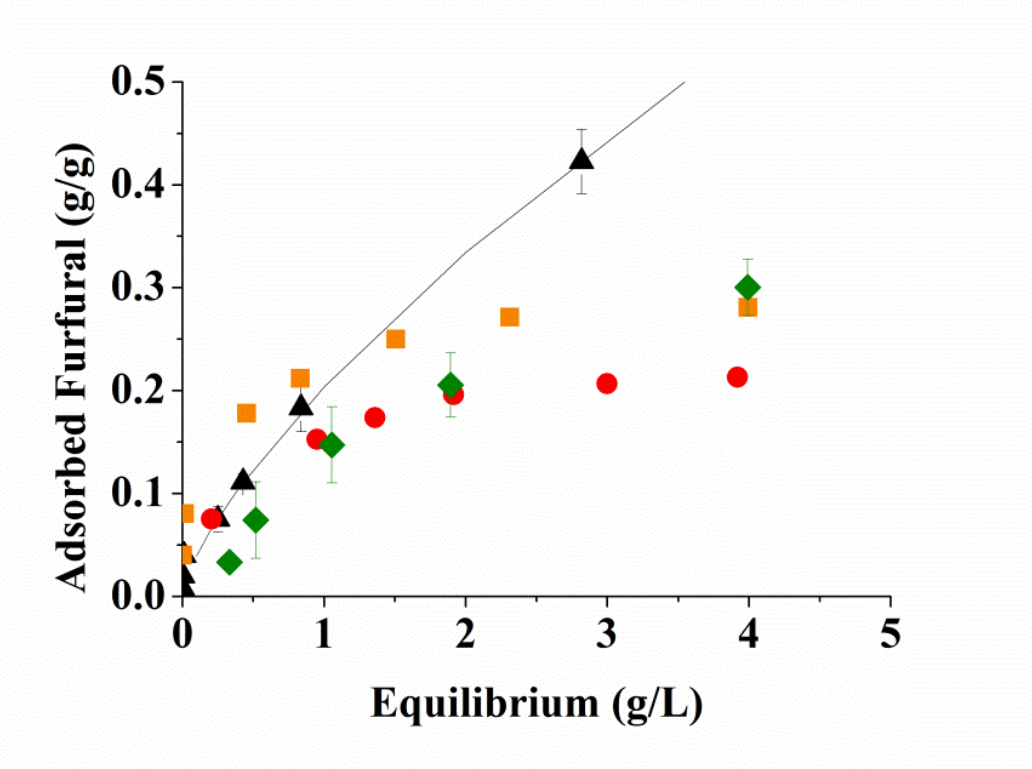

Figure 3.2 Equilibrium Isotherms. Furfural adsorption from binary furfural/water (triangles), furfural adsorption from model hydrolysate (diamonds), furfural/water adsorption on Norit 1240 (squares) and furfural/ethanol/water adsorption Norit 1240 (circles) (K. Zhang et al., 2011),

Meanwhile, the furfural adsorption results for MMCP were furthermore fit to several common isotherm models, in this case including the Langmuir, Dual-Site Langmuir, and Freundlich models. Langmuir was unable to fit the data reasonably well with a residual of ~0.65. The Dual-Site Langmuir was also a poor model for the adsorption behavior with a residual of ~0.72. The residual for the Freundlich model by contrast was ~0.997. The Freundlich fit parameters are presented in Table 3.1 along with previous results for butanol from Chapter 2 for comparison of a similarly hydrophobic analog. The Freundlich constant pertaining to loading is greater for furfural compared to butanol. This is consistent with the approximately 2 fold greater loading capacity for furfural over butanol at comparable residual concentrations. Given the log Kow ~0.47 compared to butanol ~0.88 the adsorption behavior onto a given substrate should be comparable.(D. R. Nielsen et al., 2010) The predominant adsorption mechanism is physisorption rather than chemisorption, supported by the estimated Gibbs energy of adsorption presented in Table 3.1. The small negative values are known to be consistent with the reversible attachment of physisorption (D. R. Nielsen et al., 2010), also presented in Chapter 2. It is also worthy of note that ethanol does adsorb but to a far lesser degree as seen in Table 3.1.

Table 3.1

Freundlich Isotherm Model Fit Parameters.

Compound	k_f (g/g)	n	ΔGads (kJ/mol)
Butanol	0.085	2.20	-5.38
Ethanol	0.006	1.19	-2.92
Furfural	0.204	1.40	-3.45

3.3.2 Characterizing Adsorption Kinetics of Furfural from Binary Solutions

Beyond initial adsorption capacity, the rate of adsorption is key performance metric. Whereas high adsorption loading is preferable for in situ adsorption, pretreatment benefits from rapid sorption kinetics. Rapid adsorption during pretreatment reduces the contact time for potential adsorption of valuable sugars onto the adsorbent.(S. C. Lee & Park, 2016) Equilibrium loading of furfural was reached within approximately 8 minutes compared to ~30 minutes for butanol presented in Chpater 2. Figure 3.3C illustrates the rapid equilibration between furfural and MMCPs compared to activated carbon Norit-1240. (K. Zhang et al., 2011) While both reach full equilibration at approximately 8-10 minutes, MMCPs have a greater than 80% loading fraction very rapidly at ~1 minute. Some of this performance may be due to the MMCPs being milled by hand using mortar and pestle to an average 4.8 um diameter with polydispersity index of 0.8 compared to the large granules of Norit-1240.(K. Zhang et al., 2011) The average MMCP pore diameters of 5.4 nm as discussed in Chapter 2, is greater than the ~42% of pores <2 nm with ~31% >50 nm of Norit 1240. The regularity of pore structure in MMCPs promotes rapid adsorption of furfural as it did for butanol in Chapter 2.

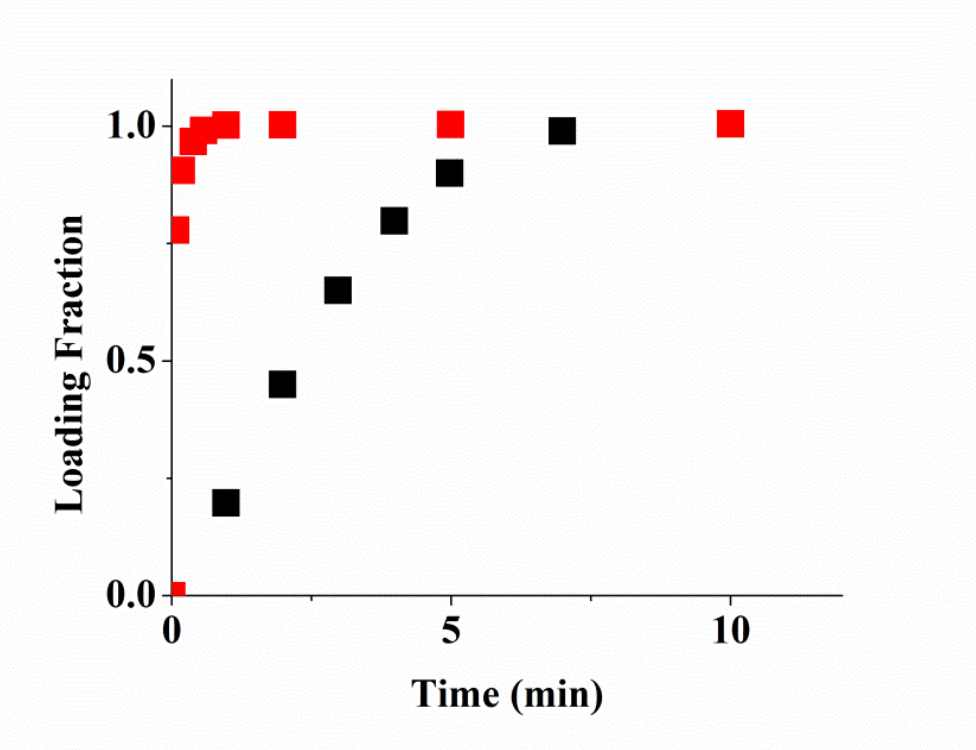

Figure 3.3 Equilibrium Kinetics from Binary Solutions. Comparison of furfural adsorption kinetics from this study (red squares) and Norit 1240 carbon (black squares),(K. Zhang et al., 2011)

3.3.3 Competitive Adsorption of Furfural

Adsorbents are known to have somewhat reduced loading capacity of a target analyte from complex media backgrounds compared to binary solutions because of competitive adsorption. (Staggs et al., 2017; Wiehn et al., 2014) For this study, model solutions included 60 g/L glucose and 25 g/L xylose with 3 g/L furfural to evaluate sugar effects on furfural adsorption. An example composition of a real hydrolysate which we intend to utilize in a follow up study following successful implementation of MMCP pretreatment is given as follows (all values in g/L): 11.2 cellobiose, 5.4 glucose, 58.8 xylose, 5.9 galactose, 7.4 arabinose, 0.7 mannose, 2.5 hydroxymethyl furan (HMF), 3.6

furfural. The competitive adsorption results of this can be seen in Figure 3.4 where residual glucose and xylose mass change by 1.8% and 3%, respectively. With glucose, xylose and ethanol present, there is a reduced loading capacity for furfural as seen in Figure 3.2 by an average of 32% across the range of the isotherm. Ethanol also reduced the loading capacity of Norit 1240 by approximately 24% across the range of the isotherm because of competitive adsorption. (K. Zhang et al., 2011)

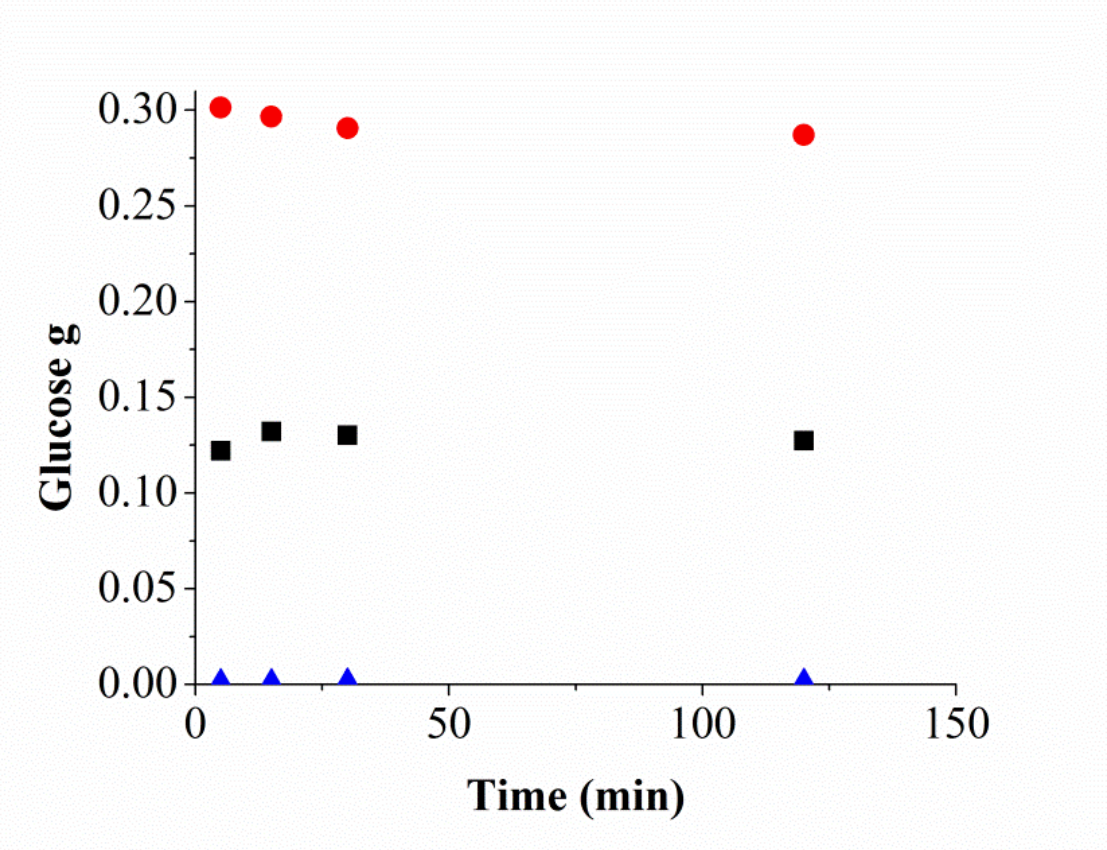

Figure 3.4 Equilibrium Kinetics from Complex Solutions. Equilibrium mass of residual aqueous furfural (triangles), Glucose (circles) and xylose (squares) mass vs time.

3.3.4 MMCP Magnetic Retrieval

In conventional applications, activated carbon adsorbents must be removed by means of filtration, with its requisite low vacuum and surface area dependence.(Balan, 2014; Dalecka et al., 2015; P. Kumar et al., 2009) Commonly activated carbons are isolated in a packed adsorption column, rather than added to aqueous slurry.(S. C. Lee & Park, 2016; Sulaymon & Ahmed, 2008; K. Zhang et al., 2011) We previously demonstrated the magnetic retrieval of MMCPs for retrieval from aqueous slurries, achieving up to 89% retrieval using a submersible magnetic device as discussed in Chapter 2. Compared to the previous magnetic retrieval mechanics presented in Chapter 2 using a simplified magnetic core, column retrieval is more readily scalable to larger process volumes. Efficiency of MMCP retrieval by column was evaluated by circulating an aqueous slurry through the column depicted in Figure 3.5. The same mass and volume as the cultures were used to study retrieval efficiency. The retrieval column was designed such that the MMCPs could be captured in a concentric ring as depicted in Figure 3.5A by modeling the magnetic flux in a cross section of the column shown in Figure 3.5B. According to the model, the magnetic field strength within the observed MMCP collection boundary is between 0.1-0.2 Tesla. After 15 minutes of circulation, the column was found to be equilibrated with the slurry as indicated by solution leaving the column changing visibly from dark slurry to a less turbid, translucent solution. Inside the column, the stages of magnetic retrieval were captured from the empty column (Figure 3.5C), to 15 minutes after circulation with the magnetic clamp in place (Figure 3.5D) and after release of the magnetic clamp (Figure 3.5E). The mass of air dried MMCPs retained in the column represented ~91% retrieval by mass; similar to the ~89% retrieval we obtained using the previously-developed, submersible magnetic device in Chapter 2.

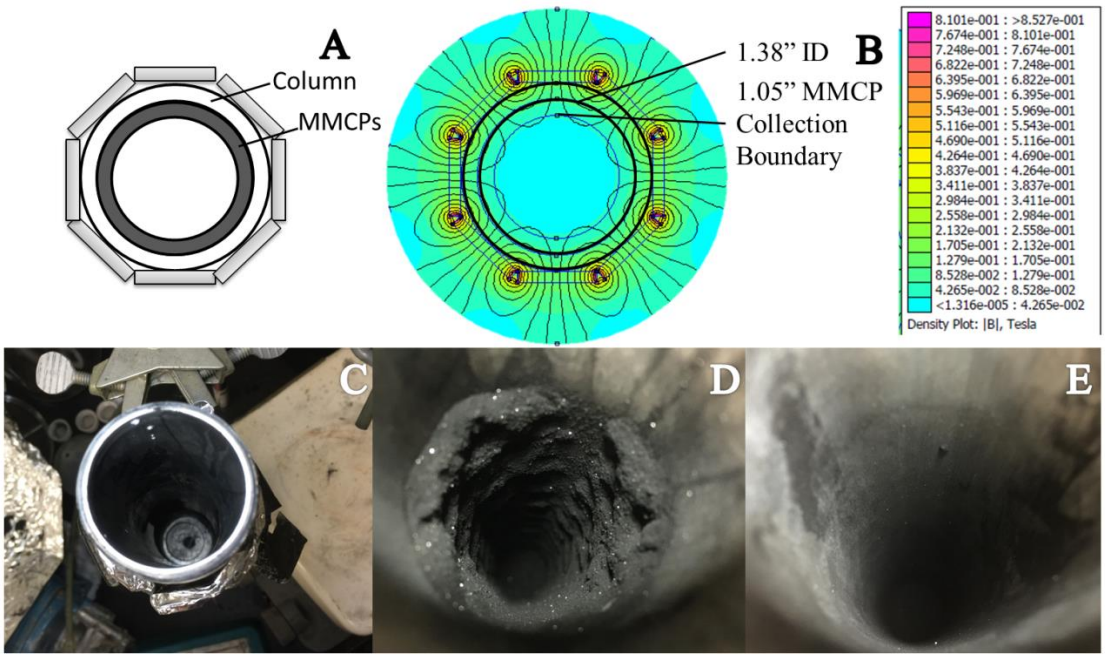

Figure 3.5 Magnetic Retrieval Column. A) Cross section of magnetic retrieval column, B) Finite element analysis of magnetic flux within the column. C) Column before carbon slurry. D) Column after magnetic capture. E) Column immediately following magnetic release.

The collection boundary modeled in Figure 3.5B corresponds to a retrieval surface area requirement of 0.0026 m^2/g of MMCP. This collection boundary for the MMCPs is visible in (Figure 3.5D). Based on the MMCP collection results, the limiting factor for MMCP retrieval is the strength of the magnetic field at a given distance from the column's inner wall. A longer column of the same design or one of greater diameter would not have an appreciably greater MMCP retrieval. The surface area required for retrieval is determined by the thickness of the film which is determined by the magnetic flux. Stronger magnetic force from stronger or thicker magnets could reduce the required

area for retrieval. Importantly, other geometries for magnetic retrieval were modeled beginning with the magnetic retrieval tool from Chapter 2. This column design with its removable magnetic clamp was determined to be the most efficient, given the type and polarization direction of the magnets. Rotation of 90 degrees in the direction of polarization would cease magnetic retrieval within the column, and is thus an important design consideration for a magnetic retrieval system.

3.3.5 Desorption and Recovery of Furfural from MMCPs for Regeneration

With the demonstrated adsorption and removal of furfural from aqueous solutions, the subsequent step for process viability was to evaluate furfural desorption and recovery as a potential value-added co-product. A first principles approach to product recovery from adsorbents often relies on the solubility of the adsorbed species in a readily available solvent such as short chain alcohols, or apolar alkanes. (Eom et al., 2013) Of several solvents studied for furfural recovery from activated carbon by Zhang *et al* DMSO was one of the most efficient, though their study ultimately used 7.5 wt% ethanol, resulting in a 42% recovery by mass compared to water at only 5% desorption.(K. Zhang et al., 2011) Accordingly, DMSO was selected as the solvent for furfural recovery for this study for comparison to thermal recovery. DMSO was equilibrated with the MMCPs in several fractions. The first DMSO/furfural fraction was visibly tinted an amber color indicating solubilized furfural and recovered 32% of the adsorbed furfural as seen in Figure 3.6A. Subsequent DMSO fractions were progressively less turbid and nearly clear after the 5^{th} fraction, where a meager 1.4% of furfural was recovered. In total, 66% of the adsorbed furfural was recovered by DMSO.

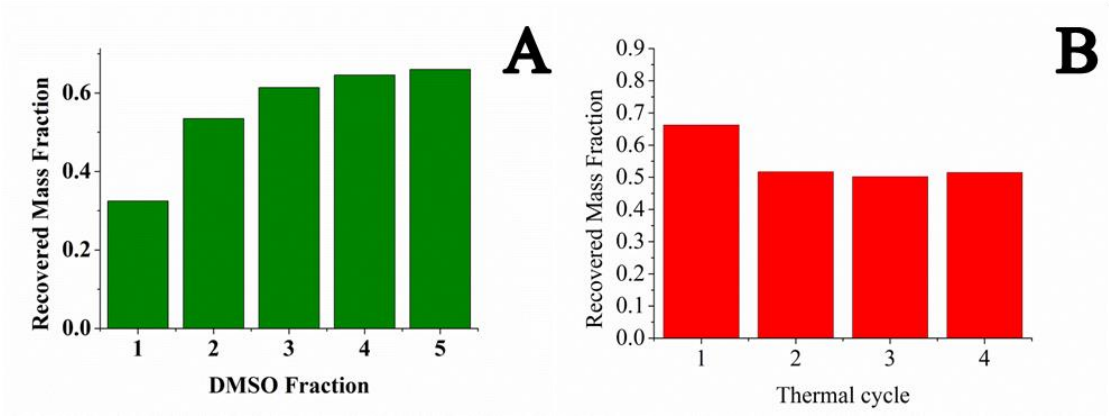

Figure 3.6 Solvent vs Thermal Recovery of Furfural. A) Mass fraction of furfural recovered by DMSO. B) Mass fraction of furfural recovered by thermal desorption.

Other hydrophobic compounds such as butanol have previously been recovered from MMCPs up to 99.7%. Butanol has also been recovered from other adsorbents such as resins by thermal treatment. (Eom et al., 2013; Wiehn et al., 2014) Some implementations of thermal desorption take the form of steam or gas stripping (Nongonierma et al., 2006; N. Qureshi, Hughes, et al., 2005a), while others use heat and vacuum.(D. R. Nielsen & Prather, 2009; Wiehn et al., 2014) For this study a fresh batch of MMCPs were equilibrated with ~3 g/L furfural for ~30 minutes, at which point equilibrium has been achieved according to kinetic results. Adsorbed furfural was recovered by heating to 95 $^{\circ}$C under vacuum while evolved vapors were captured in a cold trap acetone and dry ice as in Chapter 2 (apparatus depicted in Figure 2.13). Another 20 mL aliquot of ~3 g/L furfural was added to the same powder, which was then allowed to equilibrate before thermal regeneration was again performed. This process was repeated for a total of 4 loading-regeneration cycles to demonstrate both reproducibility as well as the reuse potential of the MMCPs. The cycle results are presented in Figure 3.6B where the thermal regeneration cycle numbers represent two fractions from 0.5 and

1 hour thermal desorption (e.g. 1 and 1.5 are the first cycle samples from 0.5 and 1 hour, 2 and 2.5 are the 0.5 and 1 hour samples from the second cycle, etc.). Each time, the specific loading at equilibrium was approximately ~0.05-0.06 g/g MMCP, indicating that adsorption behavior was not deteriorating or otherwise changing with repeated use. Thermal desorption in this study followed a similar pattern to solvent recovery, reaching ~31% and ~55%, recovery at 30 and 60 minutes, respectively. Thermal desorption results are displayed in Figure 3.5B wherein the accumulation of furfural reached 55 wt%. The recovered fraction consisted of a 3-6 g/L furfural, an up to 2-fold enrichment over the initial aqueous concentration and a ~49-fold enrichment over equilibrium concentration. This corresponds to an approximate release rate of ~4.4g/L-h. Overall, 55% of adsorbed furfural recovery from toxic feedstocks was observed, which does not match the 66% recovered by solvent extraction by DMSO. This result compares less favorably however, to the 83% recovery of butanol from resins by thermal means.(Wiehn et al., 2014) The repeatable recovery of furfural demonstrates successfully the simultaneous detoxification of a low-cost feedstock and its enriched recovery as a viable value-added byproduct.

3.3.6 Examining MMCP and Furfural Growth Inhibition

In Chapter 2, biocompatibility of MMCPs was established by growth of *E. coli* BW25113, a wild type strain, in LB media. Biocompatibility was studied here by growing wild type *E. coli* LY180 in the presence of MMCPs ranging from 4 to 160 g/L in culture tubes with LB media. At low concentrations (below 10 g/L) there is little effect on LY180 growth, as seen in Figure 3.6A. At greater than 10 g/L MMCPs, the cell density was reduced by ~50% while no growth is observed above 150 g/L. Some of the reduced growth is likely due to the adsorption of one or more key nutrients. Moreover, it is known

that activated carbon nanoparticles have their own toxicity against *E. coli* and even more resilient microorganisms such as *Pseudomonas aeruginosa.*(Karnib et al., 2013) Lignocellulose-derived feedstocks require nano- or ultrafiltration prior to use as culture media to remove particulate solids.(Balan, 2014; Dalecka et al., 2015; P. Kumar et al., 2009) The complete removal of the ~9% non-magnetically separable MMCPs by vacuum filtration enabled direct comparison of culture growth by optical density measurements at 600 nm as shown in Figure 3.7B where LY180 produces more cell mass compared to *Z. mobilis* A3.(K. Zhang et al., 2011) Also the growth inhibition of LY180 by furfural as seen in Figure 3.6C. Below 1 g/L aqueous furfural, the growth is slowed by up to ~50% while there is greatly reduced growth up to 75% at ~2 g/L and no growth at or above 3 g/L. The ethanol production is halted at 3g/L furfural compared to furfural free media fermented by Z. mobilis A3 as seen in Figure 3.6D.(K. Zhang et al., 2011)

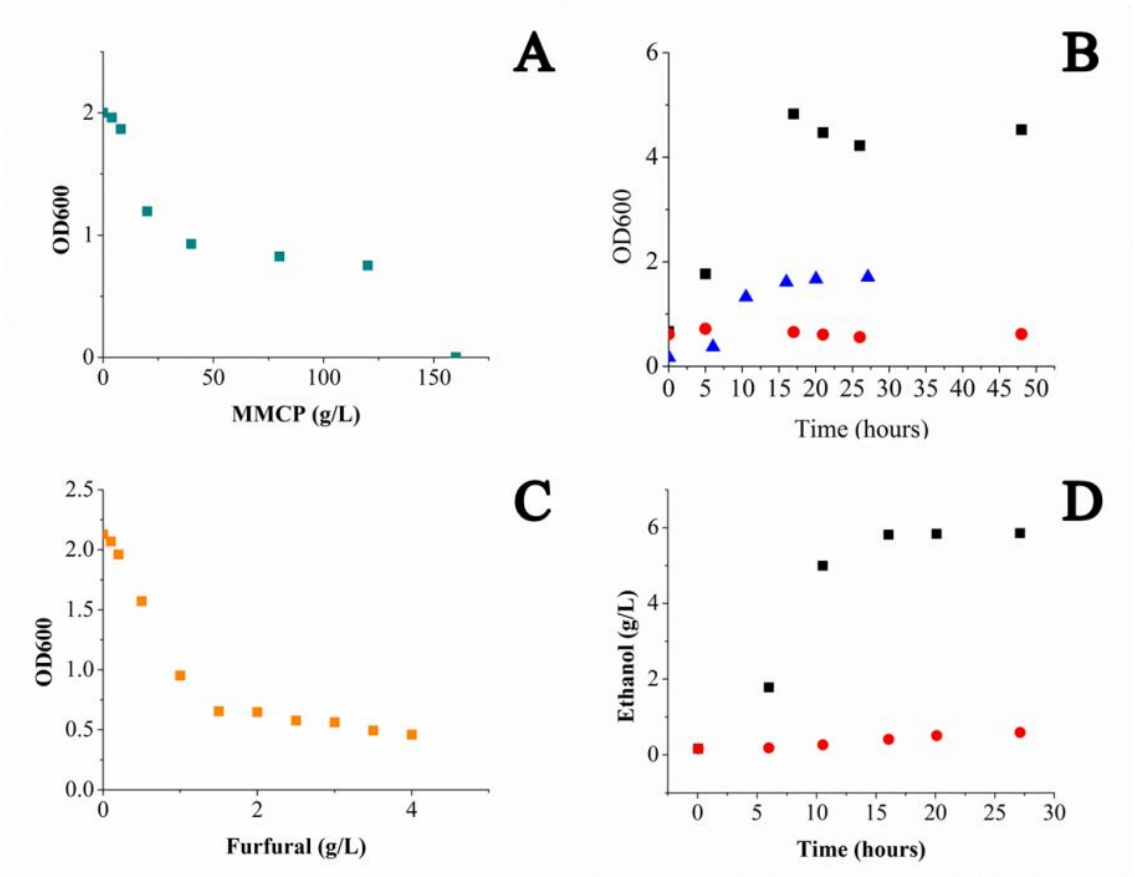

Figure 3.7 Biocompatibility and Toxicity. A) LY180 growth vs MMCP concentration (squares) at 24 hours in culture tubes. B) LY180 growth in model media (squares), growth of *Zymomonas mobilis* A3 in model media with (circles) and without (triangles) 2 g/L furfural and growth in model media (K. Zhang et al., 2011). C) LY180 growth vs furfural concentration at 24 hours in culture tubes. D) Ethanol production from model media with (circles) and without furfural (squares) by Zhang et al. (K. Zhang et al., 2011)

3.3.7 Ethanol Fermentation from Pretreated Media

From seed cultures in LB media, *E. coli* LY180 was grown in pretreated media and model lignocellulosic hydrolysate without furfural. Initial furfural concentration was 3 g/L which was reduced to 0.88 g/L following pretreatment using MMCPs and the above described magnetic column retrieval apparatus. Growth observed for model

hydrolysate without furfural was essentially no more robust than that observed for pretreated model hydrolysate as seen in Figure 3.8A. Glucose and xylose consumption and ethanol production were approximately complete by 24 hours. Total sugar utilization was 82% for the pretreated fermentations and 83% for the control. The ethanol titer rose to a high of 64.2 g/L for the control fermentations while the pretreated group achieved 62.8 g/L, both achieving approximately 95% yield on sugar. This was calculated from the theoretical yield of ethanol on sugars (glucose and xylose) at approximately 0.51g/g, which has given other LY strains approximately 90% yield or greater.(L.P. Yomano et al., 1998) By comparison to other ethanologenic strains of *E. coli*, the highest ethanol titer reported to the author's knowledge was 63.8 g/L by LY02, with most strains producing just over 60 g/L.(L.P. Yomano et al., 1998) The ethanol titers achieved here are approximately ~10-fold greater than that of *Z. mobilis* A3 from pretreated model hydrolysate by Norit 1240 activated carbon. (K. Zhang et al., 2011) Further, this co-utilization of xylose and glucose is one of the greatest improvements from the KO11 strain to the LY168 strain (L. P. Yomano, York, Shanmugam, & Ingram, 2009) which was further engineered to produce the LY180 strain. (Jarboe et al., 2010)

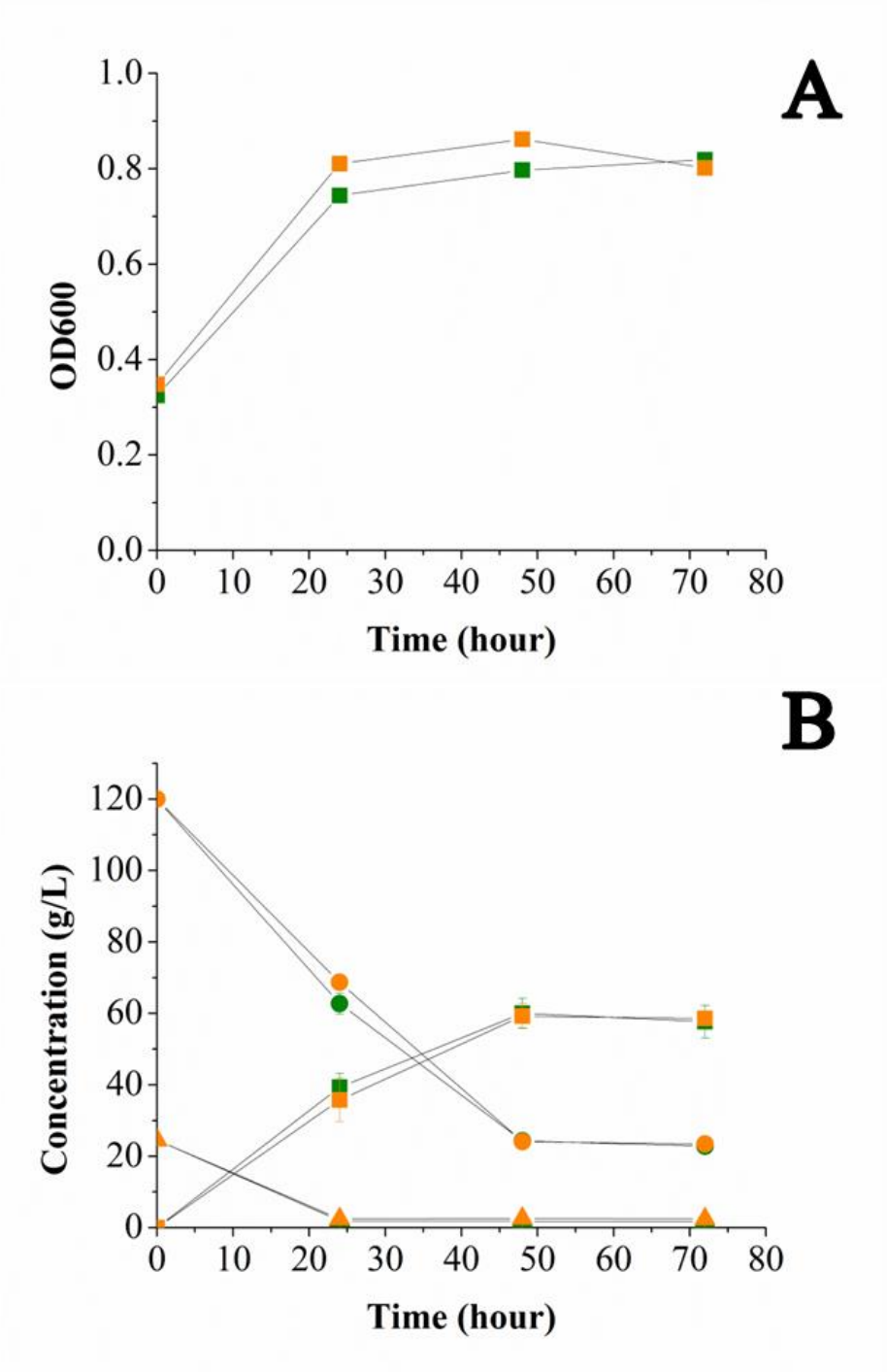

Figure 3.8 Fermentation Results. Control titers (green) and furfural pretreated media titers (orange) for ethanol (squares), xylose (circles) and glucose (triangles). Error bars represent one standard deviation.

3.3.8 MMCP Characterization

Detailed physical characterization of the MMCPs has been reported in Chapter 2. The emphasis of characterization for this study was scanning electron microscopy. Figure 3.2 shows both virgin MMCPs and MMCPs cultured with *E. coli* LY180 in LB media for 24 hours. Comparing the virgin MMCP column (left) and the fouled MMCP column (right) in Figure 3.2, it seems that there is a 'blanket' of extracellular polymeric substance (EPS) formed by LY180. This is also the case for BW25113, a wild-type strain (results not shown). A 'conditioning layer' is formed from a combination of EPS components, the surface charges of both cell and substrate, and fluid shear, all of which are known to facilitate cellular attachment and acts as a diffusion barrier to toxins, nutrients and value-added bioproducts (Bojsen, Andersen, & Regenberg, 2012; N. Qureshi, Annous, Ezeji, Karcher, & Maddox, 2005). The LY180 cells studied here do not appear to attach to the virgin carbon surface, perhaps owing to the MMCP mesoporosity. Certain fouling factors have been well investigated including strain of microorganism, substrate material, substrate roughness, finding that increasing roughness and hydrophobicity promotes fouling (Ben Chaabane et al., 2006; Ciston, Lueptow, & Gray, 2008; Diaz, Schilardi, Salvarezza, & Fernandez Lorenzo de Mele, 2011; Dohnalkova et al., 2011; B. Li & Logan, 2004; Pratt, 1998) MMCPs satisfy both the roughness and hydrophobic criteria for being fouling prone in the presence of bacterial culture. A more extensive cellular fouling study on separations materials is presented in Appendix A.

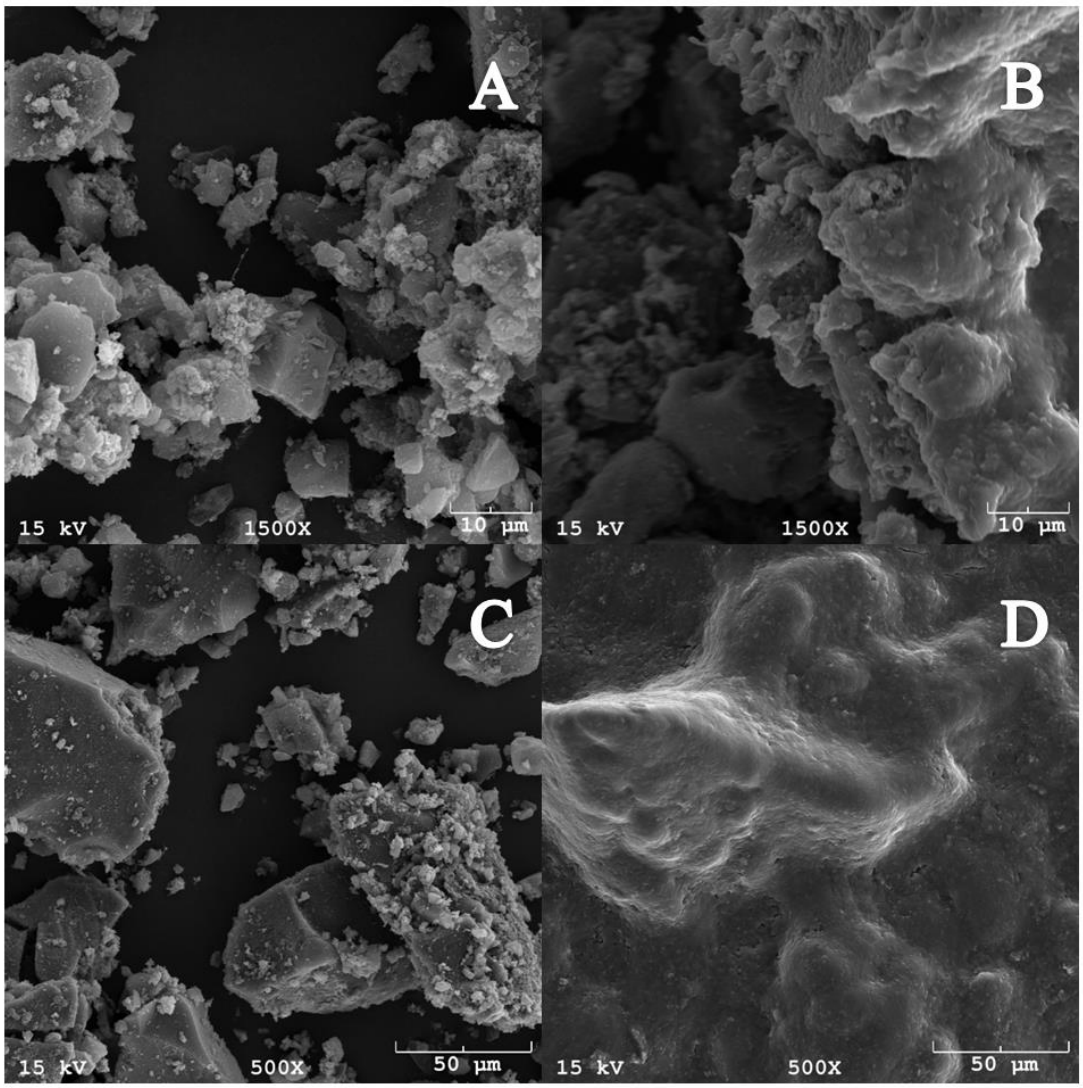

Figure 3.9 MMCP Characterization by SEM. A) Virgin MMCP at 1500x, B) MMCP cultured with *E. coli* LY180 after 24 hours at 1500 x, C) Virgin MMCP at 500x, D) MMCP cultured with *E. coli* LY180 after 24 hours at 500x.

3.4.0 Conclusion

In this work, a closed-loop process was demonstrated for simultaneous detoxification and secondary value-added product recovery. Compared to commercial carbons, the furfural adsorption capacity and kinetics of the MMCPs are competitive. Up

to 91% of the MMCP mass was recovered via magnetic column. Upon removal of the remaining fraction of MMCPs by final filtration of the model hydrolysate, *E. coli* ethanol production by LY180 was insignificantly greater that of the control cultures whereas untreaded model hydrolysate resulted in no growth. Fermentation of the model hydrolysates by E. coli LY180 resulted in up to 64.2 g/L ethanol and over 62 g/L from pretreated model hydrolysate. Moreover, MMCPs release furfural more readily than activated carbon however, with up to 66 wt% recovery of the adsorbed species. This converts the otherwise lost toxic growth inhibitor into a highly enriched value-added byproduct. MMCPs can thereby bypass toxicity bottlenecks and improve the overall value of the fermentation products from fermentation of lignocellulose-derived feedstocks without appreciable change in titer or sugar co-utilization.

3.5.0 Acknowledgments

This work was supported by the National Science Foundation (Award Nos. CBET-1067684 and CBET-1159200). The authors declare no conflicts of interest.

CHAPTER 4

4.0 SELECT VALUE-ADDED BIOPRODUCT SEPARATIONS BY MAGNETICALLY RESPONSIVE MESOPOROUS CARBON ADSORBENTS

Abstract

Here the selective capture and recovery of phenol, an aromatic useful in resin and polymer manufacturing, has been evaluated. It is easily produced from renewable feedstocks, with a theoretical toxicity limit of 1.75 g/L. Aqueous phenol titers however are often less than 420 mg/L from engineered strains which suggested a possible feedback inhibition rather than product toxicity. To evaluate this, in situ adsorption was applied to reduce the aqueous phenol content via Dowex Optipore L-493 resin and magnetically responsive mesoporous carbon. Phenol was desorbed up to 77% by mass via solvent recovery with tert-methyl butyl ether. Improvements to the media over previous study increased the aqueous phenol titers to over 500 mg/L, a higher titer than previously reported from batch culture of *Escherichia coli*. In-situ adsorption did not improve titers, eliminating the possibility of feedback inhibition. This work demonstrates the application of adsorbents to confirm a metabolic flux limitation restricting phenol titers.

Keywords: phenol; *in situ* product recovery; adsorption; mesoporous carbon; magnetic powder recovery

This work has been in preparation as a manuscript with the following authorship: Staggs, K., Thompson, B., Nielsen, D.R.

4.1.0 Introduction

Phenol is a commonly employed commodity chemical of great importance for development of polymer resins, precursors such as bisphenol A, aniline, and even salicylic acid. (Fierro et al., 2008) Phenol is thereby used in many industrial applications and found as an environmental contaminant. (Fierro et al., 2008) Whereas phenol is presently produced from petrochemical feedstocks, it can be renewably produced from biomass-derived feedstocks. (Thompson et al., 2016) Several researchers have engineered biocatalysts ranging from *Pseudomonas putida* (Wierckx, Ballerstedt, de Bont, & Wery, 2005) to *Escherichia coli*. (Kim, Park, Na, & Lee, 2014; Thompson et al., 2016)

The typical batch fermentations of phenol by *E. coli* result in titers on the order of 0.42 g/L or less.(Kim et al., 2014) Meanwhile, the typical reported phenol toxicity for *E. coli* is 1.75 g/L which is a very dilute concentration relative to bioalcohol production.(Bankar et al., 2012; Ben Chaabane et al., 2006; Ezeji et al., 2004a; Hashi et al., 2010; Ingram, 1990; J. Li et al., 2014; Thompson et al., 2016; Chuang Xue et al., 2012) As phenol is made from a tyrosine intermediate, batch fermentations often leaves unconverted tyrosine proportional to the phenol titer.(Kim et al., 2014) This unconverted tyrosine is detrimental to the phenol titer and results in decreased phenol yield. Fed batch fermentation has resulted in phenol titers as high as 1.69 g/L with a glucose yield of 0.0026 g/g (Wierckx et al., 2005), more than 100-fold less than the reported theoretical maximum yield of 0.38 g/g.(Kim et al., 2014) Certain pathway limitations are caused by phenol inhibition on tyrosine phenol lyase (TPL), which the pathways used for this study are not dependent on.(Thompson et al., 2016) While the phenol titers for the strains used here previously reached up to 0.377 g/L (Thompson et al., 2016), it was speculated that

some further feedback inhibition in the alternative pathways was causing the repression of phenol production concurrently with high tyrosine coaccumulation. *In situ* product recovery (ISPR) should improve the phenol titers from our engineered cultures.

Solvent recovery of the phenol from producing cultures has been employed as an ISPR strategy from engineered *P. putida* (Wierckx et al., 2005) as has membrane perstraction (Heerema et al., 2011) and solvent-loaded resin adsorption. (van den Berg et al., 2008) Each recovery mode has its own strengths and weaknesses. (Staggs & Nielsen, 2015) Solvent addition can cause its own solvent toxicity and induce phase separation, limiting its applications to batch and fed-batch fermentations. (Staggs & Nielsen, 2015; van den Berg et al., 2008) Membrane separations are effective, though prone to fouling by the microorganisms in the culture. (Staggs & Nielsen, 2015) Adsorbents are often biocompatible and less affected by fouling during *in situ* recovery but require column isolation or filtration. (Wiehn et al., 2014) To diagnose the existence of and potentially eliminate an internal repression improving phenol titers, *in situ* adsorption has been employed. Accordingly, phenol adsorption performance was evaluated for both magnetically responsive mesoporous carbons (MMCPs) and Dowex Optipore L-493 resins. Moreover, phenol recovery from the adsorbed phase was optimized by solvent desorption.

4.2.0 Materials and Methods

4.2.1 Bacterial Strains and Culturing

All seeds were cultured in Luria-Bertani (LB) broth at 32°C supplemented with 100mg/L ampicillin, 35 mg/L kanamycin, and/or 34 mg/L chloramphenicol, as required. All chemicals were obtained from Sigma-Aldrich (St. Louis, MO). Phenol production

was evaluated for strains cultured at 32°C in phosphate limited M9M media composed of (concentrations in parentheses, all in g/L): MgSO4_7H2O (0.5), (NH4)2SO4 (4.0), MOPS (24.7), KH2PO4 (0.3), K2HPO4 (0.7), (NH4)6 Mo7O24_4H2O (3.7*10-4), H3BO3 (2.5*10-3), CoCl2_6H2O (7.14*10-4), CuSO4 (1.6*10-4), MnCl2_4H2O (1.6* 10-3), ZnSO4_7H2O (2.88*10-4), FeCl3 (5.0*10-5), and glucose (20), supplemented with required antibiotics. Phenol was also cultured in richer M9Y media with the following composition: glycerol (10), glucose (2.5), Na_2HPO_4 (6), NaCl (0.5), KH_2PO_4 (3), NH_4Cl (1), yeast extract (1), MOPS (2). All cloning work was performed as previously described.(Thompson et al., 2016)

Control flasks of both wild type BW25113 and engineered BW25113 were grown in phosphate limited media. Control flasks and those incorporating 0.5 g of the appropriate adsorbent were autoclaved with 20 mL of deionized (DI) water before adding media components. Cells were induced with IPTG when the OD600 reached approximately 1, at ~14 hours. Flasks were pH adjusted by K2HPO4 every 12-24 hours as required. Following the completion of the phenol fermentation at approximately 144 hours for M9M and ~72 hours for M9Y, 1 mL samples were drawn for quantification by HPLC.

4.2.2 Adsorption Isotherms and Modeling

To determine the loading capacity of adsorbents, either Dowex Optipore L-493 or MMCPs were added to glass scintillation vials at a ratio of 0.1 g adsorbent/mL of solution. Phenol/water binary component solutions were added to the scintillation vials and allowed 24 hours for equilibration at 37°C overnight while mixing on an orbital shaker. Approximately 500 µL of the supernatant was aliquoted into high-pressure liquid

chromatography (HPLC) vials for analysis. To determine the equilibrium adsorption capacity (q_i) of each solute *i*, the following mass balance was performed.

$$q_i = \frac{(C_{i,0} - C_i)V}{m} \quad (4.1)$$

Where $C_{i,0}$ and C_i are initial and equilibrium aqueous concentrations of species *i*, *V* is aqueous volume, and *m* is mass of adsorbent. Adsorption data was fit according to the Langmuir and Freundlich isotherm models as shown in equations 2 and 3, respectively.

$$q_i = \frac{q_{i,max} k_{l,i} C_i}{1 + k_{l,i} C_i} \quad (4.2)$$

$$q_i = k_{f,i} C_i^{\,1/n_i} \quad (4.3)$$

Where, for the adsorbed species *i*, C_i is as defined above, q_i and $q_{i,max}$ are equilibrium and maximum equilibrium adsorption capacity, respectively and $k_{l,i}$ is the Langmuir constant, $k_{f,i}$ and n_i are the Freundlich constant and exponent, respectively.

4.2.3 Phenol Desorption and Recovery

Adsorbents were first loaded with phenol by equilibrating 4 g of adsorbent with 200 mL of approximately 2 g/L phenol in a sealed media bottle shaken overnight at 37°C. Equilibrium solution was sampled for analysis by HPLC before decanting the bulk solution. Tert-butyl methyl ether (TBME) washes of 10 mL were added to the adsorbents to extract the adsorbed phenol. The TBME washed adsorbents were shaken at 37°C for 6 hours after which 1 mL of the bulk solution was transferred to an HPLC vial for analysis. The remaining bulk TBME solution was decanted. At this point, 200 mL of fresh 2 g/L phenol solution was added to the bottle containing the regenerated adsorbent and the

entire process repeated. In total, 5 consecutive 'cycles' were preformed using the same adsorbent sample.

4.2.4 Extractive Fermentation

Seed cultures were grown as described above in 10 mL culture tubes. From seed cultures, 1 mL was added to 250 mL baffled flasks containing 25 mL of 2x M9Y media, 1 mL trace minerals, 50 uL antibiotics as needed and 20 uL IPTG with the balance sterile DI water for a total volume of 50 mL. After approximately 24 hours, 5 mL of tributyl phthalate was added and the pH adjusted with 1 mL of 40 g/L K_2HPO_4. After ~72 hours, fermentations reached completion and 1mL of culture was centrifuged at 12,000 rpm for 5 minutes before analysis by HPLC.

4.2.5 Adsorptive Fermentation

Seed cultures were grown as described above in 10 mL culture tubes. From seed cultures, 1 mL was added to 250 mL baffled flasks containing 25 mL of 2x M9Y media, 1 mL trace minerals, 50 uL antibiotics as needed and 20 uL IPTG with the balance sterile DI water for a total volume of 50 mL. After approximately 24 hours, 0.5 g of adsorbent was added and the pH adjusted with 1 mL of 40 g/L K_2HPO_4 with subsequent pH adjustments as needed. After 72 hours, fermentations reached completion and 1mL of culture was centrifuged at 12,000 rpm for 5 minutes before analysis by HPLC.

4.2.6 Analytical Techniques

Aqueous concentrations were analyzed by HPLC (1100 series Agilent; Santa Clara, CA) equipped with a refractive index detector (RID) and a diode array detector (DAD). All samples were centrifuged at 11,000 g for 3 minutes and the supernatant aliquoted into glass HPLC vials. Binary solutions for adsorption studies were separated

on a reverse-phase Hypersil GOLD aQ Polar C-18 column (4.6 x 150 mm; Thermo Scientific; Grand Island, NY) using 85% 5 mM H_2SO_4 and 15% acetonitrile as the mobile phase at 45°C 0.7 mL/min. Phenol concentration was determined by DAD at 215 nm and 275 nm for phenol. Glucose was analyzed using the RID detector and an Aminex HPX-87H column (Bio-Rad Laboratories; Hercules, CA) operated at 35°C with a constant flow rate of 0.55 mL/min 5mM H2SO4. External calibrations were used to quantify each metabolite.

4.3.0 Results and Discussion

4.3.1 Phenol Isotherms

Because phenol is a hydrophobic molecule (log Kow ~1.5) it should be readily adsorbed on hydrophobic adsorbents.(D. R. Nielsen & Prather, 2009; D. R. Nielsen et al., 2010; L. Nielsen et al., 1988; Staggs et al., 2017; van den Berg et al., 2008; Wiehn et al., 2014) Many studies involving phenol adsorption are seeking its removal from wastewater as a toxic byproduct of many industrial processes. It has been recovered by select polymeric resins (Huang et al., 2007; van den Berg et al., 2008) and activated carbons. (Fierro et al., 2008; Khan, Suidan, & Cross, 1981) Few studies have incorporated ISPR with phenol fermentation. Both perstraction with 1-octanol (Heerema et al., 2011) and adsorption using XAD-4 with and without ionic liquid loaded pores (van den Berg et al., 2008) have been integrated into *P. putida* fermentation of phenol. Ionic liquids swelled the adsorbents and improved the phenol loading capacity to 0.017 g/g at 0.2 g/L aqueous phenol, which was less than the 0.04 g/g expected from the isotherm.(van den Berg et al., 2008) Perstraction rather than decreasing the aqueous phenol concentration, it maintained approximately 0.28 g/L with the phenol production and perstraction rate nearly

equal.(Heerema et al., 2011) For this reason, adsorbents are better suited for ISPR of phenol compared to other methods. (Heerema et al., 2011)

The biocompatibility of both MMCPs and L-493 with *E. coli* BW25113 was demonstrated in Chapter 2 for butanol recovery applications. Activated carbons have been particularly efficient adsorbents of phenol, (Fierro et al., 2008) though never used for ISPR of phenol from fermentation to the author's knowledge. Commercial Norit carbons have a lesser phenol loading capacity compared to carbons activated by bases rather than acids. (Fierro et al., 2008) The phenol isotherms for base and acid prepared activated carbons are compared to the adsorption performance of phenol onto MMCPs and Dowex Optipore L-493 in Figure 4.1. Phenol adsorption onto the acid-prepared activated carbons is directly comparable to both the MMCP and L-493. The base-prepared activated carbon has a more than 2-fold greater phenol loading capacity compared to the adsorbents studied here. Activated carbons and resins alike are only separable by filtration while the MMCPs studied here are magnetically separable. As phenol is a valuable fermentation product, rather than a valueless contaminant its ultimate retrieval from the adsorbent is an important design consideration for ISPR.

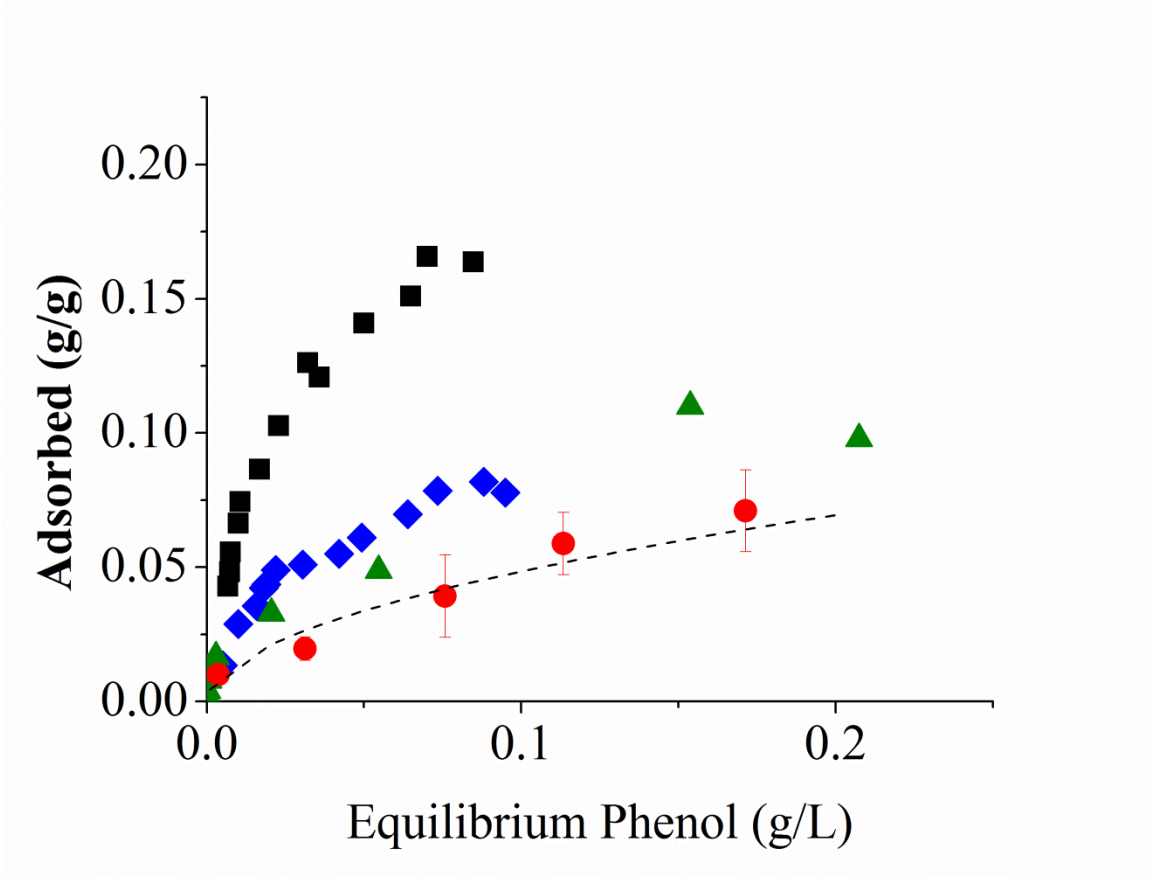

Figure 4.1. Phenol Adsorption Isotherm. Phenol isotherm for adsorption onto Dowex Optipore L-493 (crosses), and MMCPs (squares), and NaOH prepared (diamonds) and Phosphoric acid prepared (circles) activated carbon. (Fierro et al., 2008)

At the same 0.2 g/L equilibrium phenol, the MMCPs studied here are expected to have a loading of 0.07 g/g while L-493 resins should load up to ~0.11 g/g. These values are 1.7 and 2.7 fold greater than the expected phenol adsorption for XAD-4 resins, respectively.(Heerema et al., 2011) Adsorption behavior has been modeled by Freundlich, Langmuir and dual site Langmuir isotherm models to address the likelihood of multi-layer versus multi-site adsorption. Langmuir and dual-site Langmuir isotherm models were found poorly representative of either adsorbent. The Freundlich model fit both adsorbent isotherms more closely as seen in Figure 4.1. By multiplying the

Freundlich exponent by the universal gas constant and the temperature, the Gibbs energy of adsorption can be estimated (D. R. Nielsen et al., 2010; Staggs et al., 2017) which was also estimated in Chapters 2 & 3. The Gibbs energy of adsorption for phenol onto the MMCPs and L-493 were -4.74 and -6.08 kJ/mol which are both small negative values, suggesting physisorption. Taken together, the results of the data fitting suggest that multi-layer physisorption is far more likely than monolayer physisorption or chemisorption.

4.3.2 Phenol Desorption

A common method for phenol recovery from an adsorbed phase is chemical conversion to phenolate by addition of strong base such as NaOH.(van den Berg et al., 2008) Several different solvents have been evaluated for phenol recovery from adsorbents including 1-octanol.(Wierckx et al., 2005) Other alkanes evaluated for phenol recovery from aqueous culture (e.g. dodecane, dibutyl phthalate, isopropyl myristate, etc.) have been found to be low performance compared to octanol, which terminates growth.(Miao, Li, Diao, Zhang, & Ma, 2015) Solvents evaluated in this study include methanol, toluene and tert-butyl methyl ether, which was found the most effective for phenol recovery. Solvent recovery results are graphed in Figure 4.2 where the first solvent wash was methanol to aid dewatering of the adsorbents, recovering approximately ~43% of the adsorbed phenol. Subsequent washes were conducted with TBME because of greater phenol solubility allowing a total of ~77% recovered phenol by mass as seen in Figure 4.2. Because the phenol recovery method was not quantified in terms of recovered mass ratio from XAD-4 resins, (van den Berg et al., 2008) a direct comparison with our results is not feasible.

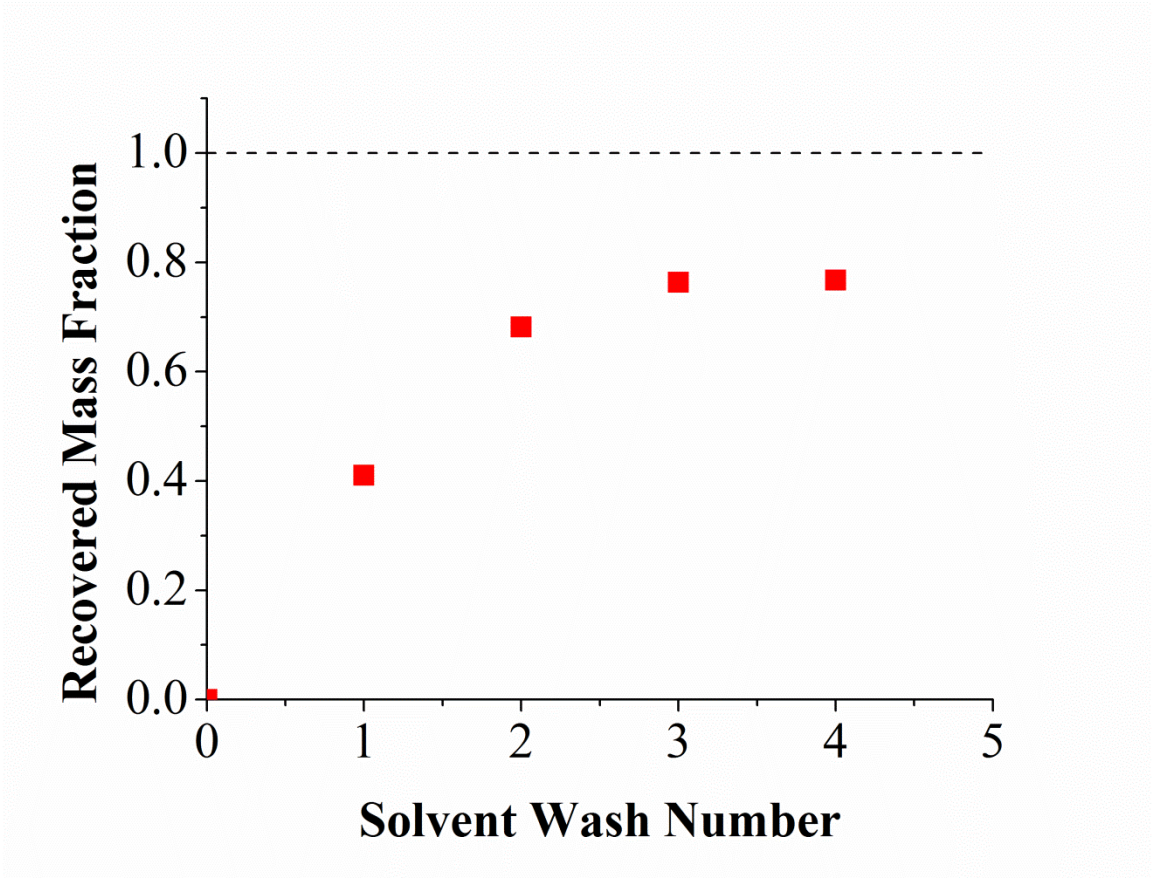

Figure 4.2. Phenol Desorption and Recovery. The total adsorbed phenol is the solid line, the additive solvent recovered phenol are the diamonds.

4.3.3 Adsorptive Fermentation

Coupled with XAD-4 resins without and with ionic liquid loaded pores, *P. putida* production of phenol improved 2.5 and 4-fold, respectively. (van den Berg et al., 2008) This produced a total combined phenol titer of 0.3 and 0.91 g/L for fed-batch control and fed-batch with solvent-loaded XAD-4 resins, respectively.(van den Berg et al., 2008) *P. putida* fermentation of phenol with in situ perstraction improved the titer from 0.38 to 0.47 g/L.(Heerema et al., 2011) Meanwhile engineered *E. coli* in minimal media (M9M) have reported batch phenol titers up to 0.42 g/L whereas with solvent extraction in a high cell density fed-batch fermentation, up to 1.75g/L has been reported.(Miao et al., 2015)

One of the main advantages to fed batch fermenter operation examined by Miao et al. was the addition of yeast extract.(Miao et al., 2015) Under minimal media conditions, adsorbents reduced growth compared to control flasks, (van den Berg et al., 2008) a trend also observed in early data for this study. By adding 2 mL of a supplement containing 20 g/L glucose and 5 g/L yeast extract to M9M, the growth of control and adsorbent loaded flasks was equalized as seen in Figure 4.3. Growth of our engineered E. coli BW25113 was further improved by the transition to M9Y media. When examining the dry cell mass with wild type *E. coli* BW25113, the control flasks grew to ~1.45 g/L compared to 1.35 g/L for MMCPs and 1.72 g/L for L-493 resins. Within the experimental error observed growing wild type *E. coli*, these cell mass results are considered essentially the same. By comparison, P. putida developed approximately 4.8 g/L biomass though perhaps with a conversion factor different than the 0.25 g/OD600 used here.

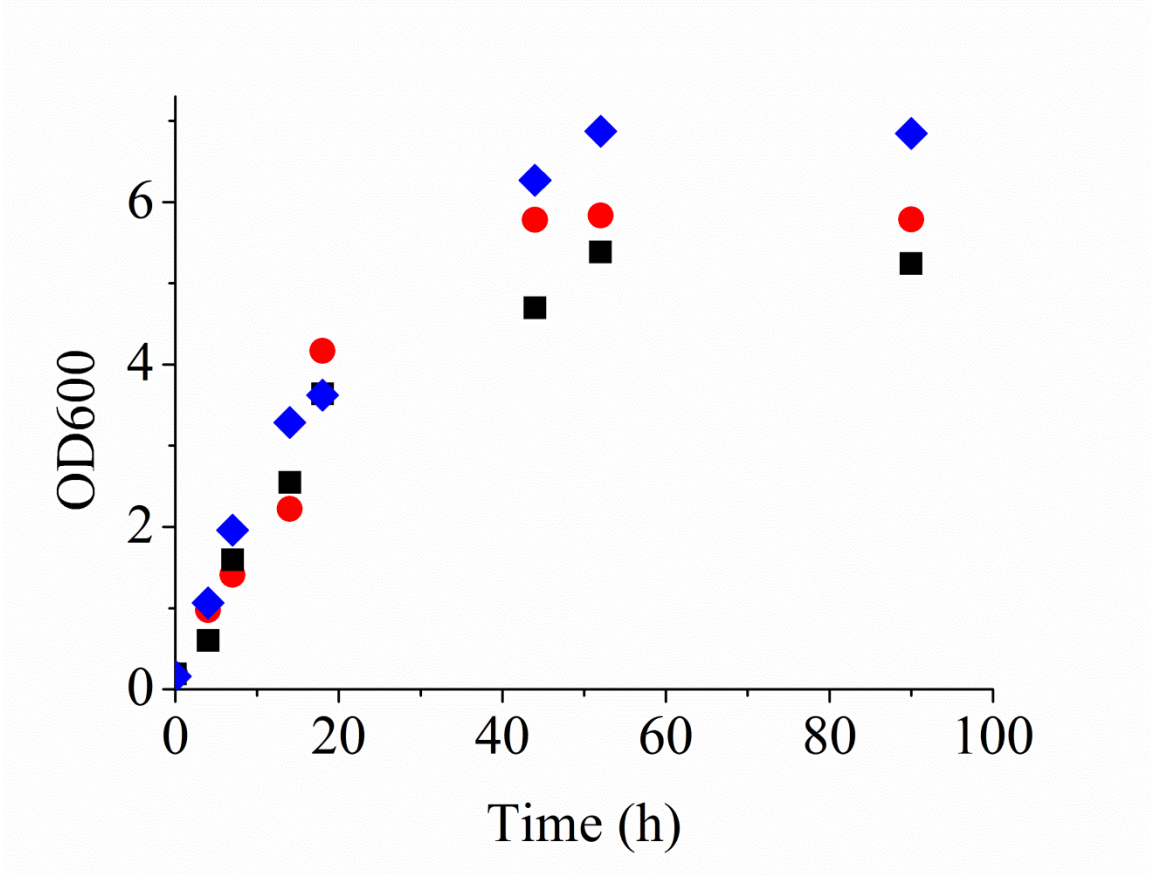

Figure 4.3. Biocompatibility of Adsorbents. Biocompatibility of Control (diamonds), Dowex Optipore L-493 resin (triangles), and MMCP-10 (squares).

Phenol batch titers in this study rose from 0.26 g/L in minimal media to 0.55 g/L in M9Y before any adsorbents were added. The comparison between batch controls and duplicate L-493 resin flasks can be observed from Table 4.1. The total recovered phenol was calculated as the sum of the remaining aqueous phenol and the total recovered from the ~5 solvent washes. At 0.55 g/L aqueous phenol titer, our control fermentations were approximately 1.4 to 1.6-fold greater than that of P. putida.(Heerema et al., 2011; van den Berg et al., 2008) Additionally, when glucose utilization was examined by HPLC, it was found to be the same for M9Y with and without adsorbent at approximately 98.9%. This

would suggest a flux limitation due to carbon source consumption, but phenol titers did not improve under fed-batch conditions.

Table 4.1.

Adsorptive Fermentation by Engineered *E. coli* NST74.

	Phenol (g/L)	Glucose Utilization %
M9Y Control	0.55 ± 0.05	98.9
M9Y L-493	0.48 ± 0.04	99.0

Because the L-493 total titer is ~87% of the control titer, it is reasonable to conclude that ISPR via adsorption does not limit the phenol titer in the richer M9Y media as it would in leaner media. Troubleshooting adsorptive fermentation results from this study follows one of three possible vectors: 1) if phenols production is feedback inhibited, adsorption would improve the phenol titer, 2) if the titer is flux-limited within or upstream from the engineered pathway, then the phenol titer would remain unchanged, and 3) if the limitation is product toxicity, then adsorption should improve both growth rates and phenol titer. Of these, clearly the second case fits the fermentation results.

4.4.0 Conclusion and Future Work

Taken together, the adsorptive fermentation results demonstrate complete biocompatibility of both MMCPs and L-493 resin at no appreciable cost to phenol titer. Additionally, adsorptive fermentation improved aqueous phenol titers to ~0.5 g/L from batch cultures, which is higher than previously reported batch cultures. Both L-493 and MMCPs have reduced the aqueous phenol to less than 10% the reported phenol toxicity limit. This has eliminated the potential bottleneck of phenol feedback inhibition. As fed-batch fermentation did not improve the phenol titer, further engineering of the strain

could increase the amount of tyrosine (phenol precursor in this engineered pathway) produced. Increased tyrosine in this engineered strain should boost phenol production in adsorptive fermentation closer to or beyond the toxicity threshold. We expect the increase in tyrosine flux to will phenol in adsorptive fermentation to over 1 g/L in batch operation, which would be the highest reported batch phenol titer known to the authors.

4.5.0 Acknowledgments

This work was supported by the National Science Foundation (Award Nos. CBET-1067684 and CBET-1159200). The authors declare no conflicts of interest.

CHAPTER 5

5.0 SUMMARY AND FUTURE WORK

Abstract

The novel application of magnetically responsive mesoporous carbons as an adsorbent for: 1) in-situ product recovery, 2) upstream feedstock detoxification, and 3) diagnostics of potential feedback inhibition. This demonstrates contributions to the field of targeted separations as a tool to assist metabolic engineering. While metabolic engineering can improve production several-fold, many factors contribute to lesser than theoretical product titers. It is important to distinguish between toxicity and inhibition, which often cannot be known a priori. Targeted separations modalities (e.g. adsorbents) are particularly effective at selective removal and recovery of products and metabolites to improve titers. Many lessons were learned throughout the course of this work particularly about MMCP retrieval and specific loading. The important lessons concerning MMCP performance are detailed in this Chapter. Future works are described including: 1) pretreatment strategy for real lignocellulosic hydrolysates by MMCPs, 2) fermentation of MMCP pretreated real lignocellulosic hydrolysates by *Escherichia coli* LY180, 3) other bioproduct fermentation from real pretreated lignocellulosic hydrolysates, and 4) An idealized design for a next generation magnetically separable adsorbent leveraging newer separations technology such as smart polymers and ionic liquids.

5.1 Introduction

This work has demonstrated the broad application of separation technologies for both improving and troubleshooting bioproduct development. MMCPs have been demonstrated to be very effective at removing hydrophobic compounds such as butanol, furfural and phenol. The MMCP loading capacity for these bioproducts and feedstock byproducts is comparable to, or greater than commercial resins or activated carbons. These MMCPs are magnetically separable from aqueous solutions up to 91% by mass. Up to 93% of butanol, 66% of furfural and 77% of adsorbed phenol by mass have been recovered from the adsorbents studied here. These MMCPs are exceptionally versatile adsorbents with proven applications for production of many bioproducts. During this research, many design considerations and key limitations of MMCPs became known.

While the MMCPs are magnetically responsive and thus magnetically separable, they are not 100% retrievable from aqueous slurries. A redesign of the magnetic retrieval column from first principles, did improve MMCP retrieval by a small 2% compared to earlier methods. While this is primarily due to the polydisperse size distribution noted in Chapter 3, certain process steps could be improved to enhance the magnetic retrieval of the MMCPs. The benefits of improved monodispersity in MMCPs are discussed in this chapter with methods of improving the magnetic retrieval further. Following improvements in magnetic retrieval, there is also room for improved specific loading performance.

Whereas the MMCPs have high specific loading for certain analytes investigated in the previous chapters, they have ~2-fold the surface area of many common commercial carbons. This should enable higher than observed equilibrium loading of certain analytes.

Such an increased equilibrium loading has not been observed, suggesting that there are potentially unoccupied pore surfaces deeper in the MMCP structure. Potentially improved specific loading may be evaluated by increasing the equilibrium temperature of adsorption. Compared to commercial activated carbon with lesser surface areas and smaller pore volumes, it would be expected that specific loading of MMCPs would greatly exceed that of commercial carbons. Elevated temperatures where this phenomenon would likely be observed (e.g. 60-90°C), are outside of the biologically relevant temperature range where 37°C is often ideal for building high cell mass. To improve specific loading and take advantage of the seemingly unused surface area, some design improvements have been suggested to leverage newly developed hybrid separations approaches.

5.2 Overview and Significance of Findings from MMCP Separations

5.2.1 Magnetic Retrieval of MMCPs

Early designs of the magnetic retrieval tool for MMCPs were derived from a common magnetic stir bar retrieval tool. This design enabled magnetic retrieval of MMCPs from aqueous solutions with multiple dips and rinses up to 89% as reported in Chapter 2. The comparison of the effect of Ni content on MMCP retrievability revealed an interesting trend not shown in Chapter 2. Several sizes of magnetic retrieval rods with increased magnetic surface area were evaluated. The trend observed for MMCP retrieval as a function of every Ni composition demonstrated a clear dependence of retrieval on magnetic surface area. The retrieval of MMCPs was influenced primarily by Ni content, though the retrieval surface area was also a factor. To increase the overall recovery

surface area, a revision to the tool increased the total number of magnets to 20 and placed it into a glass column (interior column retrieval). The MMCP slurry was flowed through the column and the retrieval was essentially complete after passing through 2 columns. This method of recovery was less efficient than expected, requiring much greater surface area than would be scalable for a large volume process. MMCPs were rinsed off the magnetic core after its removal from the glass column. This promotes mass transfer losses of MMCPs and is not suitable for aseptic protocol such that it would risk contamination of bacterial cultures. It became clear that a fundamental redesign of a magnetic column was required.

To better understand the magnetic retrieval, finite element modeling revealed that the magnetic field orientation in the column was parallel with the particle flow. Because magnetic force is a normal vector to the plane established by the flow vector and the field vector, the resultant force vectors would be primarily oriented in a rotational vector toward the column wall. This limited the effective retrieval area for a given number of magnets. By changing the orientation of the magnets in the models and thus the direction of the filed, the new direction of the force vector would be oriented toward the column wall without any significant rotational component. This allowed MMCP collection on the column wall along the path of the field lines as presented in Chapter 3. The redesigned column with the removable magnetic clamp improved the MMCP retrieval up to 91% with a single column and a single pass of the column volume. Moreover, the thickness of the MMCP retrieval layer compared to the interior column design was approximately double the thickness. The entire column could be easily sterilized and integrated with

aseptic protocol for bacterial fermentations. This column without the exterior clamp was easily rinsed with DI water and the MMCPs retrieved for thermal desorption.

5.2.2 Adsorption Kinetics Versus Desorption from MMCPs

The kinetics of adsorption presented in Chapters 2 & 3 were found to be rapid for butanol and furfural, respectively. The nature of the rapid pore loading has been ascribed to the tightly controlled pore structure as detailed in Chapter 2. Meanwhile the high surface area of MMCPs approximately 2-fold greater than common commercial activated carbons promotes high specific loading. The specific loading of each analyte is different such that there is not a singular trend for all possible analytes. What has been consistently observed is that hydrophobic analytes tend to adsorb with greater specific loadings compared to hydrophilic analytes. For example, butanol loading of MMCPs was approximately 3-fold greater than that of ethanol based on the data from Chapter 2. Based on the equilibrium adsorption data, the Gibbs energy of adsorption was estimated. Comparing these adsorption energies, butanol was approximately twice the value of ethanol. Butanol adsorbs more strongly than ethanol does and therefore should require more energy to desorb.

When comparing the desorption of analytes from adsorbents, the physical properties such as vapor pressure and boiling point are important design considerations. Thermal desorption used for both Chapters 2 & 3, took advantage of the volatility of the butanol and furfural, respectively. As butanol is particularly volatile, it is thermally recoverable up to 99.7% whereas furfural is far less volatile with its boiling point of ~162°C. Furfural was only thermally recovered with up to a maximum of 66% which

leaves some residual adsorbed furfural on the surface of the MMCPs. While there was not a significantly reduced specific loading of furfural observed for MMCPs, this would be expected with repeated adsorption/desorption cycles. It is important to note that the specific loading isn't limited by surface area as discussed in Chapter 2. Without recovering 100% of the adsorbed furfural, that remaining percentage must accumulate within the mesoporous network. This will inevitably lead to a compromise in specific loading performance. As the boiling point of furfural is ~70°C greater than the water bath temperature used for thermal regeneration, its likely 66% is the maximum achievable recovery. At an elevated temperature closer to the boiling point of furfural, it would be expected that a greater percentage would be recovered. Furthermore, as the Gibbs energy of adsorption of furfural is less than that of butanol, it is reasonable to expect that furfural should be recoverable up to a similar percentage compared to butanol.

5.3 Experimental Outlook

5.3.1 Preatreatment of Real Lignocellulosic Hydrolysates by MMCPs

With the successful pretreatment of model hydrolysate, it is reasonable to infer that real hydrolysates could also be pretreated by MMCPs. Real hydrolysate which we intend to pretreat has the following composition (all values in g/L): 11.2 cellobiose, 5.4 glucose, 58.8 xylose, 5.9 galactose, 7.4 arabinose, 0.7 mannose, 2.5 hydroxymethyl furan (HMF), 3.6 furfural. While furfural is toxic, HMF is a likewise cytotoxic furan. (H. Zheng et al., 2012) Prior to pretreating real hydrolysate, the degree of competitive adsorption between furfural and HMF must be determined. The first step is adding 0.1 g of MMCP to 2 mL of aqueous solution containing 3 g/L furfural and 3 g/L HMF and

following the HPLC analysis protocol from section 3.2.2 to develop the competitive isotherm. With the competitive sorption characteristics known, the ratio of MMCP to aqueous volume can be adjusted. It is expected that HMF and furfural will have similar adsorption characteristics, leading to a requirement to double the MMCP to aqueous ratio to 60-100 g/L. A post treatment sample of the real hydrolysate will be evaluated by HPLC using the previously described protocol for furfural to ensure furfural and HMF are below the toxic threshold.

5.3.2 Fermentation of Ethanol from Real Pretreated Lignocellulosic Hydrolysate

With the known composition of a sample real hydrolysate, the adsorptive pretreatment criteria are known. MMCPs have successfully pretreated model hydrolysates in Chapter 3. To apply the MMCP pretreatment to the real hydrolysate, 300 mL of the hydrolysate should be equilibrated with 30 g of MMCP rather to achieve a 100 g/L adsorbent ratio. The real hydrolysate contains HMF which is a furan similar to furfural and will likely coadsorb onto MMCPs. Since the degree of coadsorption of HMF with furfural has not been quantified for MMCPs, the equilibrium adsorption of furfural could be reduced by up to half. The same protocol presented in Chapter 3 should be followed with magnetic retrieval and final vacuum filtration for removal of growth inhibiting nanoparticles. The treated, filter sterilized hydrolysate will be added to the 500 mL reactor with a 300 mL working volume. Seed cultures of *E. coli* will be grown in 5 mL aliquots of LB to ensure high initial cell density. From the seed cultures, reactors will be inoculated with ~2-3% by volume. It is expected such a fermentation of real hydrolysate would result in 40-50 g/L phenol, based on the culture results from Chapter 3.

5.3.3 Fermentation of Other Bioproducts from Pretreated Real Lignocellulosic Hydrolysates

By following the same strain growth protocol presented in the previous section, several bioproducts could be fermented from the pretreated real lignocellulosic hydrolysates. Many strains are developed along the path to a final optimized metabolic pathway for a specific bioproduct such as ethanol. Almost invariably, one strain developed is a high titer producer for an intermediate metabolite such as tyrosine, chorismate, etc. (Thompson et al., 2016) Some of the metabolites of interest which can be produced from lignocellulose-derived biomass are succinic acid and lactic acid. The adsorption of both succinic and lactic acid has been observed for MMCPs as presented in Appendix B. While succinate adsorbs onto MMCPs with very low loading capacity of 0.05 g/g or less, lactate adsorbs in a multi-layer fashion up to loading capacities exceeding 1 g/g. MMCPs could thereby be used for pretreatment and removal of furfural and regenerated before in-situ recovery of lactate from an overproducing strain. Other high titer bioproducts could also be produced from pretreated lignocellulosic media including isomers of butanol, and other aromatic metabolites.

5.3.4 An Improvement on MMCP Design

From its successful implementation of MMCPs as a suitable upstream detoxification and *in situ* product recovery, the design of MMCPs leaves room for improvement. The simplest improvement of the design would require improved milling and sieving for monodisperse size distribution. Monodispersity should improve the magnetic retrievability because it creates a known average particle mass around which to design the retrieval column. The force experienced by the MMCPs from the magnetic

field is directly proportional to the particle mass and the field strength. As the MMCP mass is estimated from an average bulk density, the average particle size has a direct effect on the mass. Therefore, by controlling the MMCP size distribution the magnetic retrieval will be more consistent. The size distribution however, would be expected to have a minimal impact on the specific loading or kinetics of adsorption because the surface area and pore distribution would remain unchanged.

As the surface chemistry is directly comparable to activated carbon, which is known to be poorly selective (Khan et al., 1981; Silvestre-Albero et al., 2009; Sulaymon & Ahmed, 2008; Sutikno & Himmelstein, 1983; K. Zhang et al., 2011), there are improvements to be made in selectivity. The high surface area and pore volume of the MMCPs provide ample volume for solvent loading of the pores. From the research detailed in these chapters and from adsorption work not included in this work (Wiehn et al., 2013; Wiehn et al., 2014), the adsorbents with the highest specific loading for most hydrophobic analytes are almost always charged (e.g. ion-exchange resins such as XAD-4, L-493, etc.). This charged surface can also promote fouling by media components and whole cells which causes loss of surface area to biofilm formation as discussed further in Appendix A. Each separations technique has pros and cons which make them far more suitable for specific rather than general applications as discussed in the first part of Chapter 1. This concept has been applied for certain resins by loading the pores with ionic liquids. (van den Berg et al., 2008)

Advances in liquid-liquid separations have discovered some applications of ionic liquids with partition coefficients of up to ~245 for hydrophobic analytes such as butanol.

(Gutowski et al., 2003) Compared to any other separation performance metric, this is greater than a ~20-fold improvement from the biocompatible solvents having partition coefficients of often less than 6 as shown in Table 5.1 for butanol. The organic phases listed are biocompatible, while the solvents with greater partition coefficients are often highly toxic to bacteria. The ionic liquids with the promise of greatly improved separations also are often toxic to bacteria and suffer from decreased selectivity from complex aqueous backgrounds.

Table 5.1.

Liquid-Liquid Partition Coefficients of Butanol.

Solvent	Partition coefficient	Feed Type	Notes	Reference
Organic Phases				
Oleyl alcohol	3.3-5.75*	Quaternary	*Calculated from reported data	(Kamiński et al., 2014; Malinowski, 2001)
Butyl Laurate	1.1	Fermentation		(Barton & Daugulis, 1992)
Polymer Phases				
poly(propylene glycol) 1200	4.8	Fermentation		(Barton & Daugulis, 1992)
poly(propylene glycol) 4000	3	Fermentation		(Barton & Daugulis, 1992)
Pluronic L64 (60% PPO 40% PEO)	2.70	Fermentation		(Dhamole et al., 2012)
Ionic Liquids				
[Ph3t][NTF]	1.1	Fermentation		(Cascon et al., 2011)
[THA][DHSS]	7.99	Fermentation		(Cascon et al., 2011)
[OMA][NTF]	1.44	Fermentation		(Cascon et al., 2011)

[Ph3t][DCN]	7.49	Fermentation		(Cascon et al., 2011)
[BMIM][CL]	33-245	Binary	Addition of K3PO4 (phase separation)	(Gutowski et al., 2003)
[BMIM][PF_6]	0.85	Binary		(Fadeev & Meagher, 2001)
[OMIM][PF_6]	0.9	Binary		(Fadeev & Meagher, 2001)

To address the weaknesses of each of these separations methods, it is interesting to envision a hybridized separations modality. The ideal separations modality based on the sum of this work would take advantage of the low energy input and high surface area contact of direct adsorbent addition. It would maintain the magnetic retrieval of the MMCPs studied here. It would then leverage the extremely high partition coefficients made possible by ionic liquids. These are likely toxic to bacteria although few have been studied with fermentation. An adsorbent loaded with a highly selective solvent can combine these specific separations benefits while canceling some of the weaknesses. Because of the high toxicity of the ionic liquids, a barrier is required. This barrier could be composed of any number of newer polymers under active research. A stimulus-responsive polymer would be best suited for a barrier to prevent cell toxicity. Many such polymers have been investigated for their change in conformation resulting from pH or temperature changes. A thin film of one of these polymers would provide a minimal mass transport resistance for the target analyte. Ideally this thin film polymer would be in its condensed phase during *in situ* adsorption and expanded during the desorption phase, following magnetic retrieval. This should address the expected desorption limitations by potentially: 1) Super-concentrating the analyte from low initial aqueous concentrations,

2) Removing thin film's contribution to the mass transport resistance to desorption, 3) Tuning the ionic phases to balance adsorption and desorption, 4) Ionically extracting the analyte-loaded phase with a secondary ionic solution.

Such a follow up project would be well suited for a dissertation topic. Its scope would necessarily encompass its own review of all the design considerations of ionic liquid separations, membrane perstraction, and pervaporation. A synthesis technique would have to be developed for the covalent linkage of the thin film to the MMCPs while maintaining monodispersity. The adsorption and kinetic studies would resemble those studied here. New desorption protocols would have to be developed. Its viability for in situ adsorption would also have to be studied. Such a project is feasible and could be completed by a competent researcher in the time scale of a typical dissertation project.

REFERENCES

Abdehagh, N., Gurnani, P., Tezel, F. H., & Thibault, J. (2015). Adsorptive separation and recovery of biobutanol from ABE model solutions. *Adsorption, 21*(3), 185-194. doi:10.1007/s10450-015-9661-0

Abdehagh, N., Tezel, F. H., & Thibault, J. (2013). Adsorbent screening for biobutanol separation by adsorption: kinetics, isotherms and competitive effect of other compounds. *Adsorption, 19*(6), 1263-1272. doi:10.1007/s10450-013-9566-8

Abdehagh, N., Tezel, F. H., & Thibault, J. (2014). Separation techniques in butanol production: Challenges and developments. *Biomass Bioenerg, 60*, 222-246. doi:10.1016/j.biombioe.2013.10.003

Adnadevic, B., Mojovic, Z., & Abu Rabi, A. (2008). The kinetics of ethanol adsorption from the aqueous phase onto zeolite NaZSM-5. *Adsorption, 14*(1), 123-131. doi:DOI 10.1007/s10450-007-9077-6

Aljundi, I. H., Belovich, J. M., & Talu, O. (2005). Adsorption of lactic acid from fermentation broth and aqueous solutions on Zeolite molecular sieves. *Chemical Engineering Science, 60*(18), 5004-5009. doi:10.1016/j.ces.2005.04.034

Ang, W., & Elimelech, M. (2007). Protein (BSA) fouling of reverse osmosis membranes: Implications for wastewater reclamation. *J Membrane Sci, 296*(1-2), 83-92. doi:10.1016/j.memsci.2007.03.018

Antoni, D., Zverlov, V. V., & Schwarz, W. H. (2007). Biofuels from microbes. *Appl Microbiol Biot, 77*(1), 23-35. doi:10.1007/s00253-007-1163-x

Atsumi, S., Cann, A. F., Connor, M. R., Shen, C. R., Smith, K. M., Brynildsen, M. P., . . . Liao, J. C. (2008). Metabolic engineering of Escherichia coli for 1-butanol production. *Metab Eng, 10*(6), 305-311. doi:10.1016/j.ymben.2007.08.003

Balan, V. (2014). Current Challenges in Commercially Producing Biofuels from Lignocellulosic Biomass. *ISRN Biotechnology, 2014*, 31. doi:10.1155/2014/463074

Bankar, S. B., Survase, S. A., Singhal, R. S., & Granström, T. (2012). Continuous two stage acetone–butanol–ethanol fermentation with integrated solvent removal using Clostridium acetobutylicum B 5313. *Bioresource Technol, 106*(0), 110-116. doi:http://dx.doi.org/10.1016/j.biortech.2011.12.005

Barton, W. E., & Daugulis, A. (1992). Evaluation of solvents for extractive butanol fermentation with Clostridium acetobutylicum and the use of poly(propylene glycol) 1200. *Appl Microbiol Biot, 36*(5), 632-639. doi:10.1007/bf00183241

Bauer, F. F., Govender, P., & Bester, M. C. (2010). Yeast flocculation and its biotechnological relevance. *Appl Microbiol Biotechnol, 88*(1), 31-39. doi:10.1007/s00253-010-2783-0

Ben Chaabane, F., Aldiguier, A. S., Alfenore, S., Cameleyre, X., Blanc, P., Bideaux, C., . . . Molina-Jouve, C. (2006). Very high ethanol productivity in an innovative continuous two-stage bioreactor with cell recycle. *Bioprocess Biosyst Eng, 29*(1), 49-57. doi:10.1007/s00449-006-0056-1

Berezina, O. V., Zakharova, N. V., Yarotsky, C. V., & Zverlov, V. V. (2012). Microbial producers of butanol. *Appl Biochem Micro+, 48*(7), 625-638. doi:10.1134/s0003683812070022

Bhattacharjee, S., Chen, J. Y., & Elimelech, M. (2000a). DLVO interaction energy between spheroidal particles and a flat surface. *Colloids and Surfaces A: Physicochemical and Engineering Aspects, 165*(1–3), 143-156. doi:http://dx.doi.org/10.1016/S0927-7757(99)00448-3

Bhattacharjee, S., Chen, J. Y., & Elimelech, M. (2000b). DLVO interaction energy between spheroidal particles and a flat surface. *Colloids and Surfaces A: Physicochemical and Engineering Aspects, 165*, 143-156.

Bhattacharjee, S., Sharma, A., & Bhattacharya, P. K. (1996). Estimation and Influence of Long Range Solute. Membrane Interactions in Ultrafiltration. *Ind Eng Chem Res, 35*(9), 3108-3121. doi:10.1021/ie9507843

Bioenergy, Energy Alternatives National, P., United States. Agricultural Research, S., United States. Agricultural Research, A., United States, S., Education Administration. Agricultural, R., . . . Program, A. R. S. B. (2005). Genomics and engineering of stress-tolerant microbes for lower cost production of biofuels and bioproducts ... annual report. *Genomics and engineering of stress-tolerant microbes for lower cost production of biofuels and bioproducts ... annual report*.

Bojsen, R. K., Andersen, K. S., & Regenberg, B. (2012). Saccharomyces cerevisiae – a model to uncover molecular mechanisms for yeast biofilm biology. *FEMS Immunology & Medical Microbiology, 65*(2), 169-182. doi:10.1111/j.1574-695X.2012.00943.x

Bond-Watts, B. B., Bellerose, R. J., & Chang, M. C. Y. (2011). Enzyme mechanism as a kinetic control element for designing synthetic biofuel pathways. *Nat Chem Biol, 7*(4), 222-227.

Bowles, L. K., & Ellefson, W. L. (1985). Effects of butanol on Clostridium acetobutylicum. *Appl Environ Microbiol, 50*(5), 1165-1170.

Boyang, J., Ling, S., Guangqian, H., Guangping, W., Jian, Z., & Lijuan, W. (2011). ADSORPTION PROPERTIES OF NICKEL-BASED MAGNETIC ACTIVATED CARBON PREPARED BY PD-FREE ELECTROLESS PLATING. *BioResources, 6*(1), 70-80.

Brownlee, H. J., & Miner, C. S. (1948). Industrial Development of Furfural. *Industrial & Engineering Chemistry, 40*(2), 201-204. doi:10.1021/ie50458a005

Cai, D., Zhang, T., Zheng, J., Chang, Z., Wang, Z., Qin, P. Y., & Tan, T. W. (2013). Biobutanol from sweet sorghum bagasse hydrolysate by a hybrid pervaporation process. *Bioresour Technol*. doi:10.1016/j.biortech.2013.02.094

Campaniello, J., Engelen, C. W. R., Haije, W. G., Pex, P. P. A. C., & Vente, J. F. (2004). Long-term pervaporation performance of microporous methylated silica membranes. *Chem Commun*(7), 834-835. doi:10.1039/b401496k

Cao, T., Tang, H., Liang, X., Wang, A., Auner, G. W., Salley, S. O., & Ng, K. Y. (2006). Nanoscale investigation on adhesion of E. coli to surface modified silicone using atomic force microscopy. *Biotechnol Bioeng, 94*(1), 167-176. doi:10.1002/bit.20841

Carey, F. A., & Sundberg, R. J. (2000). *Advanced organic chemistry* (fourth ed.). New York: Kluwer Academic/Plenum Pub.

Cascon, H. R., Choudhari, S. K., Nisola, G. M., Vivas, E. L., Lee, D.-J., & Chung, W.-J. (2011). Partitioning of butanol and other fermentation broth components in phosphonium and ammonium-based ionic liquids and their toxicity to solventogenic clostridia. *Sep Purif Technol, 78*(2), 164-174. doi:http://dx.doi.org/10.1016/j.seppur.2011.01.041

Chaudhury, M. K., & Whitesides, G. M. (1991). Direct measurement of interfacial interactions between semispherical lenses and flat sheets of poly(dimethylsiloxane) and their chemical derivatives. *Langmuir, 7*(5), 1013-1025. doi:10.1021/la00053a033

Chen, C. K., & Blaschek, H. P. (1999). Acetate enhances solvent production and prevents degeneration in Clostridium beijerinckii BA101. *Appl Microbiol Biot, 52*(2), 170-173.

Chen, C. Y., Tang, X. Y., Xiao, Z. Y., Zhou, Y. H., Jiang, Y., & Fu, S. W. (2013). Adaptive evolution of Saccharomyces cerevisiae in a continuous and closed circulating fermentation (CCCF) system coupled with PDMS membrane pervaporation. *Appl Biochem Biotechnol, 169*(8), 2362-2373. doi:10.1007/s12010-013-0142-1

Chen, X., Nielsen, K. F., Borodina, I., Kielland-Brandt, M. C., & Karhumaa, K. (2011). Increased isobutanol production in Saccharomyces cerevisiae by overexpression of genes in valine metabolism. *Biotechnol Biofuels, 4*, 21. doi:10.1186/1754-6834-4-21

Chen, Y., Ren, H., Liu, D., Zhao, T., Shi, X., Cheng, H., . . . Ying, H. (2014). Enhancement of n-butanol production by in situ butanol removal using permeating-heating-gas stripping in acetone-butanol-ethanol fermentation. *Bioresource Technol, 164*, 276-284. doi:10.1016/j.biortech.2014.04.107

Cheng, H. C., & Wang, F. S. (2010). Computer-aided biocompatible solvent design for an integrated extractive fermentation-separation process. *Chem Eng J, 162*(2), 809-820.

Chibowski, E., & Perea-Carpio, R. (2002). Problems of contact angle and solid surface free enrergy determination. *Advances in Colloid and Interface Science, 98*, 245-264.

Ciston, S., Lueptow, R. M., & Gray, K. A. (2008). Bacterial attachment on reactive ceramic ultrafiltration membranes. *J Membrane Sci, 320*(1-2), 101-107. doi:10.1016/j.memsci.2008.03.065

Connor, M. R., & Liao, J. C. (2009). Microbial production of advanced transportation fuels in non-natural hosts. *Curr Opin Biotech, 20*(3), 307-315. doi:S0958-1669(09)00038-X [pii] 10.1016/j.copbio.2009.04.002

D.O.E. (1990). *Office of Energy Research, Office of Program Analysis, Membrane spearation systems, Contract No. DE-AC01-88ER30133*. Washington.

Dafoe, J. T., & Daugulis, A. J. (2014). In situ product removal in fermentation systems: improved process performance and rational extractant selection. *Biotechnol Lett, 36*(3), 443-460. doi:10.1007/s10529-013-1380-6

Dai, M., & Vogt, B. D. (2012). High capacity magnetic mesoporous carbon–cobalt composite adsorbents for removal of methylene green from aqueous solutions. *J. Colloid Interface Sci., 387*(1), 127-134. doi:http://dx.doi.org/10.1016/j.jcis.2012.06.062

Dalecka, B., Strods, M., & Mezule, L. (2015). Production of fermentation feedstock from lignocellulosic biomass: applications of membrane separation. *Agronomy Research, 13*(2), 287-293.

Dhamole, P. B., Wang, Z., Liu, Y., Wang, B., & Feng, H. (2012). Extractive fermentation with non-ionic surfactants to enhance butanol production. *Biomass Bioenerg, 40*(0), 112-119. doi:http://dx.doi.org/10.1016/j.biombioe.2012.02.007

Diaz, C., Schilardi, P. L., Salvarezza, R. C., & Fernandez Lorenzo de Mele, M. (2011). Have flagella a preferred orientation during early stages of biofilm formation?: AFM study using patterned substrates. *Colloids Surf B Biointerfaces, 82*(2), 536-542. doi:10.1016/j.colsurfb.2010.10.013

Dohnalkova, A. C., Marshall, M. J., Arey, B. W., Williams, K. H., Buck, E. C., & Fredrickson, J. K. (2011). Imaging hydrated microbial extracellular polymers: comparative analysis by electron microscopy. *Appl Environ Microbiol, 77*(4), 1254-1262. doi:10.1128/AEM.02001-10

Drobek, M., Yacou, C., Motuzas, J., Julbe, A., Ding, L., & Diniz da Costa, J. C. (2012). Long term pervaporation desalination of tubular MFI zeolite membranes. *J Membrane Sci, 415-416*, 816-823. doi:10.1016/j.memsci.2012.05.074

Elshahed, M. S., & McInerney, M. J. (2001). Benzoate Fermentation by the Anaerobic Bacterium Syntrophus aciditrophicus in the Absence of Hydrogen-Using Microorganisms. *Applied and Environmental Microbiology, 67*(12), 5520. doi:10.1128/aem.67.12.5520-5525.2001

Eom, M.-H., Kim, B., Jang, H., Lee, S.-H., Kim, W., Shin, Y.-A., & Lee, J. H. (2015). Dynamic Modeling of a Fermentation Process with Ex situ Butanol Recovery (ESBR) for Continuous Biobutanol Production. *Energy & Fuels, 29*(11), 7254-7265. doi:10.1021/acs.energyfuels.5b01031

Eom, M.-H., Kim, W., Lee, J., Cho, J.-H., Seung, D., Park, S., & Lee, J. H. (2013). Modeling of a biobutanol adsorption process for designing an extractive fermentor. *Ind Eng Chem Res, 52*(2), 603-611. doi:10.1021/ie301249z

Ezeji, T. C., Qureshi, N., & Blaschek, H. P. (2004a). Acetone butanol ethanol (ABE) production from concentrated substrate: reduction in substrate inhibition by fed-batch technique and product inhibition by gas stripping. *Appl Microbiol Biot, 63*(6), 653-658. doi:http://dx.doi.org/10.1007/s00253-003-1400-x

Ezeji, T. C., Qureshi, N., & Blaschek, H. P. (2004b). Butanol fermentation research: upstream and downstream manipulations. *Chem Rec, 4*(5), 305-314. doi:10.1002/tcr.20023

Ezeji, T. C., Qureshi, N., & Blaschek, H. P. (2007). Bioproduction of butanol from biomass: from genes to bioreactors. *Curr Opin Biotech, 18*(3), 220-227. doi:10.1016/j.copbio.2007.04.002

Ezeji, T. C., Qureshi, N., & Blaschek, H. P. (2013). Microbial production of a biofuel (acetone-butanol-ethanol) in a continuous bioreactor: impact of bleed and simultaneous product removal. *Bioprocess Biosyst Eng, 36*(1), 109-116. doi:10.1007/s00449-012-0766-5

Fadeev, A. G., & Meagher, M. M. (2001). Opportunities for ionic liquids in recovery of biofuels. *Chem Commun*(03), 295-296.

Faisal, A., Zhou, M., Hedlund, J., & Grahn, M. (2016). Recovery of butanol from model ABE fermentation broths using MFI adsorbent: a comparison between traditional beads and a structured adsorbent in the form of a film. *Adsorption*, 1-10. doi:10.1007/s10450-016-9759-z

Fierro, V., Torné-Fernández, V., Montané, D., & Celzard, A. (2008). Adsorption of phenol onto activated carbons having different textural and surface properties. *Micropor Mesopor Mat, 111*(1-3), 276-284. doi:10.1016/j.micromeso.2007.08.002

Flemming, H. C., & Wingender, J. (2010). The biofilm matrix. *Nat Rev Microbiol, 8*(9), 623-633. doi:10.1038/nrmicro2415

Fowkes, F. M. (1964). Attractive forces at interfaces. *Industrial & Engineering Chemistry, 56*(12), 40-52. doi:10.1021/ie50660a008

Garcia, V., Pakkila, J., Ojamo, H., Muurinen, E., & Keiski, R. L. (2011). Challenges in biobutanol production: How to improve the efficiency? *Renew Sust Energ Rev, 15*(2), 964-980. doi:DOI 10.1016/j.rser.2010.11.008

Gaykawad, S. S., Zha, Y., Punt, P. J., van Groenestijn, J. W., van der Wielen, L. A., & Straathof, A. J. (2013). Pervaporation of ethanol from lignocellulosic fermentation broth. *Bioresour Technol, 129*, 469-476. doi:10.1016/j.biortech.2012.11.104

Ghosh, U. K., Pradhan, N. C., & Adhikari, B. (2007). Separation of furfural from aqueous solution by pervaporation using HTPB-based hydrophobic polyurethaneurea membranes. *Desalination, 208*(1), 146-158. doi:http://dx.doi.org/10.1016/j.desal.2006.04.078

Ghosh, U. K., Pradhan, N. C., & Adhikari, B. (2010). Pervaporative separation of furfural from aqueous solution using modified polyurethaneurea membrane. *Desalination, 252*(1-3), 1-7. doi:10.1016/j.desal.2009.11.009

Gonzalez-Penas, H., Lu-Chau, T. A., Moreira, M. T., & Lema, J. M. (2014). Solvent screening methodology for in situ ABE extractive fermentation. *Appl Microbiol Biot, 98*(13), 5915-5924. doi:10.1007/s00253-014-5634-6

Groot, W. J., & Luyben, K. C. A. M. (1986a). *In situ* product recovery by adsorption in the butanol-isopropanol batch fermentation. *Appl Microbiol Biot, 25*(1), 29-31.

Groot, W. J., & Luyben, K. C. A. M. (1986b). *In situ* product recovery by adsorption in the butanol-isopropanol batch fermentation. *Applied Microbiology and Biotechnology, 25*(1), 29-31.

Groot, W. J., & Luyben, K. C. A. M. (1987). Continuous production of butanol from a glucose/xylose mixture with an immobilized cell system coupled to pervaporation. *Biotechnol Lett, 9*(12), 867-870. doi:10.1007/bf01026200

Groot, W. J., Soedjak, H. S., Donck, P. B., van der Lans, R. G. J. M., Luyben, K. C. A. M., & Timmer, J. M. K. (1990). Butanol recovery from fermentations by liquid-liquid extraction and membrane solvent extraction. *Bioprocess Eng, 5*(5), 203-216. doi:10.1007/bf00376227

Groot, W. J., van der Lans, R. G. J. M., & Luyben, K. C. A. M. (1992). Technologies for butanol recovery integrated with fermentations. *Process Biochem, 27*(2), 61-75. doi:http://dx.doi.org/10.1016/0032-9592(92)80012-R

Gudena, K., Rangaiah, G. P., & Lakshminarayanan, S. (2013). HiGee Stripper-Membrane System for Decentralized Bioethanol Recovery and Purification. *Ind Eng Chem Res, 52*(12), 4572-4585. doi:10.1021/ie302557f

Guo, B., Styles, C. A., Feng, Q., & Fink, G. R. (2000). A Saccharomyces gene family involved in invasive growth, cell-cell adhesion, and mating. *Proc Natl Acad Sci U S A, 97*(22), 12158-12163. doi:10.1073/pnas.220420397

Guo, M., Song, W., & Buhain, J. (2015). Bioenergy and biofuels: History, status, and perspective. *Renewable and Sustainable Energy Reviews, 42*, 712-725. doi:http://dx.doi.org/10.1016/j.rser.2014.10.013

Gutowski, K. E., Broker, G. A., Willauer, H. D., Huddleston, J. G., Swatloski, R. P., Holbrey, J. D., & Rogers, R. D. (2003). Controlling the aqueous miscibility of ionic liquids: aqueous biphasic systems of water-miscible ionic liquids and water-structuring salts for recycle, metahesis, and separations. *Journal of the American Chemical Society Communications, 125*, 6632-6633.

Hao, S., Xiao, X., Hu, Z., Sun, L., Han, S., Chen, D., & Liu, X. (2013). Improving the Electrochemical Performance of Li4Ti5O12 Anode through Confinement into Ordered Bimodal Porous Carbon Frameworks. *J. Phys. Chem. C, 117*(51), 26889-26895. doi:10.1021/jp408740k

Hardy, E., Kamphuis, T., Japaridze, A., Wilschut, J. C., & Winterhalter, M. (2012). Nanoaggregates of micropurified lipopolysaccharide identified using dynamic light scattering, zeta potential measurement, and TLR4 signaling activity. *Anal Biochem, 430*(2), 203-213. doi:10.1016/j.ab.2012.08.027

Hartmann, M., Vinu, A., & Chandrasekar, G. (2005). Adsorption of vitamin E on mesoporous carbon molecular sieves. *Chem Mater, 17*(4), 829-833. doi:10.1021/cm048564f

Hashi, M., Tezel, F. H., & Thibault, J. (2010). Ethanol recovery from fermentation broth via carbon dioxide stripping and adsorption. *Energ Fuel, 24*, 4628-4637. doi:Doi 10.1021/Ef901130q

Heerema, L., Wierckx, N., Roelands, M., Hanemaaijer, J. H., Goetheer, E., Verdoes, D., & Keurentjes, J. (2011). In situ phenol removal from fed-batch fermentations of solvent tolerant Pseudomonas putida S12 by pertraction. *Biochem Eng J, 53*(3), 245-252. doi:http://dx.doi.org/10.1016/j.bej.2010.11.002

Heitmann, S., Krings, J., Kreis, P., Lennert, A., Pitner, W. R., Górak, A., & Schulte, M. M. (2012). Recovery of n-butanol using ionic liquid-based pervaporation membranes. *Sep Purif Technol, 97*, 108-114. doi:10.1016/j.seppur.2011.12.033

Hijnen, W. A., Castillo, C., Brouwer-Hanzens, A. H., Harmsen, D. J., Cornelissen, E. R., & van der Kooij, D. (2012). Quantitative assessment of the efficacy of spiral-wound membrane cleaning procedures to remove biofilms. *Water Res, 46*(19), 6369-6381. doi:10.1016/j.watres.2012.09.013

Ho, Y. S., & McKay, G. (1999). Pseudo-second order model for sorption processes. *Process Biochem, 34*(5), 451-465. doi:Doi 10.1016/S0032-9592(98)00112-5

Hou, S., Gu, H., Smith, C., & Ren, D. (2011). Microtopographic Patterns Affect Escherichia coli Biofilm Formation on Poly(dimethylsiloxane) Surfaces. *Langmuir*. doi:10.1021/la1046194

Hu, S., Guan, Y., Cai, D., Li, S., Qin, P., Karim, M. N., & Tan, T. (2015). A novel method for furfural recovery via gas stripping assisted vapor permeation by a polydimethylsiloxane membrane. *Sci Rep, 5*, 9428. doi:10.1038/srep09428

Huang, J., Zhou, Y., Huang, K., Liu, S., Luo, Q., & Xu, M. (2007). Adsorption behavior, thermodynamics, and mechanism of phenol on polymeric adsorbents with amide group in cyclohexane. *J Colloid Interface Sci, 316*(1), 10-18. doi:10.1016/j.jcis.2007.07.080

Hwang, G., Yang, J.-h., Lee, C.-H., Ahn, I.-S., & Mhin, B. J. (2011). New Selection Criterion for a Base Polar Liquid in the Lifshitz–van der Waals/Lewis Acid–Base Approach. *The Journal of Physical Chemistry C, 115*(25), 12458-12463. doi:10.1021/jp200741v

Ikegami, T., Negishi, H., Nakayama, S., Kobayashi, G., & Sakaki, K. (2014). Pervaporative concentration of biobutanol from abe fermentation broths by Clostridium saccharoperbutylacetonicum using silicone rubber-coated silicalite-1 membranes. *Sep Purif Technol, 132*, 206-212. doi:10.1016/j.seppur.2014.05.030

Ikegami, T., Negishi, H., & Sakaki, K. (2011). Selective separation of n-butanol from aqueous solutions by pervaporation using silicone rubber-coated silicalite membranes. *Journal of Chemical Technology & Biotechnology, 86*(6), 845-851. doi:10.1002/jctb.2598

Ikegami, T., Negishi, H., Yanase, H., Sakaki, K., Okamoto, M., Koura, N., . . . Yanagishita, H. (2007). Stabilized production of highly concentrated bioethanol from fermentation broths byZymomonas mobilis by pervaporation using silicone rubber-coated silicalite

membranes. *Journal of Chemical Technology & Biotechnology, 82*(8), 745-751. doi:10.1002/jctb.1724

Imamoglu, S. (2002). Simulated moving bed chromatography (SMB) for application in bioseparation. *Adv Biochem Eng Biotechnol, 76*, 211-231.

Ingram, L. (1990). Ethanol tolerance in bacteria. *Crc Cr Rev Biotechn, 9*(4), 305-319.

Ishii, S., Taya, M., & Kobayashi, T. (1985). Production of butanol by *Clostridium acetobutylicum* in extractive fermentation system. *J Chem Eng Jpn, 18*(2), 125-130.

Ishizaki, A., Michiwaki, S., Crabbe, E., Kobayashi, G., Sonomoto, K., & Yoshino, S. (1999). Extractive acetone-butanol-ethanol fermentation using methylated crude palm oil as extractant in batch culture of Clostridium saccharoperbutylacetonicum N1-4 (ATCC 13564). *J Biosci Bioeng, 87*(3), 352-356. doi:http://dx.doi.org/10.1016/S1389-1723(99)80044-9

Jarboe, L. R., Zhang, X., Wang, X., Moore, J. C., Shanmugam, K. T., & Ingram, L. O. (2010). Metabolic engineering for production of biorenewable fuels and chemicals: contributions of synthetic biology. *J Biomed Biotechnol, 2010*, 761042. doi:10.1155/2010/761042

Jeon, E. J., Kim, A. S., & Lee, Y. T. (2012). Pervaporation of butanol/water mixtures using siloxane polymer/ceramic composite membranes. *Desalination and Water Treatment, 48*(1-3), 17-26. doi:10.1080/19443994.2012.698723

Jeon, Y. J., & Lee, Y. Y. (1987). Membrane-assisted extractive butanol fermentation. *Ann NY Acad Sci, 506*(1), 536-542. doi:10.1111/j.1749-6632.1987.tb23848.x

Jia, C., Li, X., Liu, Z., Xu, B., Yao, S., & Song, H. (2015). Adsorption process and mechanism for furfural separation with macroporous resin. *Desalination and Water Treatment, 56*(8), 2214-2224. doi:10.1080/19443994.2014.960455

Jones, D. T., & Woods, D. R. (1986a). Acetone-butanol fermentation revisited. *Microbiol Rev, 50*(4), 484-524.

Jones, D. T., & Woods, D. R. (1986b). Acetone-Butanol Fermentation Revisited. *Microbiol Rev, 50*(4), 484-524.

Jonsson, L. J., & Martin, C. (2016). Pretreatment of lignocellulose: Formation of inhibitory by-products and strategies for minimizing their effects. *Bioresour Technol, 199*, 103-112. doi:10.1016/j.biortech.2015.10.009

Kamiński, W., Górak, A., & Kubiczek, A. (2014). Modeling of liquid–liquid equilibrium in the quinary system of water, acetone, n-butanol, ethanol, and ionic liquid. *Fluid Phase Equilibr, 384*(0), 114-121. doi:http://dx.doi.org/10.1016/j.fluid.2014.10.017

Kang, S., & Choi, H. (2005). Effect of surface hydrophobicity on the adhesion of S. cerevisiae onto modified surfaces by poly(styrene-ran-sulfonic acid) random copolymers. *Colloids Surf B Biointerfaces, 46*(2), 70-77. doi:10.1016/j.colsurfb.2005.08.017

Kang, S., Hoek, E. M. V., Choi, H., & Shin, H. (2006). Effect of Membrane Surface Properties During the Fast Evaluation of Cell Attachment. *Separation Science and Technology, 41*(7), 1475-1487. doi:10.1080/01496390600634673

Karnib, M., Holail, H., Olama, Z., Kabbani, A., & Hines, M. (2013). The antibacterial activity of activated carbon, silver, silver impregnated activated carbon and silica sand nanoparticles against pathogenic E. coli BL21. *Int. J. Curr. Microbiol. App. Sci, 2*(4), 20-30.

Keasling, J. D., & Chou, H. (2008). Metabolic engineering delivers next-generation biofuels. *Nat Biotechnol, 26*(3), 298-299. doi:nbt0308-298 [pii] 10.1038/nbt0308-298

Keum, Y. S., Seo, J. S., & Li, Q. X. (2006). Synthesis of Bacterial Metabolites of Polycyclic Aromatic Hydrocarbons: Benzochromenones, Carboxyvinylnaphthoates, and Substituted Aryloxobutenoates. *ChemInform, 37*(8), no-no. doi:10.1002/chin.200608052

Khan, K. A., Suidan, M. T., & Cross, W. H. (1981). Anaerobic activated carbon filter for the treatment of phenol-bearing wastewater. *Journal of the Water Environment Federation, 53*(10), 1519-1532.

Kim, B., Park, H., Na, D., & Lee, S. Y. (2014). Metabolic engineering of Escherichia coli for the production of phenol from glucose. *Biotechnol J, 9*(5), 621-629. doi:10.1002/biot.201300263

Kita, H., Chen, X., Lin, X., Okamoto, K.-i., Yamamura, T., & Abe, J. (2003). Tubular Type Pervaporation Module With Silicalite Membranes For Dehydration of Biomass Alcohol. *Fuel Chemistry Division Preprints, 48*(1), 489.

Kittur, A. A., Kariduraganavar, M. Y., Kulkarni, S. S., & Aralaguppi, M. I. (2005). Preparation of zeolite-incorporated poly(dimethyl siloxane) membranes for the pervaporation separation of isopropyl alcohol/water mixtures. *J Appl Polym Sci, 96*(4), 1377-1387. doi:10.1002/app.21566

Kollerup, F., & Daugulis, A. J. (1985). Screening and identification of extractive fermentation solvents using a database. *Can J Chem Eng, 63*(6), 919-927.

Kregiel, D. (2013). Bacterial adhesion to glass surface modified with organosilanes. *Food Technology and Biotechnology, 51*(3), 245-351.

Kumar, M., & Gayen, K. (2011). Developments in biobutanol production: New insights. *Appl Energ, 88*(6), 1999-2012. doi:DOI 10.1016/j.apenergy.2010.12.055

Kumar, P., Barrett, D. M., Delwiche, M. J., & Stroeve, P. (2009). Methods for Pretreatment of Lignocellulosic Biomass for Efficient Hydrolysis and Biofuel Production. *Industrial & Engineering Chemistry Research, 48*(8), 3713-3729. doi:10.1021/ie801542g

Kwan, T. H., Hu, Y., & Lin, C. S. K. (2016). Valorisation of food waste via fungal hydrolysis and lactic acid fermentation with Lactobacillus casei Shirota. *Bioresource Technol, 217*, 129-136. doi:10.1016/j.biortech.2016.01.134

Kwok, D. Y., Li, D., & Neumann, A. W. (1994). Evaluation of the Lifshitz-van der Waals/Acid-Base Approach To Determine Interfacial Tensions. *Langmuir, 10*(4), 1323-1328. doi:10.1021/la00016a057

Larrayoz, M. A., & Puigjaner, L. (1987). Study of butanol extraction through pervaporation in acetobutylic fermentation. *Biotechnol Bioeng, 30*(5), 692-696. doi:10.1002/bit.260300516

Larsson, S., Palmqvist, E., Hahn-Hägerdal, B., Tengborg, C., Stenberg, K., Zacchi, G., & Nilvebrant, N.-O. (1999). The generation of fermentation inhibitors during dilute acid hydrolysis of softwood. *Enzyme Microb Tech, 24*(3), 151-159. doi:http://dx.doi.org/10.1016/S0141-0229(98)00101-X

Lau, M. W., Gunawan, C., Balan, V., & Dale, B. E. (2010). Comparing the fermentation performance of Escherichia coli KO11, Saccharomyces cerevisiae 424A(LNH-ST) and Zymomonas mobilis AX101 for cellulosic ethanol production. *Biotechnol Biofuels, 3*, 11. doi:10.1186/1754-6834-3-11

Lee, J., Jang, Y. S., Choi, S. J., Im, J. A., Song, H., Cho, J. H., . . . Lee, S. Y. (2012). Metabolic engineering of Clostridium acetobutylicum ATCC 824 for isopropanol-butanol-ethanol fermentation. *Appl Environ Microbiol, 78*(5), 1416-1423. doi:10.1128/AEM.06382-11

Lee, J. N., Park, C., & Whitesides, G. M. (2003). Solvent compatibility of poly(dimethylsiloxane)-based microfluidic devices *Anal Chem, 75*, 6544-6554.

Lee, S. C., & Park, S. (2016). Removal of furan and phenolic compounds from simulated biomass hydrolysates by batch adsorption and continuous fixed-bed column adsorption methods. *Bioresour Technol, 216*, 661-668. doi:10.1016/j.biortech.2016.06.007

Levario, T. J., Dai, M., Yuan, W., Vogt, B. D., & Nielsen, D. R. (2012a). Rapid adsorption of alcohol biofuels by high surface area mesoporous carbons. *Microporous Mesoporous Mater., 148*(1), 107-114. doi:http://dx.doi.org/10.1016/j.micromeso.2011.08.001

Levario, T. J., Dai, M., Yuan, W., Vogt, B. D., & Nielsen, D. R. (2012b). Rapid adsorption of alcohol biofuels by high surface area mesoporous carbons. *Microporous and Mesoporous Materials, 148*(1), 107-114. doi:http://dx.doi.org/10.1016/j.micromeso.2011.08.001

Levario, T. J., Dai, M. Z., Yuan, W., Vogt, B. D., & Nielsen, D. R. (2012). Rapid adsorption of alcohol biofuels by high surface area mesoporous carbons. *Micropor Mesopor Mat, 148*(1), 107-114. doi:Doi 10.1016/J.Micromeso.2011.08.001

Li, B., & Logan, B. E. (2004). Bacterial adhesion to glass and metal-oxide surfaces. *Colloids Surf B Biointerfaces, 36*(2), 81-90. doi:10.1016/j.colsurfb.2004.05.006

Li, J., Chen, X., Qi, B., Luo, J., Zhuang, X., Su, Y., & Wan, Y. (2014). Continuous acetone–butanol–ethanol (ABE) fermentation with in situ solvent recovery by silicalite-1 filled PDMS/PAN composite membrane. *Energ Fuel, 28*(1), 555-562. doi:10.1021/ef401706k

Li, J., Zheng, X.-Y., Fang, X.-J., Liu, S.-W., Chen, K.-Q., Jiang, M., . . . Ouyang, P.-K. (2011). A complete industrial system for economical succinic acid production by Actinobacillus

succinogenes. *Bioresource Technol, 102*(10), 6147-6152. doi:http://dx.doi.org/10.1016/j.biortech.2011.02.093

Li, Q., Cai, H., Hao, B., Zhang, C., Yu, Z., Zhou, S., & Chenjuan, L. (2010). Enhancing clostridial acetone-butanol-ethanol (ABE) production and improving fuel properties of abe-enriched biodiesel by extractive fermentation with biodiesel. *Appl Biochem Biotech, 162*(8), 2381-2386. doi:10.1007/s12010-010-9010-4

Li, S. Y., Srivastava, R., & Parnas, R. S. (2011). Study of in situ 1-Butanol Pervaporation from A-B-E Fermentation Using a PDMS Composite Membrane: Validity of Solution-Diffusion Model for Pervaporative A-B-E Fermentation. *Biotechnol Progr, 27*(1), 111-120. doi:Doi 10.1002/Btpr.535

Lin, X., Kita, H., & Okamoto, A. (2001). Silicalite Membrane Preparation, Characterization, and Separation Performance. *Ind Eng Chem Res, 40*, 4069-4078.

Lin, X., Li, R., Wen, Q., Wu, J., Fan, J., Jin, X., . . . Ying, H. (2013). Experimental and modeling studies on the sorption breakthrough behaviors of butanol from aqueous solution in a fixed-bed of KA-I resin. *Biotechnol Bioproc E, 18*(2), 223-233. doi:10.1007/s12257-012-0549-5

Lin, X., Wu, J., Fan, J., Qian, W., Zhou, X., Qian, C., . . . Ying, H. (2012). Adsorption of butanol from aqueous solution onto a new type of macroporous adsorption resin: Studies of adsorption isotherms and kinetics simulation. *J Chem Technol Biot, 87*(7), 924-931. doi:10.1002/jctb.3701

Lin, X., Wu, J., Jin, X., Fan, J., Li, R., Wen, Q., . . . Ying, H. (2012). Selective separation of biobutanol from acetone-butanol-ethanol fermentation broth by means of sorption methodology based on a novel macroporous resin. *Biotechnol Progr, 28*(4), 962-972. doi:10.1002/btpr.1553

Lin, X., Xiong, L., Qi, G., Shi, S., Huang, C., Chen, X., & Chen, X. (2015). Using Butanol Fermentation Wastewater for Biobutanol Production after Removal of Inhibitory Compounds by Micro/Mesoporous Hyper-Cross-Linked Polymeric Adsorbent. *ACS Sustainable Chem. Eng., 3*(4), 702-709. doi:10.1021/acssuschemeng.5b00010

Liu, D., Chen, Y., Ding, F.-Y., Zhao, T., Wu, J.-L., Guo, T., . . . Ying, H.-J. (2014). Biobutanol production in a Clostridium acetobutylicum biofilm reactor integrated with simultaneous product recovery by adsorption. *Biotechnol Biofuels, 7*(5), 1-13. doi:10.1186/1754-6834-7-5

Liu, D., Chen, Y., Li, A., Ding, F., Zhou, T., He, Y., . . . Ying, H. (2013). Enhanced butanol production by modulation of electron flow in Clostridium acetobutylicum B3 immobilized by surface adsorption. *Bioresource Technol, 129*(0), 321-328. doi:http://dx.doi.org/10.1016/j.biortech.2012.11.090

Liu, X., Wang, C., Wu, Q., & Wang, Z. (2015). Magnetic porous carbon-based solid-phase extraction of carbamates prior to HPLC analysis. *Microchim Acta, 183*(1), 415-421. doi:10.1007/s00604-015-1664-8

Lorite, G. S., de Souza, A. A., Neubauer, D., Mizaikoff, B., Kranz, C., & Cotta, M. A. (2013). On the role of extracellular polymeric substances during early stages of Xylella fastidiosa biofilm formation. *Colloids Surf B Biointerfaces, 102*, 519-525. doi:10.1016/j.colsurfb.2012.08.027

Lu, C., Dong, J., & Yang, S.-T. (2013). Butanol production from wood pulping hydrolysate in an integrated fermentation–gas stripping process. *Bioresource Technol, 143*(0), 467-475. doi:http://dx.doi.org/10.1016/j.biortech.2013.06.012

Lu, C., Zhao, J., Yang, S. T., & Wei, D. (2012). Fed-batch fermentation for n-butanol production from cassava bagasse hydrolysate in a fibrous bed bioreactor with continuous gas stripping. *Bioresour Technol, 104*, 380-387. doi:10.1016/j.biortech.2011.10.089

Lu, Q., Wang, J., Faghihnejad, A., Zeng, H., & Liu, Y. (2011). Understanding the molecular interactions of lipopolysaccharides during E. coli initial adhesion with a surface forces apparatus. *Soft Matter, 7*(19), 9366. doi:10.1039/c1sm05554b

Luyben, W. L. (2008). Control of the Heterogeneous Azeotropic n-Butanol/Water Distillation System. *Energ Fuel, 22*(6), 4249-4258.

Machado, G., Leon, S., Santos, F., Lourega, R., Dullius, J., Mollmann, M. E., & Eichler, P. (2016). Literature Review on Furfural Production from Lignocellulosic Biomass. *Natural Resources, 07*(03), 115-129. doi:10.4236/nr.2016.73012

Maddox, I. S. (1982). Use of silicalite for the adsorption of normal-butanol from fermentation liquors. *Biotechnol Lett, 4*(11), 759-760.

Malinowski, J. J. (2001). Two-phase partitioning bioreactors in fermentation technology. *Biotechnol Adv, 19*(7), 525-538. doi:http://dx.doi.org/10.1016/S0734-9750(01)00080-5

Mariano, A. P., Qureshi, N., Maciel Filho, R., & Ezeji, T. C. (2012). Assessment of in situ butanol recovery by vacuum during acetone butanol ethanol (abe) fermentation. *J Chem Technol Biot, 87*(3), 334-340. doi:10.1002/jctb.2717

Martarella, R. L., Rittmann, B., Lai, S. Y.-J., Chemical Engineering, P., & Barrett, T. H. C. (2015). Lipid Extraction from Microalgae Strains for Biodiesel. In.

McKenna, R., & Nielsen, D. R. (2011). Styrene biosynthesis from glucose by engineered E. coli. *Metab Eng, 13*(5), 544-554. doi:10.1016/j.ymben.2011.06.005

Menchavez, R. N., & Ha, S. H. (2013). Ultrasound-enhanced recovery of butanol/abe by pervaporation. *Appl Biochem Biotech, 171*(5), 1159-1169. doi:10.1007/s12010-013-0196-0

Meng, Y., Gu, D., Zhang, F., Shi, Y., Cheng, L., Feng, D., . . . Zhao, D. (2006). A Family of Highly Ordered Mesoporous Polymer Resin and Carbon Structures from Organic−Organic Self-Assembly. *Chem Mater, 18*(18), 4447-4464. doi:10.1021/cm060921u

Meng, Y., Gu, D., Zhang, F., Shi, Y., Yang, H., Li, Z., . . . Zhao, D. (2005). Ordered mesoporous polymers and homologous carbon frameworks: amphiphilic surfactant templating and

direct transformation. *Angew Chem Int Ed Engl, 44*(43), 7053-7059. doi:10.1002/anie.200501561

Menkhaus, T. J., & Glatz, C. E. (2005). Antibody capture from corn endosperm extracts by packed bed and expanded bed adsorption. *Biotechnol Progr, 21*(2), 473-485. doi:10.1021/bp049689s

Miao, L., Li, Q., Diao, A., Zhang, X., & Ma, Y. (2015). Construction of a novel phenol synthetic pathway in Escherichia coli through 4-hydroxybenzoate decarboxylation. *Appl Microbiol Biot, 99*(12), 5163-5173. doi:10.1007/s00253-015-6497-1

Milestone, N. B., & Bibby, D. M. (1981). Concentration of alcohols by adsorption on silicalite. *J Chem Technol Biot, 31*(12), 732-736.

Nguyen, C., & Do, D. D. (2000). Dual Langmuir Kinetic Model for Adsorption in Carbon Molecular Sieve Materials. *Fuel, 16*, 1868-1873.

Nielsen, D. R., Leonard, E., Yoon, S. H., Tseng, H. C., Yuan, C., & Prather, K. L. J. (2009). Engineering alternative butanol production platforms in heterologous bacteria. *Metab Eng, 11*(4-5), 262-273. doi:Doi 10.1016/J.Ymben.2009.05.003

Nielsen, D. R., & Prather, K. J. (2009). In situ product recovery of n-butanol using polymeric resins. *Biotechnol Bioeng, 102*(3), 811-821. doi:10.1002/bit.22109

Nielsen, D. R., Prather, K. L. J., & Amarasiriwardena, G. S. (2010). Predicting the adsorption of second generation biofuels by polymeric resins with applications for in situ product recovery (ISPR). *Bioresource Technol, 101*(8), 2762-2769. doi:10.1016/j.biortech.2009.12.003

Nielsen, L., Larsson, M., Holst, O., & Mattiasson, B. (1988). Adsorbents for extractive bioconversion applied to the acetone-butanol fermentation. *Appl Microbiol Biot, 28*(4-5), 335-339.

Nikolakis, V., Kokkoli, E., Tirrell, M., Tsapatsis, M., & Vlachos, D. G. (2000). Zeolite growth by addition of subcolloidal particles: modeling and experimental validation. *Chem. Mater., 12*(3), 845-853.

Noisuwan, A., Hemar, Y., Wilkinson, B., & Bronlund, J. E. (2011). Adsorption of milk proteins onto rice starch granules. *Carbohydrate Polymers, 84*(1), 247-254. doi:10.1016/j.carbpol.2010.11.029

Nongonierma, A., Cayot, P., Le Quere, J. L., Springett, M., & Voilley, A. (2006). Mechanisms of extraction of aroma compounds from foods, using adsorbents. Effect of various parameters. *Food Rev Int, 22*(1), 51-94.

Nunes, C. D., Pires, J., Carvalho, A. P., Calhorda, M. J., & Ferreira, P. (2008). Synthesis and characterisation of organo-silica hydrophobic clay hetero structures for volatile organic compounds removal. *Micropor Mesopor Mat, 111*(1-3), 612-619. doi:DOI 10.1016/j.micromeso.2007.09.008

O'Toole, G. A., & Kolter, R. (1998). Initiation of biofilm formation in Pseudomonas fluorescens WCS365 proceeds via multiple, convergent singnalling pathways: a genetic analysis. *Molecular Microbiology, 28*(3), 449-461.

Oliveira, L. C. A., Rios, R. V. R. A., Fabris, J. D., Garg, V., Sapag, K., & Lago, R. M. (2002). Activated carbon/iron oxide magnetic composites for the adsorption of contaminants in water. *Carbon, 40*(12), 2177-2183.

Ong, Y.-L., Razatos, A., Georgiou, G., & Sharma, M. M. (1999a). Adhesion Forces between E. coli Bacteria and Biomaterial Surfaces. *Langmuir, 15*(8), 2719-2725. doi:10.1021/la981104e

Ong, Y.-L., Razatos, A., Georgiou, G., & Sharma, M. M. (1999b). Adhesion Forces Between E. coli Bacteria and Biomaterial Surfaces. *Langmuir, 15*, 2719-2725.

Osborne, S., Leaver, J., Turner, M., & Dunnil, P. (1990). Correlation of biocatalytic activity in an organic aqueous 2-liquid phase system with solvent concentration in the cell membrane. *Enzyme Microb Tech, 12*(4), 281-291.

Oudshoorn, A., van der Wielen, L. A. M., & Straathof, A. J. J. (2009a). Adsorption equilibria of bio-based butanol solutions using zeolite. *Biochem Eng J, 48*(1), 99-103. doi:10.1016/j.bej.2009.08.014

Oudshoorn, A., van der Wielen, L. A. M., & Straathof, A. J. J. (2009b). Assessment of options for selective 1-butanol recovery from aqueous solution. *Ind Eng Chem Res, 48*(15), 7325-7336. doi:Doi 10.1021/Ie900537w

Oudshoorn, A., van der Wielen, L. A. M., & Straathof, A. J. J. (2012). Desorption of butanol from zeolite material. *Biochem Eng J, 67*, 167-172. doi:Doi 10.1016/J.Bej.2012.06.014

Paradis, G. G., Shanahan, D. P., Kreiter, R., van Veen, H. M., Castricum, H. L., Nijmeijer, A., & Vente, J. F. (2013). From hydrophilic to hydrophobic HybSi® membranes: A change of affinity and applicability. *J Membrane Sci, 428*, 157-162. doi:10.1016/j.memsci.2012.10.006

Parajo, J. C., Dominguez, H., & Dominguez, J. M. (1996). Charcoal adsorption of wood hydrolysates for improving their fermentability: influence of the operational conditions. *Bioresource Technol, 57*, 179-185.

Parial, D., Patra, H. K., Dasgupta, A. K., & Pal, R. (2012). Screening of different algae for green synthesis of gold nanoparticles. *European Journal of Phycology, 47*(1), 22-29. doi:10.1080/09670262.2011.653406

Park, N., Kwon, B., Kim, I., & Cho, J. (2005). Biofouling potential of various NF membranes with respect to bacteria and their soluble microbial products (SMP): Characterizations, flux decline, and transport parameters. *J Membrane Sci, 258*(1-2), 43-54. doi:10.1016/j.memsci.2005.02.025

Patil, M. B., Veerapur, R. S., Patil, S. A., Madhusoodana, C. D., & Aminabhavi, T. M. (2007). Preparation and characterization of filled matrix membranes of sodium alginate incorporated with aluminum-containing mesoporous silica for pervaporation

dehydration of alcohols. *Sep Purif Technol, 54*(1), 34-43. doi:10.1016/j.seppur.2006.08.015

Pfromm, P. H., Amanor-Boadu, V., Nelson, R., Vadlani, P., & Madl, R. (2010). Bio-butanol vs. bio-ethanol: A technical and economic assessment for corn and switchgrass fermented by yeast or Clostridium acetobutylicum. *Biomass Bioenerg, 34*(4), 515-524. doi:http://dx.doi.org/10.1016/j.biombioe.2009.12.017

Pierce, J. J., Fischer, E. J., Smith, M. P., Turner, C., Keshavarz-Moore, E., & Dunnill, P. (1999). Purification of a periplasmic enzyme by a stirred adsorbent, and by expanded and packed beds. *Bioprocess Eng, 20*(5), 449-457. doi:10.1007/s004490050614

Pintor, A. M. A., Vilar, V. J. P., Botelho, C. M. S., & Boaventura, R. A. R. (2016). Oil and grease removal from wastewaters: Sorption treatment as an alternative to state-of-the-art technologies. A critical review. *Chem Eng J, 297*, 229-255. doi:10.1016/j.cej.2016.03.121

Popielarska-Konieczna, M., Bohdanowicz, J., & Starnawska, E. (2010). Extracellular matrix of plant callus tissue visualized by ESEM and SEM. *Protoplasma, 247*(1-2), 121-125. doi:10.1007/s00709-010-0149-1

Pratt, L. A. K., Roberto. (1998). Genetic analysis of Esherichia coli biofilm formation: roles of flagella, motility, chemotaxis and type I pili. *Molecular Microbiology, 30*(2), 285-293.

Qiang, Z., Guo, Y. H., Liu, H., Cheng, S. Z. D., Cakmak, M., Cavicchi, K. A., & Vogt, B. D. (2015). Large-Scale Roll-to-Roll Fabrication of Ordered Mesoporous Materials using Resol-Assisted Cooperative Assembly. *ACS Appl. Mater. Interface, 7*(7), 4306-4310. doi:10.1021/am5086275

Qiang, Z., Gurkan, B., Ma, J., Liu, X., Guo, Y., Cakmak, M., . . . Vogt, B. D. (2016). Roll-to-roll fabrication of high surface area mesoporous carbon with process-tunable pore texture for optimization of adsorption capacity of bulky organic dyes. *Micropor Mesopor Mat, 227*, 57-64. doi:http://dx.doi.org/10.1016/j.micromeso.2016.02.015

Qureshi, N., Annous, B. A., Ezeji, T. C., Karcher, P., & Maddox, I. S. (2005). Biofilm reactors for industrial bioconversion processes: employing potential of enhanced reaction rates. *Microb Cell Fact, 4*, 24. doi:10.1186/1475-2859-4-24

Qureshi, N., & Blaschek, H. P. (1999). Butanol recovery from model solution/fermentation broth by pervaporation: evaluation of membrane performance. *Biomass Bioenerg, 17*, 175-184.

Qureshi, N., & Blaschek, H. P. (2000). Butanol production using Clostridium beijerinckii BA101 hyper-butanol producing mutant strain and recovery by pervaporation. *Appl Biochem Biotech, 84-86*(1-9), 225-235. doi:10.1385/abab:84-86:1-9:225

Qureshi, N., & Blaschek, H. P. (2001). Recovery of butanol from fermentation broth by gas stripping. *Renew Energ, 22*(4), 557-564. doi:Doi 10.1016/S0960-1481(00)00108-7

Qureshi, N., Hughes, S., Maddox, I. S., & Cotta, M. A. (2005a). Energy-efficient recovery of butanol from model solutions and fermentation broth by adsorption. *Bioprocess Biosyst Eng, 27*(4), 215-222. doi:10.1007/s00449-005-0402-8

Qureshi, N., Hughes, S., Maddox, I. S., & Cotta, M. A. (2005b). Energy-efficient recovery of butanol from model solutions and fermentation broth by adsorption. *Bioproc Biosyst Eng, 27*(4), 215-222. doi:10.1007/s00449-005-0402-8

Qureshi, N., & Maddox, I. S. (1995). Continuous production of acetone-butanol-ethanol using immobilized cells of Clostridium acetobutylicum and integration with product removal by liquid-liquid extraction. *J Ferment Bioeng, 80*(2), 185-189. doi:http://dx.doi.org/10.1016/0922-338X(95)93217-8

Qureshi, N., & Maddox, I. S. (2005). Reduction in butanol inhibition by perstraction. *Food Bioprod Process, 83*(1), 43-52. doi:10.1205/fbp.04163

Qureshi, N., Meagher, M. M., Huang, H. J., & Hutkins, R. W. (2001a). Acetone butanol ethanol (ABE) recovery by pervaporation using silicalite-silicone composite membrane from fed-batch reactor of Clostridium acetobutylicum. *J Membrane Sci, 187*, 93-102.

Qureshi, N., Meagher, M. M., Huang, J., & Hutkins, R. W. (2001b). Acetone butanol ethanol (ABE) recovery by pervaporation using silicalite-silicone composite membrane from fed-batch reactor of Clostridium acetobutylicum. *J. Membr. Sci. , 187*(1-2), 93-102. doi:Doi 10.1016/S0376-7388(00)00667-0

Ramaswamy, S., Huang, H.-J., & Ramarao, B. V. (2013). *Separation and purification technologies in biorefineries*.

Ramos, J. L., Duque, E., Rodríguez-Herva, J. J., Godoy, P., Haïdour, A., Reyes, F., & Fernández-Barrero, A. (1997). Mechanisms for solvent tolerance in bacteria. *J Biol Chem, 272*(7), 3887-3890.

Ras, M., Lefebvre, D., Derlon, N., Hamelin, J., Bernet, N., Paul, E., & Girbal-Neuhauser, E. (2013). Distribution and hydrophobic properties of Extracellular Polymeric Substances in biofilms in relation towards cohesion. *J Biotechnol, 165*(2), 85-92. doi:10.1016/j.jbiotec.2013.03.001

Regdon, I., Dekany, I., & Lagaly, G. (1998). A new way for calculating the adsorption capacity from surface excess isotherms *Colloid Polym Sci, 276*(6), 511-517.

Rehmann, L., Sun, B., & Daugulis, A. J. (2007). Polymer selection for biphenyl degradation in a solid-liquid two-phase partitioning bioreactor. *Biotechnol Progr, 23*(4), 814-819.

Roffler, S., Blanch, H., & Wilke, C. (1987a). In-situ recovery of butanol during fermentation. Part 1: Batch extractive fermentation. *Bioprocess Engineering, 2*, 1-12.

Roffler, S., Blanch, H., & Wilke, C. (1987b). In-situ recovery of butanol during fermentation. Part 2: Fed-batch extractive fermentation. *Bioprocess Engineering, 2*, 181-190.

Roffler, S. R., Blanch, H. W., & Wilke, C. R. (1988). In situ extractive fermentation of acetone and butanol. *Biotechnol Bioeng, 31*, 135-143.

Rudling, J. A. N. (1988). Multicomponent Adsorption Isotherms for Determination of Recoveries in Liquid Desorption of Mixtures of Polar Solvents Adsorbed on Activated Carbon. *Am Ind Hyg Assoc J, 49*(3), 95-100. doi:10.1080/15298668891379459

Sangster, J. (1989). Octanol-Water Partition Coefficients of Simple Organic Compounds. *J. Phys. Chem. Ref. Data, 18*(3), 1111-1229. doi:doi:http://dx.doi.org/10.1063/1.555833

Sano, T., Yanagishita, H., Kiyozumi, Y., Mizukami, F., & Haraya, K. (1994). Seperation of ethanol/water misture by silicalite membrane on pervaporation. *J Membrane Sci, 95*, 221-228.

Saravanan, V., Waijers, D. A., Ziari, M., & Noordermeer, M. A. (2010). Recovery of 1-butanol from aqueous solutions using zeolite ZSM-5 with a high Si/Al ratio; suitability of a column process for industrial applications. *Biochem Eng J, 49*(1), 33-39. doi:10.1016/j.bej.2009.11.008

Sasaki, K., Matsuda, F., Hasunuma, T., Ogino, C., Urairi, M., Yoshida, K., & Kondo, A. (2013). Ability of a perfluoropolymer membrane to tolerate by-products of ethanol fermentation broth from dilute acid-pretreated rice straw. *Biochem Eng J, 70*, 135-139. doi:10.1016/j.bej.2012.10.013

Schugerl, K. (2000). Integrated processing of biotechnology products. *Biotechnol Adv, 18*(7), 581-599.

Shi, G. M., Chen, H., Jean, Y. C., & Chung, T. S. (2013). Sorption, swelling, and free volume of polybenzimidazole (PBI) and PBI/zeolitic imidazolate framework (ZIF-8) nano-composite membranes for pervaporation. *Polymer, 54*(2), 774-783. doi:10.1016/j.polymer.2012.11.056

Silvestre-Albero, J., Silvestre-Albero, A., Sepulveda-Escribano, A., & Rodriguez-Reinoso, F. (2009). Ethanol removal using activated carbon: effect of porous structure and surface chemistry. *Micropor Mesopor Mat, 120*(1-2), 62-68. doi:10.1016/j.micromeso.2008.10.012

Songstad, D. D., Lakshmanan, P., Chen, J., Gibbons, W., Hughes, S., & Nelson, R. (2009). Historical perspective of biofuels: learning from the past to rediscover the future. *In Vitro Cellular & Developmental Biology - Plant, 45*(3), 189-192. doi:10.1007/s11627-009-9218-6

Soydaş, B., Dede, Ö., Çulfaz, A., & Kalıpçılar, H. (2010). Separation of gas and organic/water mixtures by MFI type zeolite membranes synthesized in a flow system. *Micropor Mesopor Mat, 127*(1-2), 96-103. doi:10.1016/j.micromeso.2009.07.004

Staggs, K. W., & Nielsen, D. R. (2015). Improving n -butanol production in batch and semi-continuous processes through integrated product recovery. *Process Biochemistry, 50*(10), 1487-1498. doi:10.1016/j.procbio.2015.06.009

Staggs, K. W., Qiang, Z., Madathil, K., Gregson, C., Xia, Y., Vogt, B., & Nielsen, D. R. (2017). High Efficiency and Facile Butanol Recovery with Magnetically Responsive Micro/Mesoporous Carbon Adsorbents. *ACS Sustainable Chemistry & Engineering, 5*(1), 885-894. doi:10.1021/acssuschemeng.6b02204

Storck, S., Bretinger, H., & Maier, W. F. (1998). Characterization of micro- and mesoporous solids by physisorption methods and pore-size analysis. *Appl. Catal., A, 174*(1–2), 137-146. doi:http://dx.doi.org/10.1016/S0926-860X(98)00164-1

Subramani, A., & Hoek, E. M. V. (2010). Biofilm formation, cleaning, re-formation on polyamide composite membranes. *Desalination, 257*(1-3), 73-79. doi:10.1016/j.desal.2010.03.003

Sulaymon, A. H., & Ahmed, K. W. (2008). Competitive adsorption of furfural and phenolic compounds onto activated carbon in fixed bed column. *Environ. Sci. Technol., 42*, 392-397.

Sutikno, T., & Himmelstein, J. (1983). Desorption of phenol from activated carbon by solvent regeneration. *Ind Eng Chem Fundam, 22*(4), 420-425.

Tan, H., Wu, Y., & Li, T. (2013). Pervaporation of n-butanol aqueous solution through ZSM-5-PEBA composite membranes. *J Appl Polym Sci, 129*(1), 105-112. doi:10.1002/app.38704

Tanaka, S., Tashiro, Y., Kobayashi, G., Ikegami, T., Negishi, H., & Sakaki, K. (2012). Membrane-assisted extractive butanol fermentation by Clostridium saccharoperbutylacetonicum N1-4 with 1-dodecanol as the extractant. *Bioresource Technol, 116*(0), 448-452. doi:http://dx.doi.org/10.1016/j.biortech.2012.03.096

Tashiro, Y., Yoshida, T., Noguchi, T., & Sonomoto, K. (2013). Recent advances and future prospects for increased butanol production by acetone-butanol-ethanol fermentation. *Eng Life Sci, 13*(5), 432-445. doi:10.1002/elsc.201200128

Thompson, B., Machas, M., & Nielsen, D. R. (2016). Engineering and comparison of non-natural pathways for microbial phenol production. *Biotechnol Bioeng*. doi:10.1002/bit.25942

van den Berg, C., Wierckx, N., Vente, J., Bussmann, P., de Bont, J., & van der Wielen, L. (2008). Solvent-impregnated resins as an in situ product recovery tool for phenol recovery from Pseudomonas putida S12TPL fermentations. *Biotechnol Bioeng, 100*(3), 466-472. doi:10.1002/bit.21790

Van Hecke, W., Kaur, G., & De Wever, H. (2014). Advances in in-situ product recovery (ISPR) in whole cell biotechnology during the last decade. *Biotechnol Adv, 32*(7), 1245-1255. doi:10.1016/j.biotechadv.2014.07.003

Van Hecke, W., Vandezande, P., Claes, S., Vangeel, S., Beckers, H., Diels, L., & De Wever, H. (2012). Integrated bioprocess for long-term continuous cultivation of Clostridium acetobutylicum coupled to pervaporation with PDMS composite membranes. *Bioresource Technol, 111*(0), 368-377. doi:http://dx.doi.org/10.1016/j.biortech.2012.02.043

van Oss, C. J. (1993). Acid-base interfacial interactions in aqueous media. *Colloids and Surfaces A: Physicochemical and Engineering Aspects, 78*, 1-49.

Vane, L. M. (2005). A review of pervaporation for product recovery from biomass fermentation processes. *J Chem Technol Biot, 80*(6), 603-629. doi:10.1002/jctb.1265

Vane, L. M. (2008a). Separation technologies for the recovery and dehydration of alcohols from fermentation broths. *Biofuels, Bioproducts and Biorefining, 2*(6), 553-588. doi:10.1002/bbb.108

Vane, L. M. (2008b). Separation technologies for the recovery and dehydration of alcohols from fermentation broths. *Biofuel Bioprod Bior, 2*(6), 553-588. doi:10.1002/bbb.108

Vane, L. M., & Alvarez, F. R. (2013). Hybrid vapor stripping-vapor permeation process for recovery and dehydration of 1-butanol and acetone/butanol/ethanol from dilute aqueous solutions. Part 1. Process Simulations. *J Chem Technol Biot*, n/a-n/a. doi:10.1002/jctb.4087

Vane, L. M., Alvarez, F. R., Rosenblum, L., & Govindaswamy, S. (2013). Efficient Ethanol Recovery from Yeast Fermentation Broth with Integrated Distillation–Membrane Process. *Ind Eng Chem Res, 52*(3), 1033-1041. doi:10.1021/ie2024917

Vermue, M., Sikkema, J., Verheul, A., Bakker, R., & Tramper, J. (1993). Toxicity of homologous series of organic-solvents for the gram-positive bacteria arthrobacter and nocardia sp and the gram-negative bacteria acinetobacter and Pseudomonas sp. *Biotechnol Bioeng, 42*(6), 747-758.

Vertes, A., Hitchins, V., & Phillips, K. S. (2012). Analytical challenges of microbial biofilms on medical devices. *Anal Chem, 84*(9), 3858-3866. doi:10.1021/ac2029997

Verwey, E. J. W., & Overbeek, J. T. G. (1948). *Theory of the stability of lyophobic colloids the interaction of sol particles having an electric double layer*. Lieden, Netherlands: Elsevier Publishing Company, Inc.

Wang, P., Wang, Y., Liu, Y., Shi, H., & Su, Z. (2012). Novel in situ product removal technique for simultaneous production of propionic acid and vitamin B12 by expanded bed adsorption bioreactor. *Bioresource Technol, 104*(0), 652-659. doi:http://dx.doi.org/10.1016/j.biortech.2011.10.047

Wang, X., & Dai, S. (2009). A simple method to ordered mesoporous carbons containing nickel nanoparticles. *Adsorption, 15*(2), 138-144. doi:10.1007/s10450-009-9164-y

Wang, Y., Tang, Y., Wang, X., Shan, W., Ke, C., Gao, Z., . . . Yang, W. (2001). Fabrication of zeolite coatings on stainless steel grids. *Journal of Materials Science Letters, 20*, 2091-2094.

Wang, Y. P., & Achenie, L. E. K. (2002). Computer aided solvent design for extractive fermentation. *Fluid Phase Equilibr, 201*(1), 1-18.

Wee, S. L., Tye, C. T., & Bhatia, S. (2008). Membrane separation process-pervaporation through zeolite membrane. *Sep Purif Technol, 63*(3), 500-516.

Wei, P., Cheng, L.-H., Zhang, L., Xu, X.-H., Chen, H.-l., & Gao, C.-j. (2014). A review of membrane technology for bioethanol production. *Renew Sust Energ Rev, 30*, 388-400. doi:10.1016/j.rser.2013.10.017

Weil, J. R., Dien, B., Bothast, R., Hendrickson, R., Mosier, N. S., & Ladisch, M. R. (2002). Removal of fermentation inhibitors formed during pretreatment of biomass by polymeric adsorbents. *Ind Eng Chem Res, 41*, 6132-6138.

Wiehn, M., Levario, T. J., Staggs, K., Linneen, N., Wang, Y., Pfeffer, R., . . . Nielsen, D. R. (2013). Adsorption of Short-Chain Alcohols by Hydrophobic Silica Aerogels. *Ind Eng Chem Res, 52*(51), 18379-18385. doi:10.1021/ie4032023

Wiehn, M., Staggs, K., Wang, Y., & Nielsen, D. R. (2014). In situ butanol recovery from Clostridium acetobutylicum fermentations by expanded bed adsorption. *Biotechnol Progr, 30*(1), 68-78. doi:10.1002/btpr.1841

Wierckx, N. J., Ballerstedt, H., de Bont, J. A., & Wery, J. (2005). Engineering of solvent-tolerant Pseudomonas putida S12 for bioproduction of phenol from glucose. *Appl Environ Microbiol, 71*(12), 8221-8227. doi:10.1128/AEM.71.12.8221-8227.2005

Wu, H., Chen, X. P., Liu, G. P., Jiang, M., Guo, T., Jin, W. Q., . . . Zhu, D. W. (2012). Acetone-butanol-ethanol (ABE) fermentation using Clostridium acetobutylicum XY16 and in situ recovery by PDMS/ceramic composite membrane. *Bioproc Biosyst Eng, 35*(7), 1057-1065. doi:10.1007/s00449-012-0721-5

Xiu, Z. L., & Zeng, A. P. (2008). Present state and perspective of downstream processing of biologically produced 1,3-propanediol and 2,3-butanediol. *Appl Microbiol Biotechnol, 78*(6), 917-926. doi:10.1007/s00253-008-1387-4

Xu, Z., Baunach, M., Ding, L., & Hertweck, C. (2012). Bacterial Synthesis of Diverse Indole Terpene Alkaloids by an Unparalleled Cyclization Sequence. *Angewandte Chemie International Edition, 51*(41), 10293-10297. doi:10.1002/anie.201204087

Xue, C., Du, G.-Q., Sun, J.-X., Chen, L.-J., Gao, S.-S., Yu, M.-L., . . . Bai, F.-W. (2014). Characterization of gas stripping and its integration with acetone–butanol–ethanol fermentation for high-efficient butanol production and recovery. *Biochem Eng J, 83*(0), 55-61. doi:http://dx.doi.org/10.1016/j.bej.2013.12.003

Xue, C., Du, G. Q., Chen, L. J., Ren, J. G., & Bai, F. W. (2014). Evaluation of asymmetric polydimethylsiloxane-polyvinylidene fluoride composite membrane and incorporated with acetone-butanol-ethanol fermentation for butanol recovery. *J Biotechnol, 188C*, 158-165. doi:10.1016/j.jbiotec.2014.08.010

Xue, C., Du, G. Q., Chen, L. J., Ren, J. G., Sun, J. X., Bai, F. W., & Yang, S. T. (2014). A carbon nanotube filled polydimethylsiloxane hybrid membrane for enhanced butanol recovery. *Sci Rep, 4*, 5925. doi:10.1038/srep05925

Xue, C., Zhao, J., Liu, F., Lu, C., Yang, S.-T., & Bai, F.-W. (2013). Two-stage in situ gas stripping for enhanced butanol fermentation and energy-saving product recovery. *Bioresource Technol, 135*(0), 396-402. doi:http://dx.doi.org/10.1016/j.biortech.2012.07.062

Xue, C., Zhao, J., Lu, C., Yang, S.-T., Bai, F., & Tang, I. C. (2012). High-titer n-butanol production by Clostridium acetobutylicum JB200 in fed-batch fermentation with intermittent gas stripping. *Biotechnol Bioeng, 109*(11), 2746-2756. doi:10.1002/bit.24563

Yang, S. T., & Lu, C. (2013). Extraction-Fermentation Hybrid (Extractive Fermentation). In S. Ramaswamy, H.-J. Huang, & B. V. Ramarao (Eds.), *Separation and purification technologies in biorefineries* (pp. 409-437). Chichester, West Sussex, United Kingdom: John Wiley & Sons Ltd,.

Yang, X., & Tsao, G. T. (1995). Enhanced acetone-butanol fermentation using repeated fed-batch operation coupled with cell recycle by membrane and simultaneous removal of inhibitory products by adsorption. *Biotechnol Bioeng, 47*(4), 444-450. doi:10.1002/bit.260470405

Yang, X. P., Tsai, G. J., & Tsao, G. T. (1994). Enhancement of *in situ* adsorption on the acetone-butanol fermentation by *Clostridium acetobutylicum*. *Separ Technol, 4*(2), 81-92.

Yapsaklı, K., Çeçen, F., Aktaş, Ö., & Can, Z. S. (2009). Impact of Surface Properties of Granular Activated Carbon and Preozonation on Adsorption and Desorption of Natural Organic Matter. *Environmental Engineering Science, 26*(3), 489-500. doi:10.1089/ees.2008.0005

Yen, H.-W., Chen, Z.-H., & Yang, I. K. (2012). Use of the composite membrane of poly(ether-block-amide) and carbon nanotubes (CNTs) in a pervaporation system incorporated with fermentation for butanol production by Clostridium acetobutylicum. *Bioresource Technol, 109*(0), 105-109. doi:http://dx.doi.org/10.1016/j.biortech.2012.01.017

Yen, H.-W., & Li, R.-J. (2011). The effects of dilution rate and glucose concentration on continuous acetone-butanol-ethanol fermentation by Clostridium acetobutylicum immobilized on bricks. *J Chem Technol Biot, 86*(11), 1399-1404. doi:10.1002/jctb.2640

Yen, H.-W., Lin, S.-F., & Yang, I. K. (2012). Use of poly(ether-block-amide) in pervaporation coupling with a fermentor to enhance butanol production in the cultivation of Clostridium acetobutylicum. *J Biosci Bioeng, 113*(3), 372-377. doi:http://dx.doi.org/10.1016/j.jbiosc.2011.10.025

Yen, H. W., Li, R. J., & Ma, T. W. (2011). The development process for a continuous acetone-butanol-ethanol (ABE) fermentation by immobilized Clostridium acetobutylicum. *J Taiwan Inst Chem E, 42*(6), 902-907. doi:Doi 10.1016/J.Jtice.2011.05.006

Yomano, L. P., York, S. W., & Ingram, L. O. (1998). Isolation and characterization of ethaol-tolerant mutants of Escherichia coli KO11 for fuel ethanol production. *J Ind Microbiol Biot, 20*, 132-138.

Yomano, L. P., York, S. W., Shanmugam, K. T., & Ingram, L. O. (2009). Deletion of methylglyoxal synthase gene (mgsA) increased sugar co-metabolism in ethanol-producing Escherichia coli. *Biotechnol Lett, 31*(9), 1389-1398. doi:10.1007/s10529-009-0011-8

Yuanzhong Zhang, Z. Q., Bryan D. Vogt. (2014). Relationship between crosslinking and ordering kinetics for the fabrication of soft templated (FDU-16) mesoporous carbon thin films. *RSC advance, 4*(85), 44858-44867. doi:C4RA08316D

Zhai, Y., Dou, Y., Liu, X., Park, S. S., Ha, C.-S., & Zhao, D. (2011). Soft-template synthesis of ordered mesoporous carbon/nanoparticle nickel composites with a high surface area. *Carbon, 49*(2), 545-555. doi:http://dx.doi.org/10.1016/j.carbon.2010.09.055

Zhang, K., Agrawal, M., Harper, J., Chen, R., & Koros, W. J. (2011). Removal of the Fermentation Inhibitor, Furfural, Using Activated Carbon in Cellulosic-Ethanol Production. *Ind Eng Chem Res, 50*(24), 14055-14060. doi:10.1021/ie2013983

Zhang, Y., Li, M., Wang, Y., Ji, X., Zhang, L., & Hou, L. (2015). Simultaneous concentration and detoxification of lignocellulosic hydrolyzates by vacuum membrane distillation coupled with adsorption. *Bioresour Technol, 197*, 276-283. doi:10.1016/j.biortech.2015.08.097

Zhang, Y., Ma, Y., Yang, F., & Zhang, C. (2009). Continuous acetone-butanol-ethanol production by corn stalk immobilized cells. *J Ind Microbiol Biot, 36*(8), 1117-1121. doi:10.1007/s10295-009-0582-3

Zheng, H., Wang, X., Yomano, L. P., Shanmugam, K. T., & Ingram, L. O. (2012). Increase in furfural tolerance in ethanologenic Escherichia coli LY180 by plasmid-based expression of thyA. *Appl Environ Microbiol, 78*(12), 4346-4352. doi:10.1128/AEM.00356-12

Zheng, Y. N., Li, L. Z., Xian, M., Ma, Y. J., Yang, J. M., Xu, X., & He, D. Z. (2009). Problems with the microbial production of butanol. *J Ind Microbiol Biot, 36*(9), 1127-1138. doi:DOI 10.1007/s10295-009-0609-9

Zhou, M. H., & Cho, W. J. (2003). Oil absorbents based on styrene-butadiene rubber. *J Appl Polym Sci, 89*(7), 1818-1824.

Zhou, W., Bi, H., Zhuang, Y., He, Q., Yin, H., Liu, T., & Ma, Y. (2017). Production of Cinnamyl Alcohol Glucoside from Glucose in Escherichia coli. *J. Agric. Food Chem., 65*(10), 2129-2135. doi:10.1021/acs.jafc.7b00076

APPENDIX A

PREDICTIVE FOULING MODEL OF *E. COLI* BW25113 ON PERVAPORATION MEMBRANES, AN XDLVO STUDY

Abstract

Here an investigation of surface fouling potential of *E. coli* as a function of substrate properties has been conducted. Certain separations modalities such as adsorption and membrane pervaporation are directly exposed to growing cultures. Fouling trends are determined in part by substrate chemistry which affects surface free energy. Surface free energy can enhance or detract from microbial attachment and subsequent fouling which undermines separation performance and overall process robustness. The organisms studied here include *Escherichia coli* (KO11 and BW25113) and *Saccharomyces cerevisiae* (BY4741, ΔYDL233W, ΔYIR019C, S288C and BY4743). Substrate properties were measured whereas surface properties of cells were drawn from literature. The extended Derjaguin Landau Verwey and Overbeek method was used to estimate the work of attachment for each cell type-substrate pairing. More hydrophobic substrates were found to be more prone to fouling than hydrophilic surfaces. Notably the positively charged alumina substrate was not conducive to biofilm formation.

Keywords: fouling; *in situ* product recovery; adsorption; pervaporation; microbial attachment

A.1.0 Introduction

Previous chapters have established the relevance of bioseparations to current research and some of the specific pros and cons for each modality. This chapter will focus on biofouling as an inevitable consequence of employing solid phase separations *in situ* with production of bioalcohols. Whereas a biofilm may be simultaneously necessary and advantageous for some applications such as water treatment, biofouling is hazardous in other applications such as medical devices (Dohnalkova et al., 2011; Drobek et al., 2012; Flemming & Wingender, 2010; Sasaki et al., 2013; Soydaş, Dede, Çulfaz, & Kalıpçılar, 2010; Vane, 2008a; Vertes, Hitchins, & Phillips, 2012). Biofouling refers to the attachment of cells (e.g bacteria), and 'cellular debris' (high molecular weight polysaccharides, lipids, phosphates, proteins, nucleic acids, flagella, pili, and free amino acids) to a substrate (Dohnalkova et al., 2011; Vertes et al., 2012). These foulants are often grouped under the terms extended glycocalyx or extracellular polymeric substances (EPS). A 'conditioning layer' is formed from a combination of EPS components, the surface charges of both cell and substrate, and fluid shear all of which facilitate cellular attachment and acts as a diffusion barrier to toxins, nutrients and value-added bioproducts (Bojsen et al., 2012; N. Qureshi, Annous, et al., 2005). From these factors, fouling is a grand challenge in bioenergy applications such as alcohol fermentations (Aljundi et al., 2005; Drobek et al., 2012; Gaykawad et al., 2013; Ong, Razatos, Georgiou, & Sharma, 1999b; Sasaki et al., 2013; Xiu & Zeng, 2008).

While conventional separation of bioalcohols relies on distillation (Vane, 2008a), the dilute concentrations necessitate multi-stage separation processes (C. Y. Chen et al., 2013; Vane, 2005, 2008a; Vane & Alvarez, 2013; Vane et al., 2013). Many alternative

separation strategies have been explored (Cai et al., 2013; C. Y. Chen et al., 2013; Gudena et al., 2013; Paradis et al., 2013; Patil et al., 2007; Shi et al., 2013; Vane, 2008a; Vane & Alvarez, 2013) often employing economical materials such as polydimethylsiloxane (PDMS), zeolites (Aljundi et al., 2005; Cai et al., 2013; C. Y. Chen et al., 2013; Kita et al., 2003; Kittur et al., 2005; Xiao Lin et al., 2001), and carbons (Fierro et al., 2008; Khan et al., 1981; T. J. Levario, M. Dai, W. Yuan, B. D. Vogt, & D. R. Nielsen, 2012b; Silvestre-Albero et al., 2009). Commonly these separation studies use model broth and avoid the effects of fouling (Aljundi et al., 2005; Gaykawad et al., 2013; Sasaki et al., 2013; Vane, 2008a; Vane & Alvarez, 2013; Vane et al., 2013; Xiu & Zeng, 2008). Biofouling inevitably causes degradation of separation performance (Gaykawad et al., 2013) and few *in situ* separations studies reach beyond 20 days of continuous operation (C. Y. Chen et al., 2013; Sasaki et al., 2013) and most lack predictive models or preventive measures (C. Y. Chen et al., 2013; Hijnen et al., 2012; Subramani & Hoek, 2010). Certain studies have attempted to map fouling trends across varied species and substrates (B. Li & Logan, 2004). Potential contributors to biofouling have been well investigated including strain of microorganism, substrate material, substrate roughness, finding that increasing roughness and hydrophobicity promotes fouling. (Ben Chaabane et al., 2006; Ciston et al., 2008; Diaz et al., 2011; Dohnalkova et al., 2011; B. Li & Logan, 2004; Pratt, 1998) Whereas some aim to investigate the biofouling of resuspended cells on static substrates (B. Li & Logan, 2004), others attempt to quantify attachment in flow cells (S. Kang & Choi, 2005; Seoktae Kang, Hoek, Choi, & Shin, 2006). The length of time used to develop cellular attachment also varies by study, ranging from to 2 hours

(B. Li & Logan, 2004) to 10 days (Kregiel, 2013). The variety of protocols, attachment substrates and organisms prevents detailed comparisons.

The biofouling context of this study is a semi-continuous fermentation wherein the substrate exposure to cell-containing media occurs on the scale of days. This is meant to represent in situ adsorption or pervaporation of an ethanol or butanol fermentation. The substrates include silicalites, polydimethylsiloxane and alumina. While many types of organisms can foul substrates, the 2 types of microorganisms included in this study are *Escherichia coli* and *Saccharomyces cerevisiae*. *E. coli* and *S. cerevisiae* represent industrial work horse organisms and *S. cerevisiae* is a model eukaryote. To estimate the surface free energy, Gibbs energy of attachment, and better understand the cellular attachment, an extension of the mathematical model developed by Derjaguin Landau Verwey and Overbeek (DLVO) will be applied. (Verwey & Overbeek, 1948) The goals of this work were to: 1) Characterize the surface free energy of common separations substrates, 2) Evaluate the fouling potential by *E. coli* and *S. cerevisiae* via an extended DLVO (XDLVO) analysis which estimates the Gibbs energy of attachment, 3) Compare the fouling potential by media components forming a 'conditioning layer' and for whole cells, and 4) Evaluate cellular fouling by *S. cerevisiae* strains with deletions of the Flo11 gene suspected to cause fouling.

A.2.0 Materials and Methods

A.2.1 Substrate Preparation

Silicone (PDMS) sheet was obtained from Specialty Silicone Fabricators (Tustin, CA) in 12" x 12" sheets of 0.004" thickness. Silicone films were cut into approximately

1” squares for placement in the base of 6 well microplates. Silicalite membranes were grown on supports of either alumina or yittria-supported zirconia (YSZ) by collaborators from Prof. Jerry Lin’s laboratory at Arizona State University. YSZ supports were synthesized by pressing and sintering YSZ powders of 2 μm in particle size. Silicalite was seeded onto the YSZ supports by dip-coating into a stable nano-sized silicalite sol and calcined. Multiple dip-coatings ensured improved quality of the seed layer. Synthesis was optimized toward ethanol selectivity by varied synthesis conditions. Silicalite substrates measured approximately 0.85” diameter and 0.065” thick and the support side was scored with a sharp knife and snapped. Alumina discs of 25 mm diameter and 2 mm thickness were purchased from Spectrum Chemical MFG (Gardena, CA). These alumina substrates were likewise scored with a sharp knife and snapped into 4 pieces.

A.2.2 Substrate Zeta Potential

Substrate surface charge was determined by zeta potential measurements performed on a Zetasizer Nano ZS (Malvern Instruments, Westborough, MA). Disposable Zeta cuvettes, and zeta calibration standards were obtained from Malvern Instruments (Westborough, MA). PDMS particles were prepared from silicone tubing ground up under liquid nitrogen in a mortar and pestle. Aqueous suspension of the silicone particles selected the particles averaging less than 10 μm in diameter as they were buoyant. Some silicalite seed crystals used for synthesis were also used for zeta analysis. Alumina particles were obtained from Sorbent Technologies (Atlanta, GA) to be used as a positively charged fouling surface control. Sample powders were suspended in DI water, 10 mM and 100 mM NaCl solutions for zeta measurement. 1 mL of powder suspension was deposited into the zeta cuvettes by 1 mL syringe with several aspiration

cycles to displace air bubbles. Each sample material was measured to determine average particle diameter and zeta potential. Zeta potential was averaged from 30 cycles. Conductivity of the aqueous solutions ranged from 0.35- 0.02 mS/cm for 0- 100 mM NaCl solutions, respectively.

A.2.3 Substrate Characterization by Goniometry

A Kruss Easy Drop DSA14 goniometer (Matthews, NC) was used for receding contact angle measurements on the substrates. Droplet volumes of 1-2 μL were applied to the surface in 3-5 sites for 3 replicates such that the reported values were averaged over at least 11 measurements. For PDMS substrates, solvent triads were selected based on swelling parameters studied for microfluidic applications (J. N. Lee, Park, & Whitesides, 2003). A common liquid triad used for goniometry is water, glycerol and an apolar alkane such as hexane, or hexadecane. Ethanol and butanol were used as well as glycerol and dimethylformamide based on their small swelling coefficients with PDMS compared to (Chaudhury & Whitesides, 1991).

A.2.4 Microorganisms and Growth Conditions

E. coli KO11, which was developed by the Ingram Lab at the University of Florida, was obtained from the American Type Culture Collection (ATCC, Manassas, VA). *E. coli* BW25113 was obtained from the Coli Genetic Stock Center (CGSC) at Yale University. *S. cerevisiae* BY4741, BY4743, ΔYDL233W, ΔYIR019C, and S288C were obtained from (Prather Lab, MIT). All bacterial and yeast seeds were grown in 12 mL culture tubes overnight at 37°C in 5 mL Nutrient Broth (NB) plus glucose in a shaking incubator at 200 rpm. All substrates were added to 6 well plates and sterilized

with 200 proof ethanol for 20 minutes. Residual ethanol was removed from the wells by pipette. All seed cultures were centrifuged at 3000 rpm for 5 minutes and cells were resuspended in 5 mL of fresh NB glucose media before being added to the microplate wells. Bacterial and yeast cultures were added to the 6 well plates and cultured at 37 °C in a shaking incubator at 120 rpm with NB glucose media exchanged every 2 days for 4 weeks.

A.2.5 SEM Preparation

Spent media was decanted from each microplate well and gently rinsed twice with 1 mL of double deionized water. Cellular function was ceased by adding 2 mL of a 2.5% gluteraldehyde solution. After 1.5 hours, wells were washed 5 times each with 2 mL of double deionized water and the remaining wash solution decanted. Cellular fixation was performed by adding 2 mL of 1% osmium tetroxide (OsO_4) solution and allowed a 1.5 hour equilibration time. Wells were washed 5 times each with double deionized water and the solutions decanted. Water was then exchanged with 2 mL of ethanol/water solutions of increasing concentration to ensure substrate dehydration (10% ethanol, 20%, 40%, 60%, 80% and three exchanges with 100% ethanol). Critical point drying was then performed on a Balzers CPD020 (Brunswick, OH). Substrates were placed into a stainless basket and placed into the chamber submerged in 100% ethanol. Liquid CO_2 was added to the chamber, mixed with the ethanol, ~60% of the solution was evacuated and refilled with liquid CO_2. Full ethanol removal required ~9 CO_2 exchanges at 5°C and mixed for 2 minutes. Following 9 exchanges, substrates were dried at 45°C and approximately 73 bar which is above the critical point for CO_2. Substrates were mounted on carbon tape adhered to pin stubs and either gold or carbon sputter coated using a

Technics Hummer V sputter coater (Anatech, Union City, CA). The sputter coating chamber was held between 100-125 mTorr with argon gas flow under partial vacuum. Substrates were sputter coated for 5 minutes maintaining approximately a 7-10 microamp current. Imaging was performed on a JEOL JSM6300 Scanning Electron Microscope (Peabody, MA). Virgin and fouled substrates were imaged at 15 kV for optimum contrast and clarity with minimum charging.

A.2.6 Atomic Force Microscopy

Substrates were prepared for atomic force microscopy (AFM) by ethanol rinse and air drying, substrates from cultures in well plates were simply rinsed with deionized water and air dried for 24 hours. Silicon nitride cantilevers were used on a Digital Instruments Dimension 3000 surface probe microscope (Bruker, Satna Barbara, CA). All images were taken in tapping mode with frequencies near 270 kHz and driving amplitudes of approximately 1.1 Volts. Amplitude and height data were imported into Gwyddion software and overlaid in the 3D visualization mode to export images for figures.

A.2.7 Bradford Total Protein Assay

Bovine serum albumin (BSA) was obtained from New England BioLabs (Ipswich, MA). BSA was mixed with DI water to give concentrations ranging from 0.2 to 1 mg/mL for initial controls. Higher ionic strength BSA solutions were prepared in 100 mM NaCl potassium phosphate buffered at pH 4.7 (the isoelectric point for BSA). The aqueous BSA controls, silicalite and PDMS samples were mixed thoroughly in 4 mL glass vials and allowed 24 hour equilibration. From the supernatant, 100 μL aliquots were

mixed with 0.9 mL of ¼ diluted coomasie blue (R form) dye from Bio-Rad (Hercules, CA) and placed into in cuvettes. BSA concentrations were measured on a Beckman Coulter DU600 spectrophotometer (Indianapolis, IN) at 595 nm.

A.2.8 XDLVO Theory and Its Biofouling Application

Traditional surface energy analysis attempts to capture the components of surface free energy as follows.

$$U_S^{Total} = U_S^{LW} + U_S^{AB} \quad \text{(A.1)}$$

Where the total free energy of a surface is determined by the sum of the Lifschitz-van der Waals (LW) and Lewis acid-base (AB) interactions. Equation A.1 describes the overall energy as being composed of acid-base interactions and short-range interactions. This premise results in the following equation for surface tension, a term often interchanged with surface energy.

$$\gamma_i = \gamma_i^{LW} + \gamma_i^{AB} \quad \text{(A.2)}$$

Where γ_i is the surface tension for component i, γ_i^{LW} and γ_i^{AB} are the Lifshitz van der Waals and Lewis acid-base components of the surface tension also known as Fowke's equation. (Fowkes, 1964) Equation A.2 describes surface tension as a function of the 2 classically assumed surface tension contributions. These cannot be measured directly and therefore must be estimated. Often a liquid solvent is used to interrogate the properties of a solid substrate via goniometry by the following relation.

$$\gamma_s = \gamma_i \cos\theta_i + \gamma_{sl} \quad \text{(A.3)}$$

Where γ_i is defined as above, γ_s is the energy of the substrate, and γ_{sl} is the substrate-solvent interaction energy and θ is the contact angle of solvent *i*. Equation A.3 is known as the Young's equation which relates the surface energy to the contact angles with solvents. This replaces the indirectly measurable quantity with a measurable correlation. In general, the interfacial free energy between two phases (namely the substrate-solvent interface) can be defined as follows.

$$\gamma_{12} = \gamma_1 + \gamma_2 - W_a \tag{A.4}$$

Where γ_1 and γ_2 are the interfacial surface tension components and W_a is the work of adhesion to a substrate. The work of adhesion has been expressed as equation A.5 also termed the Young-Dupré equation (Chaudhury & Whitesides, 1991).

$$W_a = \gamma_1(1 + \cos\theta_a) \tag{A.5}$$

Where W_a is as defined above, θ_a is the contact angle of solvent 1, and γ_1 is the total surface tension of solvent 1. When combined, Equations A.3 and A.4 express the work of adhesion as a function of contact angle as follows in Equation A.6. Also, Equations A.5 and A.6 can be combined into Equation A.7 which can be used in a traditional 3 solvent system to solve for the substrate surface energy components.

$$W_a = 2\left[(\gamma_1^{LW}\gamma_2^{LW})^{1/2} + (\gamma_1^{+}\gamma_2^{-})^{1/2} + (\gamma_1^{-}\gamma_2^{+})^{1/2}\right] \tag{A.6}$$

$$\gamma_1(1 + \cos\theta_a) = 2\left[(\gamma_1^{LW}\gamma_2^{LW})^{1/2} + (\gamma_1^{+}\gamma_2^{-})^{1/2} + (\gamma_1^{-}\gamma_2^{+})^{1/2}\right] \tag{A.7}$$

Where W_a, γ_i^{LW}, and θ_a are as defined above, γ^+ is the electron acceptor component γ^- is the electron donor component and γ_1 is the total surface tension of the solvent. It is

important to note that the subscripts 1 and 2 designate the known and unknown properties, respectively. Equation A.6 is known as the van Oss-Chaudhury-Good (OCG) thermodynamic approach for surface free energy determination using 3 solvents with known properties. (Fowkes, 1964) As the work of adhesion cannot be measured directly, Equation A.7 uses the measured contact angles and known solvent properties to solve for the unknown substrate properties. This method does not account for electrostatic contributions to surface energy however, prompting development of the extended DLVO model (XDLVO) with the following energy contributions.

$$U_S^{Total} = U_S^{LW} + U_S^{EL} + U_S^{AB} \tag{A.8}$$

Where U is the total interaction energy, AB and LW are as defined above and EL is the electrostatic free energy component. In conjunction with Equation A.7, Gibbs free energy per unit area for each interaction type can be determined as follows (S. Kang & Choi, 2005).

$$\Delta G_0^{LW} = 2 * \left[\sqrt{\gamma_b^{LW}} - \sqrt{\gamma_w^{LW}}\right] * \left[\sqrt{\gamma_w^{LW}} - \sqrt{\gamma_s^{LW}}\right] \tag{A.9}$$

$$\Delta G_0^{AB} = 2 * \left[\sqrt{\gamma_w^+}\left(\sqrt{\gamma_b^-} + \sqrt{\gamma_s^-} - \sqrt{\gamma_w^-}\right) + \sqrt{\gamma_w^-}\left(\sqrt{\gamma_b^+} + \sqrt{\gamma_s^+} - \sqrt{\gamma_w^+}\right) - \left(\sqrt{\gamma_b^+\gamma_s^-} + \sqrt{\gamma_b^-\gamma_s^+}\right)\right] \tag{A.10}$$

$$\Delta G_0^{EL} = \frac{\varepsilon_0 \varepsilon_r \kappa}{2}\left(\Psi^2{}_b + \Psi^2{}_s\right)\left[1 - \coth(\kappa h_0) + \frac{2\Psi_b \Psi_s}{\Psi^2{}_b + \Psi^2{}_s}\operatorname{csch}(\kappa h_0)\right] \tag{A.11}$$

Where γ, LW, AB, and EL are as defined above, ε_0 and ε_r are the dielectric permittivity of free space and water, respectively, Ψ is the zeta potential, κ is the inverse Debye length,

h_0 is the minimum approach distance, ΔG_0 is the Gibbs free energy of adhesion per unit area, and the subscripts are w for water, s for substrate and b for bacteria. From the above adhesion energies, the interaction energies as a function of separation distance may be calculated for each component as listed below (S. Kang & Choi, 2005). Sphere and plate geometry are typically used for AB and LW components whereas infinite plate-infinite plate geometry is typically used for EL components (Bhattacharjee, Chen, & Elimelech, 2000b) as follows.

$$U_S^{LW} = \frac{2\pi h_0^2 * \Delta G_0^{LW} * a}{h\left(1+{}^{14h}/_{\lambda}\right)} \tag{A.12}$$

$$U_S^{AB} = 2\pi\lambda_1 * \Delta G_0^{AB} * e^{{}^{(h_0-h)}/_{\lambda_1}} \tag{A.13}$$

$$U_S^{EL} = \pi\varepsilon\varepsilon_0 a\left[2\Psi_b\Psi_s ln\left(\frac{1+e^{-\kappa h}}{1-e^{-\kappa h}}\right) + (\Psi_b^2 + \Psi_s^2) ln(1-e^{-2\kappa h})\right] \tag{A.14}$$

Where γ, LW, AB, EL, ε_0, ε_r, Ψ, κ, h_0, ΔG_0, and U are as defined above, a is the cell radius, h is the separation distance, λ is the characterstic wavelength of interaction (assumed to be 100 nm) (B. Li & Logan, 2004), and the subscripts are w for water, s for substrate and b for bacteria.

A.2.9 XDLVO Predictions from Experimental Data

Goniometry data was input to a Matlab script to determine the roots of Equation A.7 from 3 distinct liquid triads for each substrate. Following simple algebraic manipulation, the right side of equation A.7 was factored to form a 3 x 3 matrix (A) of known solution properties multiplied by a 3 x 1 vector (X) of substrate unknowns. The

left side of equation A.7 formed a 3 x 1 vector (B). The unknown vector X was solved for by simple matrix division for efficient, rapid calculation. From the roots of Equation A.7, the Gibbs free energy of adhesion was calculated for both microorganisms. The cell surface tension components required for estimating Gibbs free energy of adhesion were used from tabulated data for *E. coli* (B. Li & Logan, 2004), and *S. cerevisiae* (S. Kang & Choi, 2005). Other factors such as Debye length, 5 nm separation and a minimum separation distance of 0.164 nm were used with Equations A.9-A.11. The Gibbs energies of adhesion were used to estimate the total interaction energies of attachment for each of the 2 organisms on each of the 3 substrate materials by Equations A.12-A.14.

A.3.0 Results and Discussion

A.3.1 Substrate and Cell Characterization by Zeta Potential

As bacteria approach the surface of a separations substrate such as a membrane or adsorbent, the charge interaction between the cell and surface occurs first. Attractive and repulsive forces are most simply characterized by the differences in surface charge. Surface charge can be directly measured by determining the electrophoretic mobility of a particle, which can be converted back to a zeta potential. This is done automatically in modern instruments designed for quantifying zeta potential. Zeta potentials were determined for particles of 3 type of substrate common to separations processes (alumina, silicalite, and PDMS). Zeta potential of a charged particle varies with the ionic environment however. Ionic strength of media is important not only for cellular growth but also for its implications on fouling. For example, addition of NaCl has been observed to reduce the repulsion between *E. coli* and mica because of the phenomenon of charge screening (Ong et al., 1999b). This occurs as suspended ions in aqueous solutions are

attracted to the opposing charge on a submerged surface. Fewer of the surface charges are 'experienced' by the remaining aqueous solution, reducing the effective surface charge as ionic strength increases.

Surface charges of bacteria tend to primarily be negative, so both positively and negatively charged substrates were evaluated in this study. The first step of characterization was to determine particle size distributions. Alumina, silicalite and PDMS particles were found to have average diameters of 0.53 μm, 0.2 μm and 3 μm, respectively. The zeta potential for each substrate was then evaluated for 0, 10 and 100 mM NaCl aqueous suspensions. The resultant zeta potentials are presented in Table A.1. Of the substrates studied here, silicalite had the most electronegative surface charge at -45.6 mV in deionized water. At low ionic strength and pH range of 7-8 others have also observed zeta potentials of silicalite colloids to range from approximately -40 mV (Y. Wang et al., 2001) down to -50 mV. (Nikolakis, Kokkoli, Tirrell, Tsapatsis, & Vlachos, 2000) At higher ionic strength and pH 7-8, the reported silicalite zeta potential rises to -20 mV because of ionic screening (Y. Wang et al., 2001) which compares well with the -19.4 mV observed at 100 mM NaCl for silicalite in this study. Zeta potentials of other substrates decreased in absolute value with increasing ionic strength as seen in Table A.1.

Table A.1.

Substrate Zeta Potential vs Ionic Strength.

Zeta Potentials (mV)	PDMS	Silicalite	Alumina
0 mM	- 30.7 ± 7.0	-45.6 ± 5.4	30.6 ± 4.5
1 mM	-18.2 ± 4.0	-49.1 ± 6.2	13.9 ± 4.2
10 mM	- 16.7 ± 5.3	-42.9 ± 4.8	12.1 ± 3.8
100 mM	- 6.3 ± 4.6	-19.4 ± 5.1	- 5.33 ± 4.2

Cellular surface charges fluctuate with changes in the pH of the aqueous background as the plasma membrane tends to be polarized and protonated differently as a function of pH (S. Kang & Choi, 2005). *S. cerevisiae* surface properties used in this study were measured by Kang et al. (S. Kang & Choi, 2005) while the *E. coli* properties were determined from adhesion studies on coated glass surfaces (B. Li & Logan, 2004). The zeta potentials used for this study are reported in Table A.2. As with the substrates, zeta potential decreases in absolute value with increasing ionic strength. Notably, the zeta potentials of both cells and substrate are directly comparable in magnitude. In an ionically complex media, it might be expected that some cellular repulsion from substrates would exist. High osmolarity and high ionic strength of the aqueous background increase microbial adhesion even robust biofilm formers such as *P. fluorescens* on polymer substrates (O'Toole & Kolter, 1998). Other correlations between ionic strength and increased cell-surface adhesion are very linear, though ionic strength alone is not an accurate predictor of cellular adhesion compared to surface free energy. (B. Li & Logan, 2004) Meanwhile bulk cell growth is largely unaffected by ionic strength of the media ranging from 0-0.4 M. (O'Toole & Kolter, 1998)

Table A.2.

Cellular Zeta Potential vs Ionic Strength.

Zeta Potentials (mV)	***S. cerevisiae***	***E. coli***	**Reference**
1 mM	—	−53 ± 5	(B. Li & Logan, 2004)
10 mM	−8.7 ± 1.5	—	(S. Kang & Choi, 2005)
100 mM	—	−32 ± 6	(B. Li & Logan, 2004)

150 mM	−9.4	—	(S. Kang & Choi, 2005)

A.3.2 Substrate and Cell Characterization by Goniometry

Increasing hydrophobicity of the substrate has also been correlated with increased cellular adhesion but cannot be determined by zeta potential, rather the contact angle is the only reliable indicator of relative hydrophobicity. (B. Li & Logan, 2004; Sano, Yanagishita, Kiyozumi, Mizukami, & Haraya, 1994) The susceptibility of a substrate to cellular fouling has also been studied with respect to surface roughness and hydrophobicity with lesser and greater effects, respectively. (Park, Kwon, Kim, & Cho, 2005) The high swelling coefficient of many alkanes and organic solvents, determining the free surface energy of polymers such as PDMS are challenging by sessile drop methods. (Chaudhury & Whitesides, 1991) Among the substrates studied here, the most hydrophobic (having the greatest water contact angle) was the PDMS whereas the most hydrophilic was silicalite as seen in Figure A.1B and C&D, respectively. The contact angles for both virgin and fouled substrates have been collected in Table A.3. Both virgin and fouled substrates were compared via the attachment energies before and after cellular attachment. Figure A.1A & F show electron micrographs of PDMS before and after exposure to E. coli KO11, while Figure A.1 E & J show the same electron micrographs for silicalite. The fouled substrate contact angles are presented in Figure A.1G, H&I for PDMS and silicalite. Silicalite has a far lesser water contact angle compared to alumina and PDMS and is therefore least hydrophobic of the substrates. The alumina substrate had consistent contact angles before and after growth in the well plates. Following cellular attachment, the contact angles for all substrates decreased, reflecting the changes

in surface properties and a transition from hydrophobic to hydrophilic properties. This difference is most pronounced for PDMS with its 80% decrease in water contact angle compared to a 15% decrease for silicalite. Silicalite contact angle for water decreased slightly whereas the contact angles for other solvents increased with DMSO contact angles remaining essentially constant as seen in Table A.3.

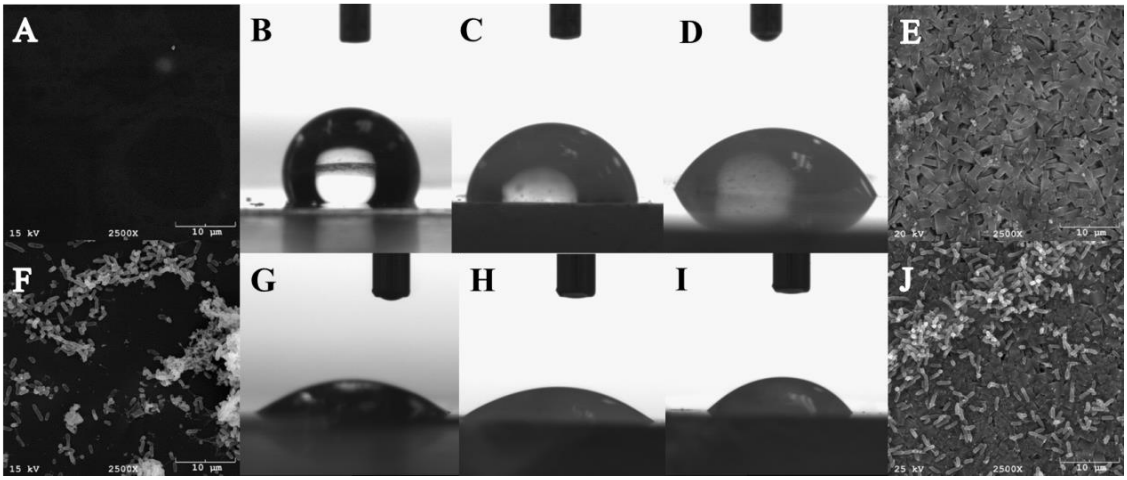

Figure A.1. Goniometry Before and After Cellular Fouling. A) Electron micrograph of virgin PDMS, water contact angle of B) virgin PDMS, C) alumina and D) yittria-supported zirconia substrates coated in silicalite, E) virgin silicalite, F) electron micrograph of fouled PDMS, water contact angles on G) fouled PDMS, fouled H) alumina and I) Yittria-supported zirconia substrates coated in silicalite, J) electron micrograph of fouled silicalite.

Table A.3.

Substrate Contact Angle.

	Virgin Substrate			Fouled Substrates		
Contact Angle (degrees)	PDMS	Silicalite	Alumina	PDMS	Silicalite	Alumina
Water	113 ± 3	54 ± 6	85 ± 7	22 ± 2	41 ± 3	85 ± 7
Glycerol	106 ± 3	75 ± 5	—	—	—	—
Hexadecane	47 ± 5	Wetting	—	8 ± 1	13 ± 1	—
Dodecane	50 ± 3	Wetting	—	—	—	—

Ethylene Glycol	101 ± 3	33 ± 4	57 ± 5	59 ± 4	51 ± 6	57 ± 5
Dimethyl Formamide	93 ± 2	20 ± 3	—	—	—	—
Diiodomethane	86 ± 8	44 ± 4	65 ± 2	52 ± 1	50 ± 3	65 ± 2
DMSO	93 ± 2	24 ± 3	46 ± 9	31 ± 4	24 ± 2	46 ± 9

Such large change in apparent surface properties of PDMS was likely the result of the extra-cellular matrix (ECM) formed between cells, which is also contextually referred to as EPS, or the glycocalyx, and often forms as a stress response (Popielarska-Konieczna, Bohdanowicz, & Starnawska, 2010). EPS is composed of high MW polysaccharides, lipids, phosphates, proteins, nucleic acids, flagella, pili, cellular debris all up to 95% water by mass (Dohnalkova et al., 2011; Vertes et al., 2012). Each of these components has distinct physical chemical properties and together are responsible for the majority of cellular attachment forces measured by AFM at cell-substrate separation distances less than 20 nm (Ong, Razatos, Georgiou, & Sharma, 1999a). EPS is approximately 10-fold greater mass in biofilm compared to cells. (Lorite et al., 2013; Vertes et al., 2012) The cellular contact angles used for this study are listed in Table A.4. It is interesting to note that the cellular contact angles for *E. coli* compared closely to those of fouled PDMS for water (19° and 22°, respectively) and diiodomethane (43° and 52°, respectively). While not identical, the substrate surface clearly becomes more hydrophilic after cellular attachment begins. This is likely to promote further and more rapid fouling of the substrates. In the case of an adsorbent or pervaporation membrane, this fouling would inhibit separations performance. It is therefore important to understand how substrate and cell properties effect the mechanism of the substrate fouling.

Table A.4.

Cellular Contact Angles.

Contact Angle (degrees)	*E. coli* JM109	*S. cerevisiae*
Water	19 ± 2	25 ± 2
Glycerol	40 ± 4	—
Ethylene Glycol	—	32 ± 2
Diiodomethane	43 ± 2	64 ± 3
Reference	(B. Li & Logan, 2004)	(S. Kang & Choi, 2005)

A.3.3Modeling Bacteria-Substrate Attachment Energies

The most effective means of estimating the likelihood of a substrate to foul in the presence of any given microorganism is to first estimate the energy of attachment between substrate and cell. These analytical methods rely on surface characterization of both cells and substrates. Substrate properties are readily determined from contact angle goniometry with judicious choice of an apolar alkane (having neither electron donor, nor electron acceptor component energies) in the liquid triad. The substrate's Lifschitz-van der Waals component energy is easily determined from Equation A.7 when the alkane is not swelling or solvating the substrate. Substrate swelling is a particular challenge with polymeric substrates such as PDMS. (Chaudhury & Whitesides, 1991; J. N. Lee et al., 2003) Many solvent properties have been tabulated (Fowkes, 1964) for a number of liquid triads. Depending on the liquid triad chosen, the calculated surface energies will differ often due to the degree of surface adsorption of one or more of the solvents, which is difficult to quantify. (Chibowski & Perea-Carpio, 2002) This can also result in overestimation of the surface tension components when 'negative' values result from solving the roots of Equation A.7 (Hwang, Yang, Lee, Ahn, & Mhin, 2011; Kwok, Li, & Neumann, 1994). Accordingly, it is best to estimate the surface energies by using a

multiple solvent triads since there is no direct method to measure the surface free energy of a substrate. (Chibowski & Perea-Carpio, 2002)

Substrates were interrogated by surface chemistry analytical techniques including contact angle goniometry and zeta potential determination. Using the XDLVO method rooted in the earlier DLVO method (Verwey & Overbeek, 1948) for cell-substrate attachment energy from analytical chemistry data is a common practice. (Bhattacharjee, Chen, & Elimelech, 2000a; Bhattacharjee, Sharma, & Bhattacharya, 1996; B. Li & Logan, 2004; Ong et al., 1999a). For this study substrates were interrogated using the following solvents: water, glycerol, hexane, hexadecane, dimethylformamide, dimethylsulfoxide and diiodomethane. The first substantive energetic analysis by which to compare substrates is the OCG method calculated by Equation A.6, as presented in Table A.5. Whereas for PDMS the work of attachment decreases by ~17% after fouling, it decreases for silicalite by ~88 % and is unchanged for alumina which remained unchanged after exposure to culture. This indicates that once fouling of a separations surface begins, the cells attach more readily. Also clear from this initial estimate is that silicalite has ~4-fold greater work of attachment than alumina and ~1.7-fold greater than that of PDMS. From these results, it seems that the alumina, PDMS and silicalite should undergo cellular attachment in the order of the work of attachment. This parameter doesn't account for cellular or electrostatic contributions to attachment and therefore doesn't provide an accurate fouling prediction.

Table A.5.

Estimated Work of Attachment.

OCG Work of Attachment	PDMS (mJ/m^2)	Silicalite (mJ/m^2)	Alumina (mJ/m^2)
Virgin substrates	78.2	129.1	32.1
Fouled substrates	64.7	16.0	—

By including the contact angles of not only the substrate but also *E. coli* and *S. cerevisiae*, a more complete comparison can be made. The virgin substrate energies for each of the 3 separations materials are presented in Table A.6 as calculated from the DLVO method. It would seem from this estimation that alumina and PDMS would foul similarly. From the energy of attachment calculated by the XDLVO method in Table A.6 for *E. coli* attachment, it becomes clear that attachment to PDMS requires only ~36% of the energy required to attach to alumina and silicalite. It would therefore be expected that the cellular attachment to PDMS would be significantly greater than for silicalite or alumina. The attached *E. coli* KO11 cells counted from several scanning electron micrographs are also presented in Table A.6. There were ~5.7-fold more cells attached to PDMS compared to silicalite and none observed for alumina. For the attachment of E.coli then, the results expected from the XDLVO model are consistent with the experimental observations. Energy of attachment for S. cerevisiae to the substrates was also estimated in Table A.6. From these values, it would be expected that cellular attachment of yeast should be comparable between PDMS and silicalite. While *S. cerevisiae* was observed to attach to PDMS, no attachment was observed for alumina or silicalite as shown in Table A.6. A closer examination of the energy of attachment contributions calculated from Equations A.12-A.14 shows the acid-base interactions are dominant. Specifically, the acid-base contributions to the energy of attachment are 10-fold larger than the other

contributions at ~5nm approach distance. The calculated acid-base contributions to energy of attachment for PDMS and silicalite are approximately 2-fold that of the Polyethersulfone membranes studied by Bhattacharjee et al. (Bhattacharjee et al., 1996) This is likely due to differences in both the polymer chemistries and the liquid triads used for characterization, but demonstrates the calculated values are reasonable. The dominance of the acid-base interactions often leads to the conclusion that hydrophobicity has the strongest correlation between substrate properties and cellular attachment. (B. Li & Logan, 2004) This is important to understand for judicious choice of adsorbents in particular where longer contact times with culture will allow cellular attachment to begin. (Wiehn et al., 2014)

Table A.6.

XDLVO Attachment Energies and Attached Cell Counts.

XDLVO	Virgin substrate energies (mJ/m^2)	E. coli attachment energy (J)	E. coli KO11 (cells/µm2)	S. cerevisiae BY4741 attachment energy (J)	S. cerevisiae BY4741 (cells/µm2)
PDMS	24.6	1.8E-13	4.00E+07	2.94E-13	6.49E+06
Silicalite	87.3	6.5E-14	7.13E+06	2.88E-13	—
Alumina	32.3	5.9E-14	—	—	—
E. coli JM109 surface energy (mJ/m^2)	215.4				

An important factor to consider for separations, specifically bioalcohol adsorption is the influence of the product (e.g. ethanol) on the energy of attachment to substrates. For *in situ* recovery by adsorbents such as L-493 resins (Wiehn et al., 2014) or activated carbons (Sulaymon & Ahmed, 2008) it is common to start product adsorption after ~12-24 hours. (Ezeji et al., 2013; Xiaoqing Lin et al., 2013) This means that a model cellular attachment environment would necessarily include the effects of ethanol, though such an XDLVO analysis of separations materials has not been investigated to the author's

knowledge. The same characterizations were carried out with ethanol/water contact angles used to solve for ethanol-dependent roots of Equation A.7. The ethanol contact angles change compared to deionized water because of changes in the surface tension. The energy of attachment for both *E. coli* and *S. cerevisiae* on silicalite and PDMS were calculated by XDLVO with the results presented in Table A.7. As the ethanol concentration increases, the energy of attachment of E.coli decreased for both silicalite and PDMS. At 5% ethanol the energy of attachment of *E. coli* to PDMS becomes a negative value, which would be expected to promote biofilm formation on the surface. This would be coincident with the ethanol stress on E. coli which would further promote biofilm formation as a stress response. Interestingly the energy of attachment increases for *S. cerevisiae*, which implies that lesser attachment should be observed for increased ethanol concentration. Also presented in Table A.7, the fouled substrate attachment energy for *E. coli* is nearly the same for both substrates and the attachment energy for 5% ethanol on silicalite. It would therefore be expected that cellular attachment leading to biofilm formation becomes much greater once cellular attachment is established on a substrate. As the XDLVO method does not entirely capture the fouling potential of a substrate for all organisms, another important factor to consider is the contributions to forming the 'conditioning layer' on the substrates.

Table A.7.

XDLVO Attachment Energy on Substrates.

Energy of Attachment	PDMS (J)	Silicalite (J)
Virgin Substrate & *E. coli* JM109	1.8E-13	2.7E-13
3% EtOH & *E. coli* JM109	1.8E-13	2.8E-13
5% EtOH & *E. coli* JM109	-1.5E-14	5.1E-14

Fouled Substrate & *E. coli* JM109	4.7E-14	5.0E-14
Virgin Substrate & *S. cerevisiae* BY4741	6.5E-14	5.1E-14
5% EtOH & *S. cerevisiae* BY4741	2.9E-13	2.9E-13

A.3.4 Conditioning Layer Formation by Media Components

There are many organic components present in aqueous media capable of initiating formation of a 'conditioning layer'. A diagram of a generalized fouling mechanism is presented in Figure A.2 where the conditioning layer promotes early cellular attachment, leading to biofilm formation. One significant contributor to conditioning the substrate for cellular attachment are the lipopolysaccharides (LPS) from *E. coli*, for example, which have a negative surface charge (Hardy, Kamphuis, Japaridze, Wilschut, & Winterhalter, 2012). LPS-substrate adhesion is known to be inversely proportional to LPS length (B. Li & Logan, 2004), meaning that as cell-substrate separation distance decreases, the LPS-substrate adhesion increases. The attachment of robust biofilm formers such as *P. aeruginosa* to surfaces increased with increasing LPS length at low ionic strength, though not at high ionic strength (B. Li & Logan, 2004). This is of particular interest to adsorbents with the long contact times for in situ product recovery.

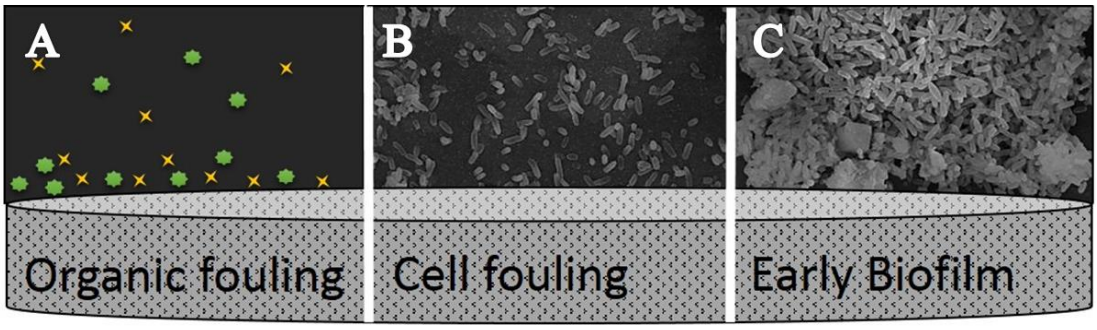

Figure A.2. General Biofouling Development. A) Conditioning film of proteins, lipids and cellular debris, B) Cellular attachment to the conditioning layer, C) Early biofilm.

As this supposed 'conditioning layer' has not been rigorously characterized to the author's knowledge, an experiment was devised. To evaluate the effect of media components on 'conditioning layer' formation, substrates were ethanol sterilized and submerged in sterile cell-free Luria-Bertani media for 24 hours in a shaking incubator at 37°C and 120 rpm. AFM was performed on the substrates following media exposure to determine changes in the surface roughness caused by the formation of a 'conditioning layer' which would otherwise not be directly observable. The AFM results are displayed in Figure A.3 for both silicalite and PDMS. The roughness measured by AFM increased for PDMS while it decreased for silicalite. As these substrates were rinsed by deionized water, the changes in roughness were the result of substrate fouling rather than particle sedimentation. In the case of silicalite the high initial roughness leaves troughs and valleys of the crystalline surface which become partially occluded by adsorbed material. While this method shows qualitative fouling by media components, it provides no quantitative insights about what media components adsorbed. It is thought the adsorbed media components include primarily proteins and polysaccharides (Ras et al., 2013) perhaps from yeast extract present in LB media.

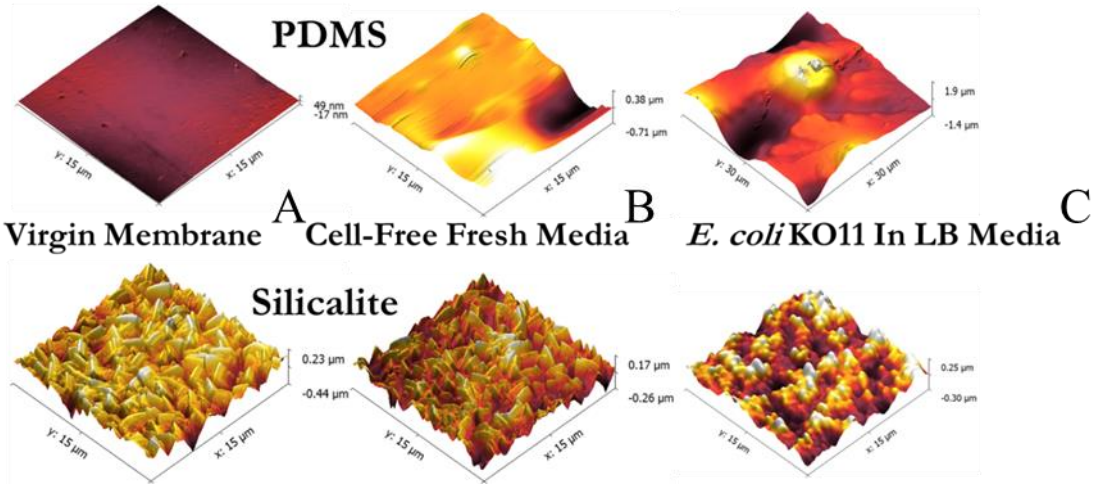

Figure A.3. Biofouling of Media Components. A) Conditioning film of proteins, lipids and cellular debris, B) Cellular attachment to the conditioning layer, C) Early biofilm.

To evaluate the likelihood of protein fouling of substrates, Bovine Serum Albumin was chosen as a model protein for an adhesion study. Substrates were immersed in varied concentrations of BSA in glass vials and the aqueous solution dyed with coomasie blue dye before being quantified by optical density at 595 nm. The adsorption isotherms for BSA onto PDMS and silicalite are displayed in Figure A.4. It is clear that BSA adhered to both silicalite and PDMS, with PDMS having the greater BSA adsorption. Adhesion of BSA to silicalite seemingly reaches equilibrium at ~0.003 g/g whereas the PDMS substrate accumulates what may be multiple BSA layers. Langmuir-type isotherm behavior is often observed for protein adsorption onto silicalites whereas multilayer adsorption profiles have been observed for other substrates (Noisuwan, Hemar, Wilkinson, & Bronlund, 2011; Oudshoorn et al., 2009a). These adsorption studies were conducted at 100 mM ionic strength where foulant-foulant interactions are often more energetically favorable than foulant-substrate interactions (Ang & Elimelech,

2007). Electrostatic interactions between BSA molecules were not a factor for this study as the isoelectric point for BSA was used. Silica materials are known to have primarily repulsive interactions with proteins which can slow protein adsorption. (van Oss, 1993) It is also known that proteins tend to adhere to substrates with higher energy surfaces such as hydrophobic polymers (van Oss, 1993) which is consistent with the BSA isotherm behavior for PDMS. While BSA adsorption is more quantitative than the AFM results above, it does not characterize a complete fouling mechanism. Other factors such as surface roughness are also important to consider.

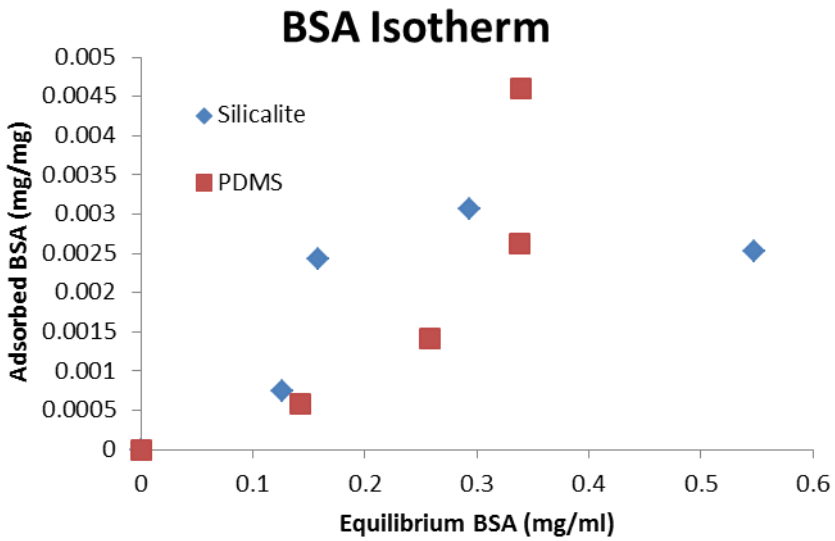

Figure A.4. *Bovine Serum Albumin Isotherm***.** Isotherm for bovine serum albumin adsorption onto silicalite (diamonds) and polydimethyl siloxane (squares)

A.3.5 Effects of Roughness on Whole-Cell Fouling

Substrate roughness does effect fouling by microorganisms, but to a lesser degree than other factors for bacteria. (B. Li & Logan, 2004) Both virgin substrates and cell fouled substrates were examined after being rinsed with deionized water and air dried

overnight. Virgin silicalite samples had roughness values approximately 10-fold greater than PDMS. Fouled silicalite membranes increased in roughness due to the presence of cells as seen in Figure A.5. It is clear that the substrate roughness of the silicalite did not prevent cellular attachment. The effects of ethanol on cellular attachment were also qualified with this study where increasing ethanol content reduced the cellular attachment to silicalite.

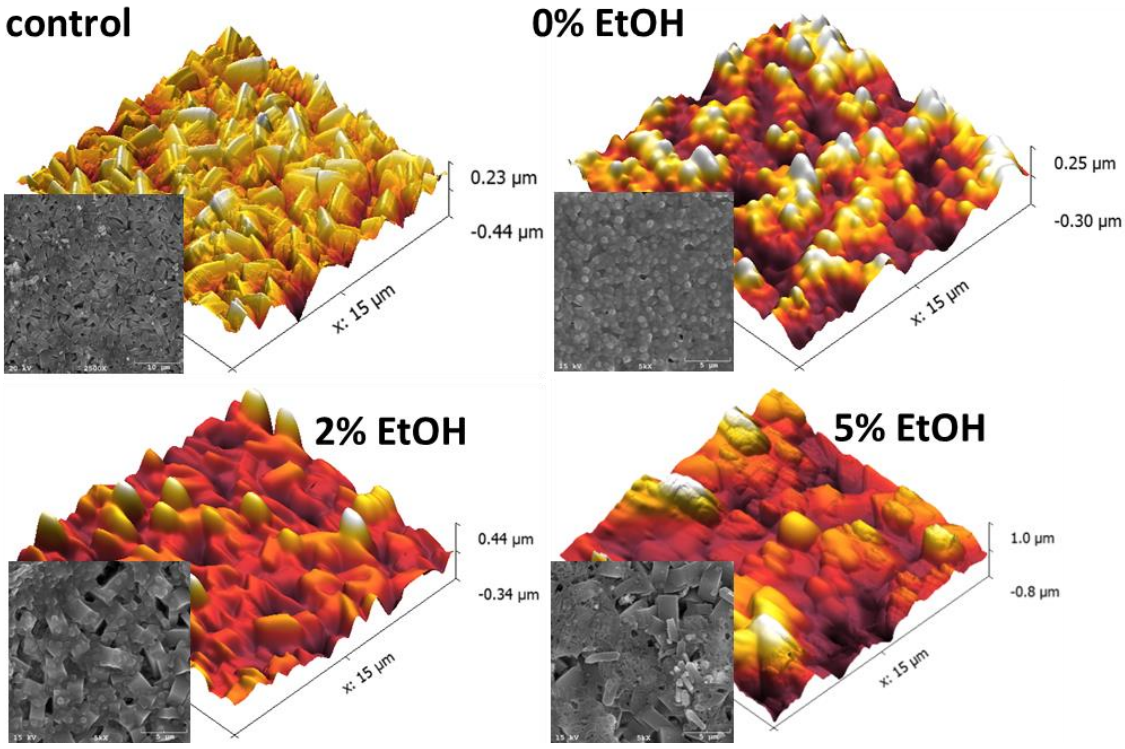

Figure A.5. AFM of Virgin and Fouled Alumina-Supported Silicalite Effects of Ethanol. Top row: Virgin and E. coli KO11 biofouled alumina supported silicalite with 0% ethanol. Bottom Row: Biofilm grown on alumina supported silicalite with 2 and 5 wt% ethanol content.

Similarly to alumina supported silicalite, the YSZ-supported silicalite membranes increased in overall roughness with fouling as seen in Figure A.6. Likewise with the

increase in ethanol concentration, the cellular attachment decreased qualitatively. Also similar to the alumina-supported silicalite, the surface roughness did not prevent cellular attachment.

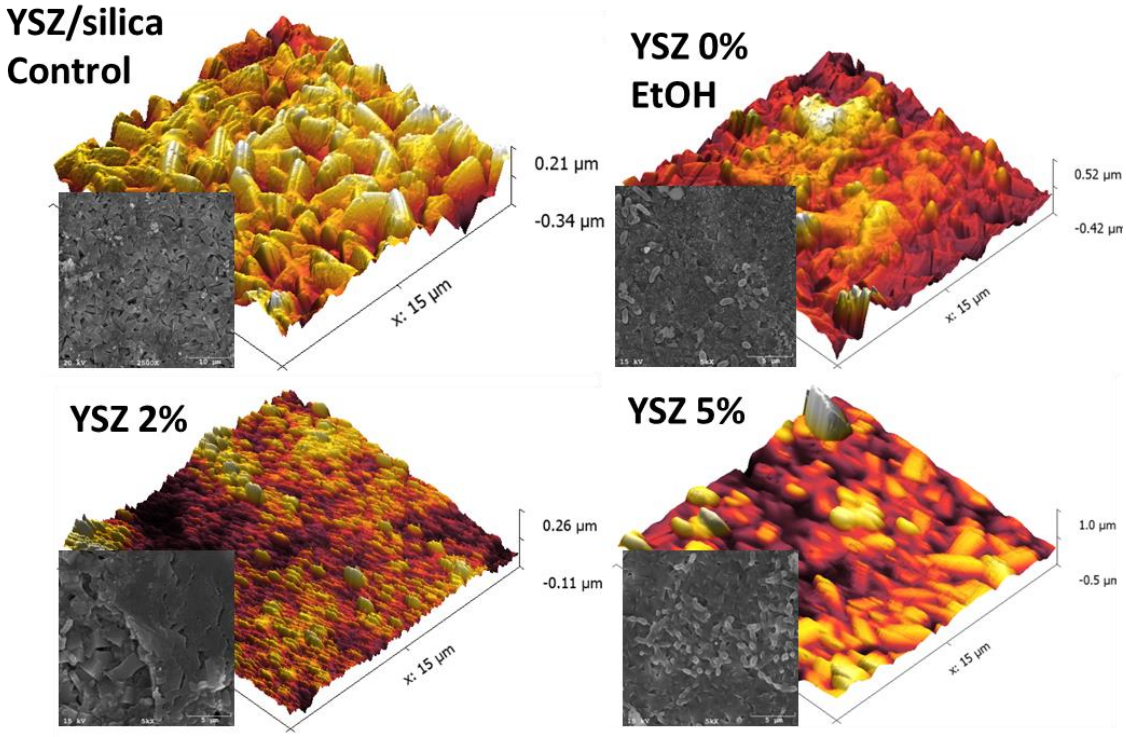

Figure A.6. AFM of Virgin and Fouled YSZ-Supported Silicalite Effects of Ethanol. Top row: Virgin and E. coli KO11 biofouled YSZ supported silicalite with 0% ethanol. Bottom Row: Biofilm grown on YSZ supported silicalite with 2 and 5 wt% ethanol content.

PDMS roughness was found to increase by approximately 200-fold following fouling. AFM results taken alone suggest that the less rough surface of the PDMS was somehow more favorable for cellular attachment than the silicalite. The effects of ethanol on cellular attachment to PDMS are presented in Figure A.7. The increased roughness

from cellular attachment was consistent across ethanol concentrations, but qualitatively cell fouling at 5% ethanol was greater than for any other case studied.

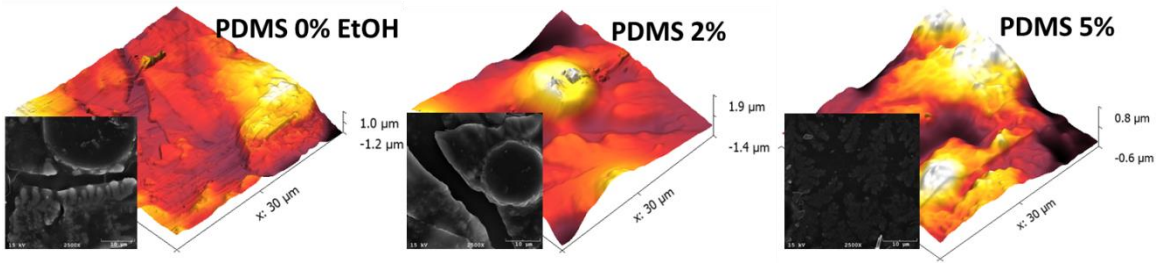

Figure A.7. AFM of Fouled PDMS Effect of Ethanol. PDMS fouling as influenced by ethanol concentration from 0% (left) to 5% (right).

The most significant changes in the substrates quantified by AFM investigation occurs for PDMS. This study does not quantify the changes in energy of interaction between the AFM probe and the virgin or fouled substrates. Other groups have studied substrate roughness often with no conclusive correlation to cellular attachment (Cao et al., 2006; Ciston et al., 2008; B. Li & Logan, 2004; Q. Lu, Wang, Faghihnejad, Zeng, & Liu, 2011). Substrate roughness between 0.04 and 1.24 µm have been observed to promote biofilm formation while more roughened surfaces are more resistant to biofilm formation given the same chemistry. (Hou, Gu, Smith, & Ren, 2011) Taken together, the XDLVO results and the AFM characterizations show that once the conditioning layer begins to form, the substrates become increasingly similar both physically and in surface energy. Once *E. coli* attachment has occurred, the substrates are not distinguishable by roughness and are nearly identical in the required energy of attachment. Aside from alumina, these results suggest that it is expected most substrates will undergo cellular attachment. Since substrate material alone can only slow attachment, extended

applications of *in situ* product recovery by adsorption or pervaporation could greatly benefit from reduction of the ability of the organism to attach to substrates.

A.3.6 Effect of Gene Deletion on S. cerevisiae Attachment

Several strains of *S. cerevisiae* were obtained with and without the Flo11 gene thought to be responsible for the flocculation of yeast. (Bauer, Govender, & Bester, 2010; B. Guo, Styles, Feng, & Fink, 2000) Substrates were ethanol sterilized and added to 6 well plates with NB glucose media as with the previous attachment studies. The substrates were cultured for 48 hours to allow sufficient growth of the yeast strains. Substrates were then chemically fixed for SEM imaging using the protocol previously described. The electron micrographs are presented in Figure A.8 where the top row represents silicalite substrates and the bottom row represents PDMS attachment. Yeast attachment to silicalite was generally poor, with only some cellular attachment observed. PDMS was observed to have significant attachment of yeast strains, particularly by BY4741 as seen in Figure A.8. This is consistent with the energy of attachment predictions from the XDLVO method. When the primary flocculation gene was deleted from BY4741, the cellular attachment decreased approximately 94%. S288C is a yeast strain known for its high flocculation and low substrate adhesion. Without Flo11, the S288C strain reduced cellular attachment to PDMS by ~51%. While there was no significant quantitative difference between *S. cerevisiae* attachment to silicalite with and without Flo11, the results for PDMS are significant. While not an all-inclusive gene deletion study, it is clear that some clever genetic engineering of the organism in combination with judicious substrate choice, the cellular attachment may be well controlled. More extensive studies would likely develop a strategy for the prevention of

cellular attachment on the separations substrates leading to improved performance for longer duration *in situ* product recovery. This is of particular interest for a process where semi-continuous operation with *in situ* product recovery is the objective.

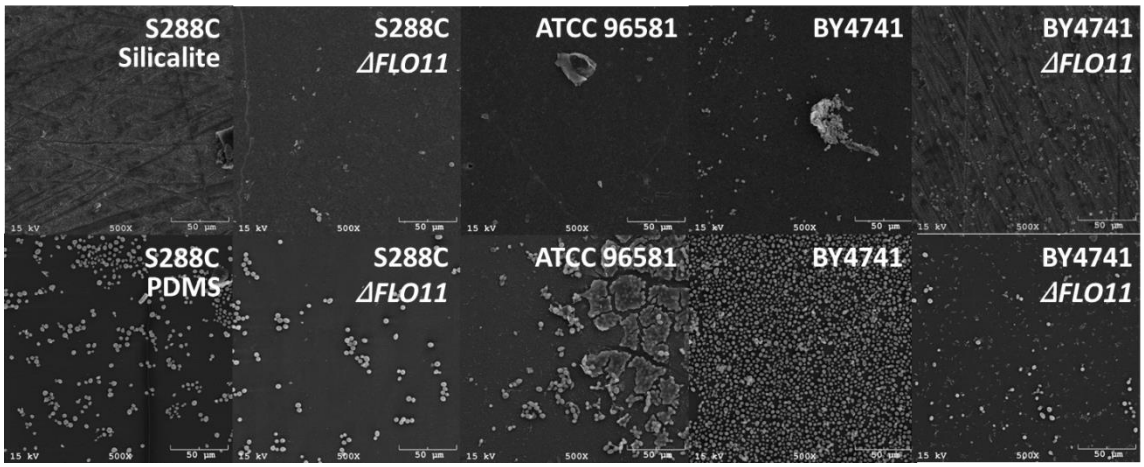

Figure A.8. Electron Micrographs of Yeast Attachment to Substrates. Top row: Electron micrographs from SEM of a few S. cerevisiae strains grown on silicalite membranes. BY4741 and its child strain ΔYDL233W missing Flo11 followed by ATCC96581 and BY4741 with and without Flo11. Bottom row: Electron micrographs of the same S. cerevisiae strains grown on PDMS membranes.

A.4.0 Conclusion and Future Work

It is clear that polymeric substrates (e.g. pervaporation membranes) will foul, not only from media components, but undergo whole cell fouling. *E. coli* attachment to both PDMS and silicalite substrates can be reasonably predicted from XDLVO estimation of the energy of attachment. The formation of a conditioning layer by media components, particularly proteins prior to cellular attachment has been established for both PDMS and silicalite substrates. While the substrate roughness did not provide a meaningful correlation with cellular attachment, the relative hydrophobicity defined by contact

angles did. The more hydrophobic substrate was prone to increased fouling not only by model proteins but also whole cells. Even within 48 hours in rich media, dense cell layers were observed to form by all organisms on PDMS, with only moderate attachment to silicalite. By deleting certain genes involved in cellular attachment, cell fouling can be reduced, though not eliminated. In combination, both judicious strain engineering and substrate choice could greatly reduce the impact of fouling on separations substrates for *in situ* product recovery.

This study would greatly benefit from the inclusion of *B. subtilis* and *P. aeruginosa* for the XDLVO modeling and attachment studies. *B. subtilis* is a model Gram-positive bacteria which can often be found in biofilms, while *P. aeruginosa* is a well-known infectious microorganism and a robust biofilm former. (B. Li & Logan, 2004) These microorganisms along with the current study of E. coli and S. cerevisiae would represent a broad cross section of bioprocesses, giving this study greater relevance across many industrial applications. The cellular attachment could perhaps also be characterized with techniques such as environmental SEM to capture the cellular attachment before the harsh chemical actions of cell fixation. This study would also be further enhanced by the inclusion of more substrate materials such as activated carbon and glass as both materials are industrially ubiquitous for bioprocessing.

A.5.0 Acknowledgments

This work was supported by the National Science Foundation (Award Nos. CBET-1067684 and CBET-1159200). The authors declare no conflicts of interest.

APPENDIX B

ADSORPTION OF OTHER METABOLITES ONTO MMCPS

B.1.0 Adsorption of Other Bioproducts

Adsorption studied were conducted as described in the chapters with 100 g/L ratio of adsorbents to aqueous phase. The adsorption of xylose, glucose, succinate and lactate were evaluated. Figure B.1 shows the limited adsorption of select sugars from lignocellulosic feedstocks and select bioproducts. Xylose in Figure B.1A does not appreciably adsorb onto MMCPs, nor does glucose as seen in Figure B.1B. Sodium succinate adsorbs onto MMCPs up to ~0.05g/g which may be considered low adsorbent loading as can be seen in Figure B.1C. Lactate does adsorb onto MMCPs likely, multi-layer adsorption given its linearity as seen in Figure B.1D.

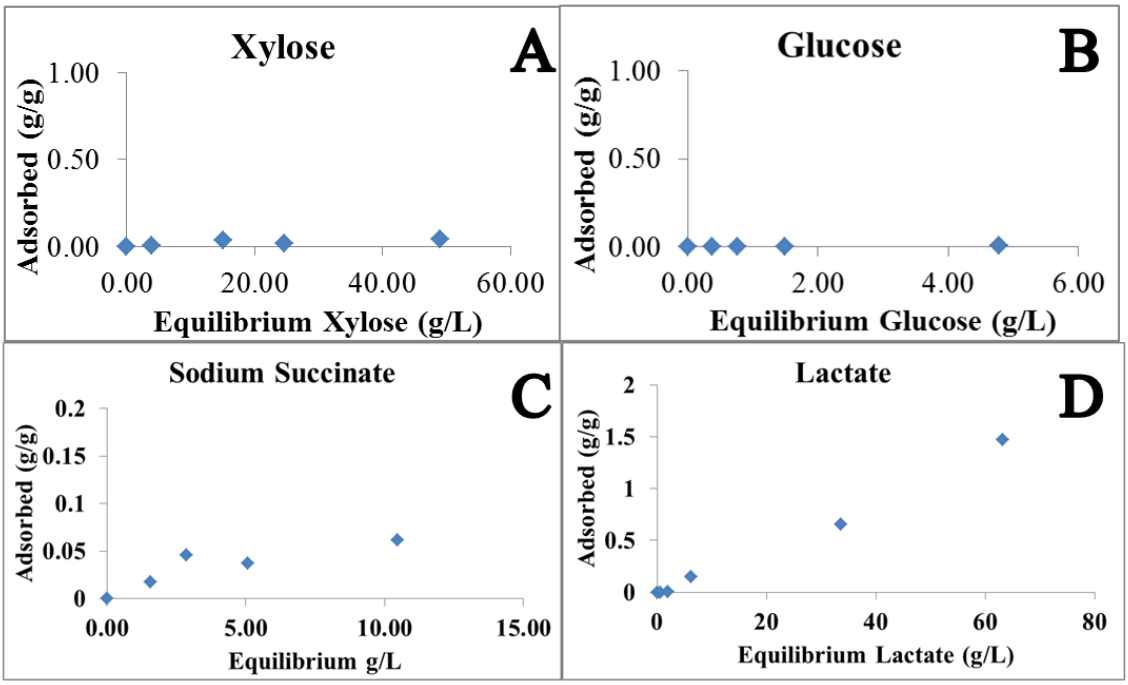

Figure B.1. Adsorption of Other Bioproducts. Equilibrium adsorption of A) xylose, B) glucose, C) Succinate, D) Lactate.